AD_____

Award Number: DAMD17-01-1-0635

TITLE: Combining Electron with Intensity Modulated Photon Beams for Breast Cancer

PRINCIPAL INVESTIGATOR: Lei Xing, Ph.D.

CONTRACTING ORGANIZATION: The Leland Stanford Jr. University
Stanford, California 94305-5401

REPORT DATE: July 2002

TYPE OF REPORT: Annual

PREPARED FOR: U.S. Army Medical Research and Materiel Command
Fort Detrick, Maryland 21702-5012

DISTRIBUTION STATEMENT: Approved for Public Release;
Distribution Unlimited

REPORT DOCUMENTATION PAGE

Form Approved
OMB No. 074-0188

1. AGENCY USE ONLY (Leave blank)	2. REPORT DATE	3. REPORT TYPE AND DATES COVERED
	July 2002	Annual (1 Jul 01 - 30 Jun 02)

4. TITLE AND SUBTITLE
Combining Electron with Intensity Modulated Photon Beams for Breast Cancer

5. FUNDING NUMBERS
DAMD17-01-1-0635

6. AUTHOR(S)
Lei Xing, Ph.D.

7. PERFORMING ORGANIZATION NAME(S) AND ADDRESS(ES)
The Leland Stanford Jr. University
Stanford, California 94305-5401

e-mail:
lei@reyes.stanford.edu

8. PERFORMING ORGANIZATION REPORT NUMBER

9. SPONSORING / MONITORING AGENCY NAME(S) AND ADDRESS(ES)
U.S. Army Medical Research and Materiel Command
Fort Detrick, Maryland 21702-5012

10. SPONSORING / MONITORING AGENCY REPORT NUMBER

11. SUPPLEMENTARY NOTES

12a. DISTRIBUTION / AVAILABILITY STATEMENT
Approved for Public Release; Distribution Unlimited

12b. DISTRIBUTION CODE

13. ABSTRACT *(Maximum 200 Words)*

We developed a hybrid technique of electron and intensity modulated photon beams for breast cancer. The electron beam was used to treat the bulk of the tumor volume, whereas IMRT beams were used to improve target dose homogeneity. The weight of the electron beam as well as the fluence profiles of the IMRT beams were optimized using a dose-based objective function. We have worked on: (i) developed an effective dose optimization algorithm for the hybrid treatment, with regional dose modifiable by a voxel-dependent penalty scheme; (ii) developed software tools to incorporate MLC transmission and head scatter into dynamic delivery process to ensure the accurate delivery of the planned dose distribution; (iii) demonstrated the dosimetric advantage of the hybrid treatment; and (iv) evaluated the matching of electron and IMRT beam against the setup errors as well as the match-line dose uniformity. It was found that the hybrid approach provides a viable alternative for clinically difficult breast cases. Using the technique, the high doses to the ipsilateral lung and, in the case of the left-breast cancer patient, the heart were markedly reduced with minimal increase in the dose to other normal structures when compared with plans generated using the tangential field technique.

14. SUBJECT TERMS
breast cancer, photon beams, IMRT

15. NUMBER OF PAGES
136

16. PRICE CODE

17. SECURITY CLASSIFICATION OF REPORT	18. SECURITY CLASSIFICATION OF THIS PAGE	19. SECURITY CLASSIFICATION OF ABSTRACT	20. LIMITATION OF ABSTRACT
Unclassified	Unclassified	Unclassified	Unlimited

Table of Contents

Cover.....1

SF 298.....2

Table of Contents.....3

Introduction.....4

Body.....4

Key Research Accomplishments.....9

Reportable Outcomes.....9

Conclusions.....11

References.....12

Appendices.....13

I. INTRODUCTION

This Concept Award was awarded to the principal investigator (PI) for the period of July 1, 2001—June 30, 2002. Because of the late arrival of the postdoctoral fellow (Dr. David Y. Yang) for this project, we have filed a no-cost extension to June 31, 2003 (see attached Assistance Agreement). This proposal is aimed at developing a hybrid treatment method of intensity modulated radiation therapy (IMRT) and conventional electron for breast cancer and exploring the potential benefit of the approach. The specific aims of the proposal are: (1) to demonstrate that the combination of the two modalities can lead to more conformal dose distributions that would not otherwise be possible for breast cancer treatment; and (2) to show that substantially improved dose distributions can be realized in practice. Under the generous support from the U.S. Army Medical Research and Materiel Command (AMRMC) , the PI has contributed significantly to breast cancer research by applying physics and engineering knowledge to breast cancer research. A number of conference abstracts and refereed papers have been resulted from the support. The preliminary data obtained under the support of the grant has also enabled the PI to start new research initiatives and significantly advanced my academic career. In this report, I summarize the highlights of my past year's research.

II.RESEARCH AND ACCOMPLISHMENTS

Radiation therapy is accepted as an effective treatment modality in the management of both invasive and non-invasive breast cancer [1-3]. In practice, breast irradiation has been associated with a number of potential complications, which include radiation pneumonitis, necrosis, cardiac toxicity, and radiation-induced secondary cancer [4-6]. Adjuvant treatment with chemotherapy may further aggravate these effects. Many approaches have been proposed to improve the current tangential-fields treatment aiming at reducing cardiac and pulmonary toxicity. Among them, use of electron for breast cancer has attracted much attention because of its rapid fall-off beyond the treatment range. These include, but not limited to, helical electron avoidance therapy (HEART) [7] using a scanning axial magnetic collimator to generate helical electron beams, and intensity- and energy-modulated electron therapy (IEMET) [8, 9]. While HEART and IEMET can modify the axial transport properties of an electron beam, the range of electrons is still predominantly determined by the incident energy and is difficult to be extended by intensity modulation or a magnetic field. Furthermore, as the electron energy increases (e.g., >18 MeV), the rapid fall-off feature starts *diminishing* and an enface treatment using any type of electron would considerably increase the risk of excessively irradiating the heart or the lung. In addition, it is practically impossible to maneuver the incident direction of an electron beam because of the extremely short distance between the electron applicator and the patient's skin. As a result, electron beam alone (conventional, HEART, IEMET) is only suitable, at best, for treating

chest wall for post-mastectomy patients or patients with small-sized breast. Considering the fact that the distance between the nipple and the chest wall for majority of breast cancer patients is much larger than 2~4cm (the fall-off range of 6~15MeV electrons), it is less likely for electron alone to make a genuine impact on breast cancer treatment.

On the other hand, it is well known that photon beam has high penetration power. Breast irradiation is conventionally delivered with wedged tangential fields, optimized using a single central-axis isodose distribution. Intensity-modulated tangential beam irradiation has been recently studied on five left and five right breasts by the research group of Memorial Sloan Kettering Cancer Center [10] and notable improvement in the doses to critical structures were achieved. Compared with a standard-wedged plan prescribed to 46 Gy, the dose from IMRT plan encompassing 20% of the coronary artery region decreased by 25% (from 36 Gy to 27 Gy) for patients treated to the left breast; the mean dose to the contra-lateral breast decreased by 42% (from 1.2 to 0.7 Gy); the ipsilateral lung volume receiving more than 46 Gy decreased by 30% (from 10% to 7%); the volume of surrounding soft tissue receiving more than 46 Gy decreased by 31% (from 48% to 33%). The dose homogeneity within the target volume improved greatest in the superior and inferior regions of the breast (approximately 8%), although some decrease in the medial and lateral high-dose regions (approximately 4%) was also observed. While these data illustrate the advantage of intensity modulation, rooms for further improvement exist. For instance, 7% of the ipsilateral lung volume receiving a dose higher than the prescribed dose is still quite substantial considering the large volume of a lung. Because of the half-moon shape of a breast target, it is inevitable that part of the lung (and part of the heart for left breast irradiation) will be in the treatment fields even for intensity-modulated beams. We have examined the feasibility of using multiple (3~7) intensity-modulated beams for breast cancer[11]. Figure 1 shows an example of this type of treatment. The technique can treat the breast target as well as nodal sites with a single set of IMRT fields, which simplifies the treatment when the regional lymph nodes (supraclavicular, axillary and internal mammary nodes) are involved and eliminates the potential overdosing/underdosing caused by matching the supraclavicular/axillary field with the tangential fields.

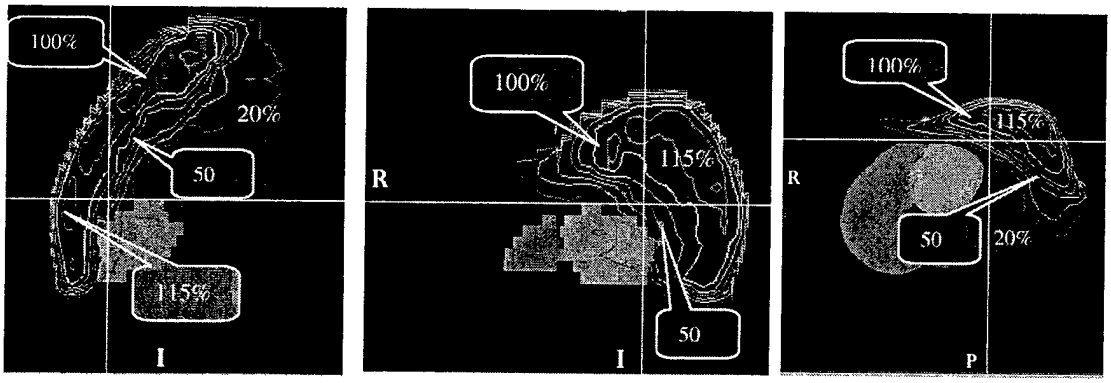

Fig. 1 Isodose distribution on a sagittal, coronal, and axial plane of a breast plan with inclusion of supraclavicular, axillary and internal mammary lymph nodes.

However, IMRT alone does not reduce the doses to the heart and lung because of the exiting photons. These photons in IMRT often result in an excessive volume of normal tissue exposed to low, moderate and even high dose, increasing the risk of late effects. In short, an effective method to prevent/reduce the primary or scatter photon from passing through the sensitive structures is strongly needed in order for breast cancer patients to benefit more from state-of-the-art IMRT technology.

Based on the above discussion, it seems logical to combine the electron and IMRT to take advantage of the desirable features of the two modalities. The attempt to combine the conventional electron and photon beams for breast cancer has, however, been hindered by distinctly different penumbra characteristics of the two modalities. Excessive hot/cold spots exist in the match-line region and the match is extremely sensitive to the patient setup error and organ motion. Using intensity-modulated field can significantly improve the situation because it allows one to fine-tune the dose on an individual beamlet level and to deliver a predetermined (not necessarily uniform) radiation field. The strategy is to irradiate the shallow part of a breast tumor in the medial region using an anterior (enface) electron beam (<15 MeV) and then to fill in the dose to the remaining target volume using intensity-modulated photons. In Fig. 2, we show that by properly designing the photon fluence profile in the abutting region it is possible to achieve a perfect match at a certain depth. In addition, the matching becomes significantly less sensitive to a set-up error or organ

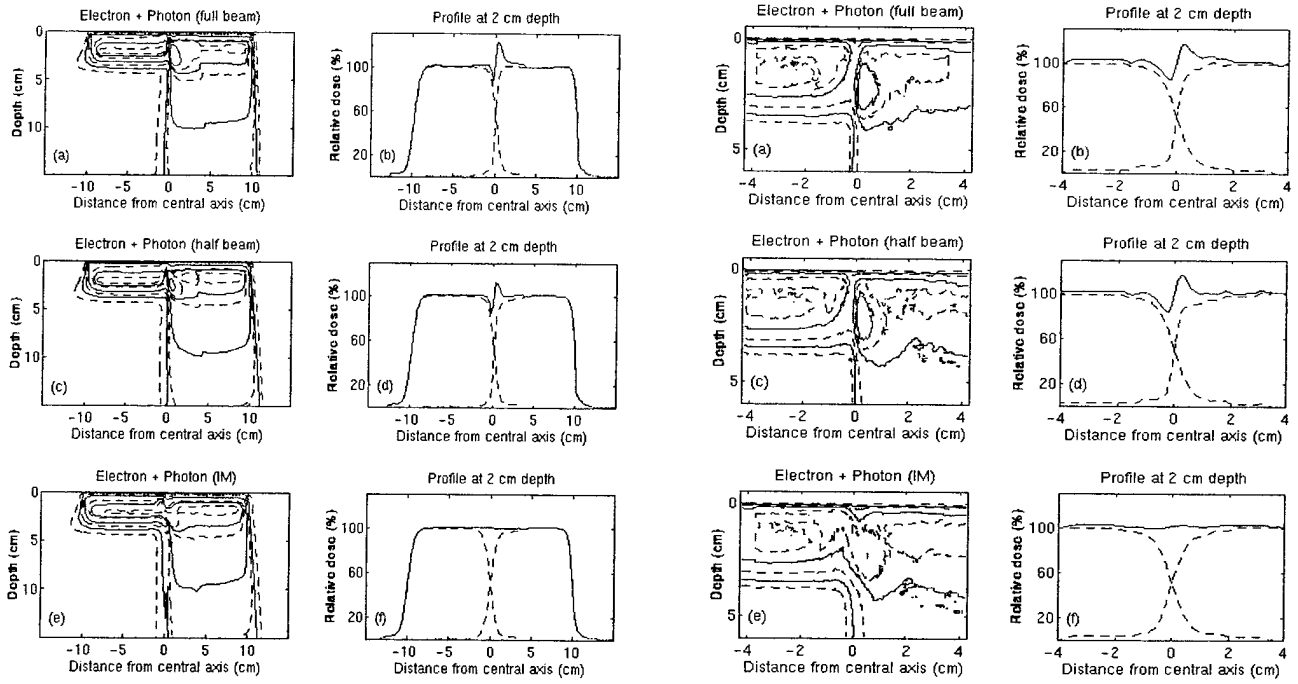

Fig. 2 Matching of electron-photon fields. The left two columns are theoretical calculations and the right two columns are film measurements. A divergent (full-beam), non-divergent (half beam) and intensity modulated photon beams were used in obtaining the results shown in the first, second and the third rows. As indicated by the first two rows, there are always hot/cold spots (over 20%) in the abutting region when we match a conventional photon beam (without intensity modulation) with an electron beam. A perfect match at 2cm depth is achieved using intensity modulated photon beam. The dynamic MLC serves as a photon penumbra generator, effectively broadening the photon penumbra and complementing the electron penumbra.

motion.

In Fig. 3 we show a comparison of a tangential field treatment, IMRT treatment, and a composite plan obtained using an electron and intensity modulated photon beams for a left-sided breast cancer patient. The corresponding dose-volume histograms (DVHs) are plotted in Fig. 4. Two major concerns are the radiation dose to the heart and the lung. Typically, between 4%~10% of the heart volume is inevitably included in the tangential fields (left panel of Fig. 3), resulting in a high radiation dose to this small volume of the heart. For the particular patient in Fig. 3, it was also difficult to exclude the contralateral breast from the tangential field without overdosing the lateral chest wall, resulting in a hot spot in the medial part of the contralateral breast. The IMRT treatment plan (middle panel of Fig. 3) reduced the high dose to the ipsilateral lung, the heart, and the contralateral breast. However, larger volumes of these structures as well as the contralateral lung received low doses of radiation. For example, for the ipsilateral lung, 40% of the volume received doses of more than 1,400 cGy, compared with ~17% of the volume for the tangential field plan. The volumes of the critical structures receiving low doses of radiation were significantly reduced with the combined electron and IMRT technique (right panel of Fig. 3), as well as reduction in the high dose to the ipsilateral lung, the heart, and the contralateral breast when compared with the tangential field plan. For the ipsilateral lung, the volume receiving doses of more than 1,400 cGy was reduced to 15%, and the reduction in the maximum dose was similar to that achieved with IMRT.

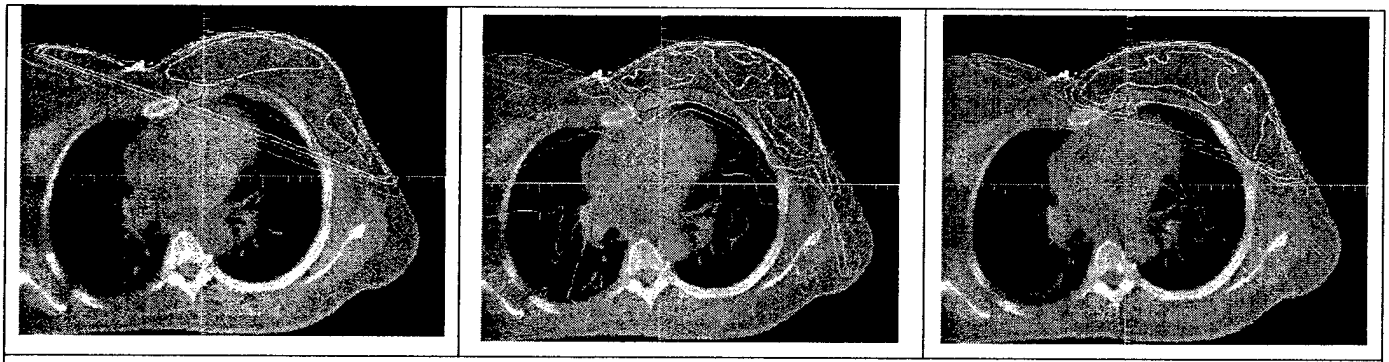

Figure 3 Comparison of the isodose distributions of the treatment plans in the transverse section of the left-sided breast cancer patient using the tangential field technique (a), IMRT (b), and the combined electron and IMRT technique (c). Target volume includes the whole breast and the internal mammary nodes. Isodose levels are shown at 100%, 90%, 70%, 50%, 30%, and 10%, with 100%=5600 cGy.

We have also introduced a general method for fine-tuning of an "optimal" IMRT solution, which has significant potential to facilitate the dose optimization process of hybrid treatment of IMRT and electron. In practice, ranking of treatment plans is variable and subjective, reflecting different criteria among physicians and patient and implying that an "optimal" plan may need to be "tweaked" in a clinical setting. Moreover, this tweaking frequently needs to be done in one or more subvolumes in a patient. For instance, in breast treatment one may wish to shift the high dose region away from the lung or heart to reduce the influence of

breathing motion and avoid potential complication. Currently, the modification can only be achieved by adjusting structure dependent system parameters (e.g., prescription, importance factors) in the dose optimization process, which influence the regional doses in an implicit and complicated fashion. The lack of a mechanism to fine-tune the doses has been known as a major deficiency of inverse planning and makes IMRT planning labor intensive. We have, for the first time, pointed out that the local dosimetric behavior can be effectively controlled by introducing a voxel-dependent penalty scheme and demonstrated the utility of the approach using a few examples [12]. We expect that the method will have widespread application in therapeutic dose optimization.

The Concept Award for Breast Cancer from US Amy Medical Research and Materiel Command also provides a unique educational opportunity for training junior researcher through the participation of research activities. In this aspect, the postdoctoral fellow, David Yong Yang, has been benefited greatly from the support. After obtaining his Ph.D. degree in Medical Physics from Chinese Academy of Medical Sciences in Beijing, China, Dr. Yang jointed my group in December of last year. Since he came here, he has had opportunity to learn the clinical breast treatment planning, simulation, and quality assurance and many aspects of radiation treatment of breast cancer. He has also learnt film dosimetry and other dosimetric measurements. He has developed an elegant and clinically practical method for incorporating both multileaf collimator transmission and head scatter into IMRT leaf sequencing process [13], making it possible to ensure the optimal hybrid treatment plans on the treatment planning computer will be accurately achieved in a clinical environment. He is now working under the PI's supervision on developing a practical quality assurance procedure of the hybrid treatment of IMRT and

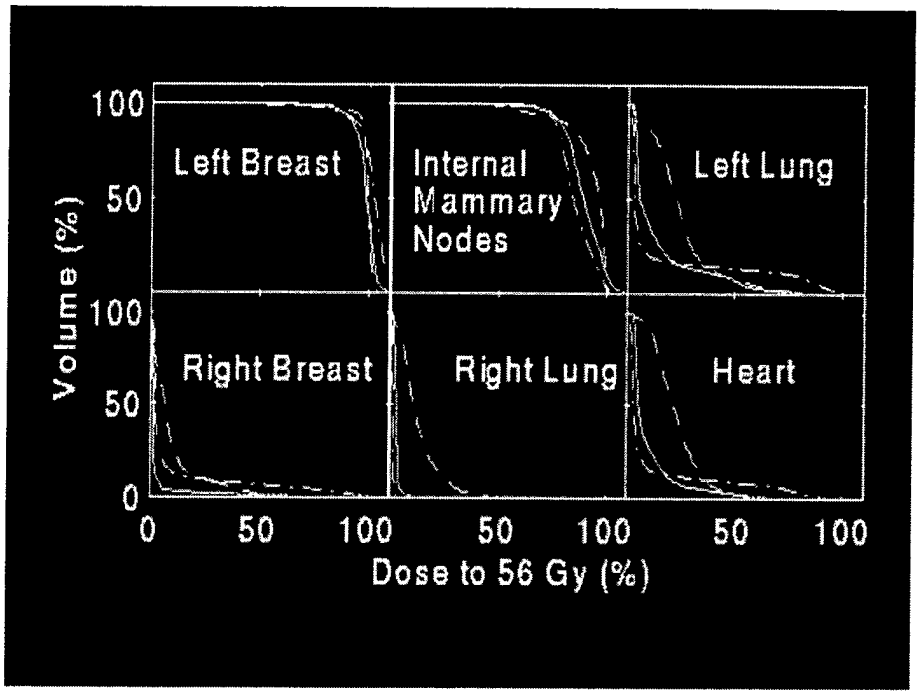

Figure 4 Dose-volume histograms for the targets and normal structures for the treatment plans of the left-sided breast cancer patient as shown in Fig. 3. Dash-dotted lines: tangential field plan. Dashed lines: IMRT plan. Solid lines: combined electron and IMRT plan.

electron for breast cancer. Given his training obtained under the support of this grant and his performance in the past year, I expect that he will become a leading researcher in the fields of medical physics and breast radiotherapy in the years to come.

III. KEY RESEARCH ACCOMPLISHMENTS

- Developed an effective inverse planning algorithm for optimizing the photon beam profiles and electron beam weight, with the capability of fine-tuning the final dose distributions by using voxel-dependent importance factors.
- Demonstrated the dosimetric advantage of hybrid breast treatment using IMRT and conventional electron.
- Developed an effective method for incorporating MLC transmission and head scatter into MLC leaf sequencing process, which makes it possible to accurate deliver the optimal treatment plans.
- Performed dosimetric measurements to experimentally evaluate the quality of hybrid treatment of IMRT and electron in terms of sensitivity against the setup errors, match-line dose uniformity, and compared with the theoretical prediction.

IV. REPORTABLE OUTCOMES

The following is a list of publications resulted from the grant support. Copies of the publication materials are enclosed with this report.

Refereed publication:

1. Cotrutz C and **Xing L**: "Using Voxel Dependent Importance Factors for DVH-Based Interactive Planning", Physics in Medicine and Biology 47, 1659-69, 2002.
2. **Xing L**, Pawlicki T, Yuen L, Crooks S, Dugan J, Li C, Halberg F, Cotrutz C, Lehmann J, Donaldson S, Luxton G, Boyer A, Goffinet D: "A comprehensive method of breast-conserving radiation therapy using forward multiple segment planning and step-and-shoot delivery", *Journal of Applied Clinical Medical Physics*, submitted, 2002.
3. Pugachev A and **Xing L**: "Incorporating Prior Knowledge into IMRT Beam Orientation Optimization", *International Journal of Radiation Oncology, Biology, Physics*, accepted.
4. Cotrutz C, **Xing L**: " IMRT Dose Shaping with a Regional Penalty Scheme", Medical Physics, submitted, 2002.
5. Yang Y and **Xing L**, "Incorporating leaf transmission and head scatter corrections into step-and-shoot leaf sequences for IMRT". International Journal of Radiation Oncology, Biology, Physics, submitted, 2002.

Published Abstracts:

The PI's group has also been active in disseminating our research results. The following are some of the presentations given in various national/international meetings.

L. Xing, J.G. Li, Y. Song, D.Y. Yang, D. Goffinet, A.L. Boyer, "Combining electron with intensity modulated photon beams for breast cancer", the Era of Hope 2002 DOD Breast Cancer Research Program Meeting, Orlando, Florida, September 25-28, 2002.
L Xing, T. Pawlicki, L Yuen, C. Cotrutz, J. Dogan, C. Li, F. Halberg, A. Boyer, G. Luxton, D. Goffinet, "Multiple Segment Radiation Therapy for Breast Cancer Treatment After Breast-Conserving Surgery", poster presentation in 2001 Annual Meeting of American Society of Therapeutic Radiology and Oncology (ASTRO), San Francisco, CA.
Y Yang, L Xing, "An Algorithm to Incorporate Leaf Transmission and Head Scatter Corrections Into Step-And-Shoot Leaf Sequences for IMRT", oral presentation in 2002 American Association of Physicists in Medicine (AAPM) Annual Meeting, Montreal, Canada.
C Cotrutz, L. Xing, "Inverse Treatment Planning with Interactively Variable Voxel-Dependent Importance Factors", oral presentation in 2002 AAPM Annual Meeting, Montreal, Canada.
A Pugachev, L Xing, "Incorporating Prior Knowledge into Beam Orientation Optimization in IMRT", oral presentation in 2002 AAPM Annual Meeting, Montreal, Canada.
L Xing, J Lian, C Cotrutz, Y Yang, G Luxton, A Boyer, "Inverse Treatment Planning with Inclusion of Model Parameter Uncertainty", oral presentation in 2002 AAPM Annual Meeting, Montreal, Canada.
C Cotrutz, L Xing, "IMRT Dose Shaping Using a Regional Penalty Scheme", oral presentation in 2002 ASTRO Annual Meeting, New Orleans, LA.

US Patent:

Cotrutz C. and Xing L., *Fine-tuning a dose distribution after dose optimization*, US Provisional Patent Application filed in March 2002. Stanford Office of Technology Reference #: S01-261/Prov.

Invited talks:

The PI has been invited as abstract review and session chair in several national/international meetings and has given a number of invited talks. The following is a partial list of the relevant activities in last year.

- *IMRT and its Combination with Electron for Breast Cancer*, invited talk in 2002 Northern California Society of Radiation Therapists conference, Greenbrae, CA.
- *Multiple Segment Radiation Therapy for Breast Cancer*, in 2002 Stanford IMRT Course.
- *Recent Progress in IMRT Inverse Treatment Planning*, in 2002 AAPM Annual Meeting, Montreal, Canada.
- *Fast Optimization and the Selection of Beam Angles*, invited speaker, NCI-NSF Sponsored Workshop---Operations Research Applied to Radiation Therapy, 2002, Bethesda, MD.
- *Overview of Inverse Planning Systems for IMRT*, invited talk in 2001 American College of Medical Physics Anal Meeting, June, Hershey, PA.
- *Recent progress in IMRT*, invited talk in the 2001 Annual Meeting AAPM Missouri-Valley Chapter, May, Ozarks, MO.
- *Monitor Unit Calculation for Intensity Modulated Photon Beam*, invited talk in AAPM Symposium entitled "MU Calculation and Verification in IMRT", 2001 AAPM Annual Meeting, Salt Lake City, UT.
- *Computer-Controlled Radiation Delivery,* instructor in AAPM "Therapy Physics Review Course", 2001 AAPM Annual Meeting, Salt Lake City, UT.
- *Breast Radiotherapy Using Intensity Modulated photons and its Combination of Electron,* invited talk in Workshop on IMRT, Rio de Janeiro, Brazil, 2003, to be delivered.

V. CONCLUSIONS

A combined electron and IMRT technique has been developed and evaluated for the treatment of breast cancer. The electron beam was used to treat the bulk of the tumor volume, whereas intensity modulated photon beams were used to improve target dose homogeneity. The weight of the electron beam as well as the beam fluence profiles of the intensity modulated photon beams were optimized using a dose-based objective function. It was found that high doses to the ipsilateral lung and, in the case of the left-breast cancer patient, the heart were markedly reduced with minimal increase in the dose to other normal structures when compared with treatment plans generated using the tangential field technique. In addition, technique of incorporating MLC transmission and head scatter has been developed to ensure that the accuracy of IMRT delivery and an effective method of fine-tuning a planned dose distribution has been established. It is expected these tools will greatly facilitate the planning, delivery, and quality assurance of the hybrid breast treatment.

References

1. Perez, CA, Brady LW. *Principles and Practice of Radiation Oncology*. Philadelphia, Lippincott Williams & Wilkins.
2. Asrari, F, Gage I. Radiation therapy in management of breast cancer. *Current Opinion in Oncology* 1999, **11**, 463-7.
3. Fisher, B, Redmond C, Poisson R, Margolese R, Wolmark N, Wickerham L, Fisher E, Deutsch M, Caplan R, Pilch Y, et al. Eight-year results of a randomized clinical trial comparing total mastectomy and lumpectomy with or without irradiation in the treatment of breast cancer [published erratum appears in N Engl J Med 1994 May 19;330(20):1467] [see comments]. Comment in: N Engl J Med 1989 Sep 7;321(10):689-90. *New England Journal of Medicine* 1989, **320**, 822-8.
4. Arbetter, KR, Prakash UB, Tazelaar HD, Douglas WW. Radiation-induced pneumonitis in the "nonirradiated" lung [see comments]. Comment in: Mayo Clin Proc 1999 Jul;74(7):743-4. *Mayo Clinic Proceedings* 1999, **74**, 27-36.
5. Boice, JD, Jr., Harvey EB, Blettner M, Stovall M, Flannery JT. Cancer in the contralateral breast after radiotherapy for breast cancer [see comments]. Comment in: N Engl J Med 1992 Aug 6;327(6):430; discussion 431-2. Comment in: N Engl J Med 1992 Aug 6;327(6):431; discussion 431-2. *New England Journal of Medicine* 1992, **326**, 781-5.
6. Dobbs, HJ. Radiation therapy for breast cancer at the millennium. *Radiotherapy & Oncology* 2000, **54**, 191-200.
7. Phaisangittisakul, N, Ma L. Range-Modulated Electron Radiotherapy with Longitudinal Magnetic Field Collimation. *2002 Annual Meeting of AAPM*. Montreal, Canada, 2002.
8. Hyodynmaa, S, Gustafsson A, Brahme A. Optimization of conformal electron beam therapy using energy- and fluence-modulated beams. *Medical Physics* 1996, **23**, 659-66.
9. Ma, CM, Pawlicki T, Lee MC, Jiang SB, Li JS, Deng J, Yi B, Mok E, Boyer AL. Energy- and intensity-modulated electron beams for radiotherapy. *Physics in Medicine & Biology* 2000, **45**, 2293-311.
10. Hong, L, Hunt M, Chui C, Spirou S, Forster K, Lee H, Yahalom J, Kutcher GJ, McCormick B. Intensity-modulated tangential beam irradiation of the intact breast. *International Journal of Radiation Oncology, Biology, Physics* 1999, **44**, 1155-64.
11. Williams, SS, Xing L, Boyer AL, Goffinet D. Intensity modulated treatment of breast cancer with inclusion of supraclavicular and internal mammary lymph nodes. *International Journal Radiation Oncology, Biology, Physics* 1998, **42**, 370.
12. Cotrutz, C, Xing L. Using voxel-dependent importance factors for interactive DVH-based dose optimization. *Physics in Medicine & Biology* 2002, **47**, 1659-1669.
13. Yang, Y, Xing L. Incorporating leaf transmission and header scatter corrections into MLC leaf sequences for IMRT. *International Journal of Radiation Oncology, Biology, Physics* 2002, submitted.

List of personnel receiving pay from the research effort: 10% of PI's salary was supported by the grant during the funding period. In addition, 65% of Dr. David Yong Yang (Postdoctoral fellow)'s effort was supported by the grant. There are no other personnel who receive pay from the research effort.

INSTITUTE OF PHYSICS PUBLISHING PHYSICS IN MEDICINE AND BIOLOGY

Phys. Med. Biol. 47 (2002) 1659–1669 PII: S0031-9155(02)32605-8

Using voxel-dependent importance factors for interactive DVH-based dose optimization*

Cristian Cotrutz and Lei Xing

Department of Radiation Oncology, Stanford University School of Medicine, 300 Pasteur Drive, Stanford CA 94305-5304, USA

E-mail: cristian@reyes.stanford.edu and lei@reyes.stanford.edu

Received 11 January 2002
Published 2 May 2002
Online at stacks.iop.org/PMB/47/1659

Abstract

Intensity modulated radiation therapy (IMRT) inverse planning is usually performed by pre-selecting parameters such as beam modality, beam configuration and importance factors and then optimizing the fluence profiles or beamlet weights. In reality, the IMRT dose optimization problem may be ill-conditioned and there may not be a physical solution to account for the chosen parameters and constraints. Planner intervention is often required to conduct a multiple trial-and-error process where several parameters are sequentially varied until an acceptable compromise is achieved. The resulting solution reflects a balance between the conflicting requirements of the target and the sensitive structures. A major problem of the conventional inverse planning formalism is that there exists no effective mechanism for a planner to fine-tune the dose distribution on a local level or to differentially modify the dose–volume histograms (DVHs) of the involved structures. In this paper we introduce a new inverse planning scheme with voxel-dependent importance factors and demonstrate that it provides us with an effective link between the system parameters and the dosimetric behaviour at a local level. The planning proceeds in two steps. After a conventional trial-and-error inverse planning procedure is completed, we identify the dose interval at which the fractional volume on the DVH curve needs to be changed. The voxels that receive dose in the selected range are then located and their voxel-dependent importance factors are adjusted accordingly. The fine-tuning of the DVHs is iterative in nature and, using widely available computer graphic software tools, the process can be made graphically interactive. The new IMRT planning scheme is applied to two test cases and the results indicate that our control over the differential shapes of the DVHs of the involved structures is greatly enhanced. Thus the technique may have significant practical implications in facilitating the IMRT treatment planning process.

* US Patent pending.

0031-9155/02/101659+11$30.00

1. Introduction

IMRT represents one of the most important advancements in radiation therapy, and aims at delivering high radiation doses to the target volumes while maximally sparing the adjacent critical structures. The beam profiles of an IMRT treatment are usually obtained using inverse planning systems that employ various approaches for dose optimization (Webb 1989, Bortfeld *et al* 1990, Rosen *et al* 1995, Morrill *et al* 1995, Xing and Chen 1996, Olivera *et al* 1998, Spirou and Chui 1998, Wu and Mohan 2000, Gopal and Starkschall 2001, Cotrutz *et al* 2001). Most inverse planning algorithms developed to date require dose–volume prescriptions. At the dose optimization level, these algorithms can be categorized into two classes: (i) minimization of a dose–volume histogram (DVH)-based objective function (Togane *et al* 1998, McGary 2001) and (ii) minimization of a quadratic objective function with dose–volume constraints (Cho *et al* 1998, Spirou and Chui 1998, Bortfeld 1999, Wu and Mohan 2000). The latter approach attempts to satisfy the dose–volume constraints either by constantly penalizing those voxels that exceed the permitted fractional volume (Spirou and Chui 1998) or by adopting a volume sensitive variable penalization scheme (Cho *et al* 1998) of the same voxels. The final solution is determined by the choice of DVH prescriptions and the structure specific importance factors that prioritize the relative importance of the clinical goals of the involved structures. In general, the optimized plan complies to a certain degree with the prescriptions and constraints set to the target and critical structures, but hardly meets all the requirements. Therefore, several trial-and-error adjustments of the system parameters are often necessary to achieve a good compromise solution.

A main problem of the currently available inverse planning systems is that there is no explicit way to fine-tune the shapes of the final DVHs. While the shape of the optimized DVH curve of a given structure often differs from the desired one, at which dose bin(s) the fractional volume exceeds the expected value(s) is somewhat random and out of the user's control. There is no explicit way for a user to differentially modify the DVH curves according to the clinical requirement after a trial optimization is completed. When the need arises, the user often refers to the prescribed DVHs and/or the structure-specific importance factors, hoping that the resulting solution will be more consistent with his/her expectation.

In this work, we report an effective method for interactively controlling the shapes of the final DVHs of the target and sensitive structures. We introduce the concept of voxel-dependent importance factors and relate it to the local dosimetric behaviour of the system. After an optimal solution is reached by using the conventional approach, further refinement of the dose distribution is accomplished by modifying the importance factors of user-defined voxels. This process proceeds interactively driven by the user's clinical judgement.

In section 2 we introduce the concept of local importance factors and describe in detail the interactive planning procedure. Also, the technique is exemplified using two test cases. Our physical insight on the approach is given along with the presentation of the results. We conclude in section 4.

2. Method

2.1. Local importance factors

The inverse radiotherapy problem is to determine a vector of beamlet weights, w, with the goal of achieving a prescribed dose distribution or DVHs. In a vectorial form, the dose to the points in the treatment region depends upon the beamlet weights as

$$D_c = d \cdot w \tag{1}$$

where $\boldsymbol{d}$ represents the dose deposition coefficient matrix, expressing the dose deposited to any calculation point when irradiated with a set of unit weight beamlets.

A commonly used method to find the optimal solution of the inverse IMRT problem is to minimize a quadratic objective function (Webb 1989, Bortfeld *et al* 1990, Mageras and Mohan 1993, Xing and Chen 1996) defined by

$$F = \frac{1}{N}\sum_{n} r_\sigma [D_c(n) - D_0(n)]^2 \tag{2}$$

where D_c and D_0 are the calculated and prescribed doses, respectively, N is the total number of voxels within a structure σ, n is the voxel index and r_σ is the importance factor that controls the relative importance of a structure σ. Different sets of importance factors result in different 'optimal' solutions and multiple trial-and-error are often needed to find a set of clinically acceptable values. Several methods have been proposed to use the computer to facilitate the trial-and-error determination of the importance factors (Xing *et al* 1999a, 1999b, Cotrutz *et al* 2001, Wu and Zhu 2001).

While the inverse planning formalism with structure-specific importance factors can provide us with acceptable solutions, there is no mechanism for the user to differentially modify the shapes of the DVHs of the final solution or the regional dose within a structure when a such clinical need arises. To give an example, imagine the behaviour of a system comprising two very closely located anatomical structures, e.g. planning target volume (PTV) and one critical structure volume (CSV). In the most probable instance, neither the PTV, nor CSV prescription doses will be met at the common boundary region. Therefore, it would be less advisable to penalize the voxels in the high-gradient region with the same importance factor as for those located in the bulk of the structures. Here we propose a general inverse planning framework with non-uniform importance factors. In this new formalism, the importance at a voxel n is expressed as a product of two factors, r_σ and r_n (see equation (3)), where r_σ characterizes the importance of the structure σ as an entity relative to other structures, and r_n modulates the importance in obtaining an optimal solution at a regional level of the structure. The voxel-specific importance factor provides an effective means for us to prioritize the inner structural importance. The objective function now reads

$$F = \sum_{\sigma=1}^{n_\sigma}\left[\frac{1}{N_\sigma}\sum_{n=1}^{N_\sigma} r_\sigma r_n [D_c(n) - D_0(n)]^2\right] \tag{3}$$

where N_σ represents the total number of voxels of a structure. In equation (3), $D_0(n)$ is the prescription dose. Note that conventional inverse planning scheme represents a special case of the more general formalism proposed here when all the r_n have unit values.

2.2. *Strategy of the optimization process*

The overall planning process is schematically shown in the flow chart of figure 1. The operations included within rectangle I are part of the conventional inverse planning process, where system parameters, such as structure-specific importance factors and beam angles, are determined through trial-and-error. For each trial, the optimization results are assessed using dose distributions and DVH tools. This process can be realized by any inverse planning system.

After the conventional IMRT plan is obtained, we proceed to the next stage of interactive planning shown in rectangle II of figure 1. The flow of operations follows the same pattern as in the case of conventional planning (rectangle I), but the adjusting parameters are now the

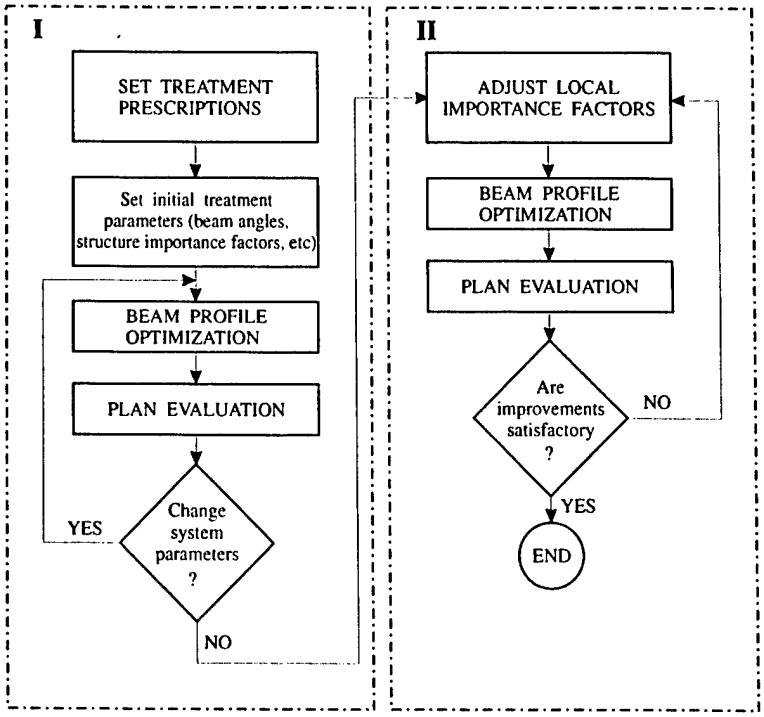

Figure 1. Flow chart depicting the strategy followed by the interactive inverse planning algorithm with voxel-dependent importance factors. The operations incorporated in the left rectangle define the classical inverse planning process. Further refinement of dose distributions and DVHs is achieved by interactively modifying the voxel-dependent importance factors. This latter process is schematically shown in the right rectangle.

local importance factors. Every cycle of this iterative procedure begins with the assessment of the dose distributions and DVHs resulted from the precedent loop.

The planner selects the dose interval(s) for which further refinement of structure DVH(s) is sought. The indices of the voxels belonging to the selected dose interval(s) are automatically detected and 'turned on.' The local importance factors of these voxels are then increased or decreased accordingly. Obviously, increasing the values of the local importance factors will increase the penalization level at the considered voxels and generally lead to better compliance of the resulting dose distribution with the prescription in that region. Conversely, decreasing the importance factors will have an opposite effect and relax the compliance. The amount of change in the importance factors is empirical and we usually proceed by assigning a value 15–50% higher/lower than their previous values after the corresponding voxels are identified. For every change in the importance factors, the dose is re-optimized and the plan is then re-evaluated. The planning process proceeds in an iterative fashion, as shown in figure 1.

The introduction of the local importance factors makes it possible for us to identify the system parameters that are most responsible for the dosimetric behaviour at a local level. Once this link is established, the dose distribution can be fine-tuned more directly. The adjustment of the local importance factors can be performed sequentially or simultaneously

for a few structures. According to our experience, two to three iterations are often sufficient to significantly improve the final solution.

2.3. Beam profile optimization and voxel selection

The algorithm used for beam profile optimization belongs to the gradient-based methods and has been extensively described elsewhere (Cotrutz *et al* 2001). The dose calculation engine is based on a radiological pathlength algorithm (Cotrutz *et al* 1998). The system was modified to take into account the voxel-based importance factors defined in relation (3). The capability for a user to graphically identify one or more regions on a DVH curve of interest was added as a new feature of the planning system. Alternatively, dose distribution layouts can be used to guide the user to geometrically select the regions where the dose(s) need to be modified by changing the local importance factors.

Subsequent to user's selection of the DVH dose interval of interest (or the outlined volumes of interest) the indices of the voxels receiving a dose in that range are identified and the corresponding values of the voxel-specific importance factors are ready to be assigned with a new value. The plan is re-optimized after the importance factors are updated. The above procedure is performed interactively until the best possible solution is obtained.

3. Results and discussion

Two test cases were used to assess the dose optimization approach proposed in this paper. The first was an elliptical phantom case with a C-shaped tumour and an abutting circular critical structure. The second one was a nasopharynx tumour. The considered critical structures included the eyes, optic chiasm and the brain stem.

3.1. The C-shaped tumour case

The configuration of the C-shaped tumour case is shown in figure 2. Nine 6 MV equispaced beams were used in the treatment (0°, 40°, 80°, 120°, 160°, 200°, 240°, 280° and 320°—respecting the IEC convention). The prescribed dose to the PTV was set to 100 arbitrary dose units and 20 units were assigned as tolerance dose of the critical structure volume (CSV).

Using the conventional inverse planning procedure, we found that the values of the structure-specific importance factors were $r_{PTV} = 0.8$ and $r_{CSV} = 0.2$. This set of importance factors provided a reasonable overall trade-off between dose coverage of the tumour and the protection of the critical structure. The black lines in figure 3 show the tumour and critical structure DVHs for the plan optimized with this set of structure-specific importance factors.

Assuming that our clinical concern was the dose to the CSV, we wanted to lower the maximum dose and the fractional volume receiving dose in the interval AB shown in figure 3. To accomplish this, we first identified the responsible voxels by analysing the dose distribution in the critical structure. These voxels represent ~25% of the structure volume and are marked in figure 2 by plain dots. Their distribution is along the periphery of the CSV's contour, with a larger density within the part proximal to the PTV. In a first attempt, the local importance factors for these voxels labelled by the plain dots were increased from 1.00 to 1.35, while the importance factors of the rest of the CSV voxels remained unchanged and fixed at unit value. Upon re-optimization of the system, the new DVHs are shown in grey lines in figure 3. The target coverage remains practically unchanged, but the CSV sparing is greatly improved. In particular, the maximum dose is decreased by almost 8 dose units as compared to the plan performed with only structure-specific importance factors. With the use of the local

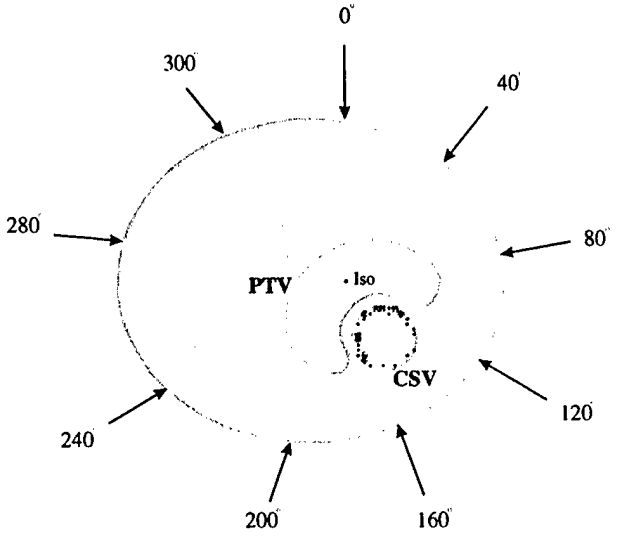

Figure 2. Sketch of the C-shaped tumour test case and the nine-beam set-up used for dose optimization. Dose prescription is set 100 dose units (arbitrary units) to the tumour (PTV) and 20 units to the circular critical structure (CSV).

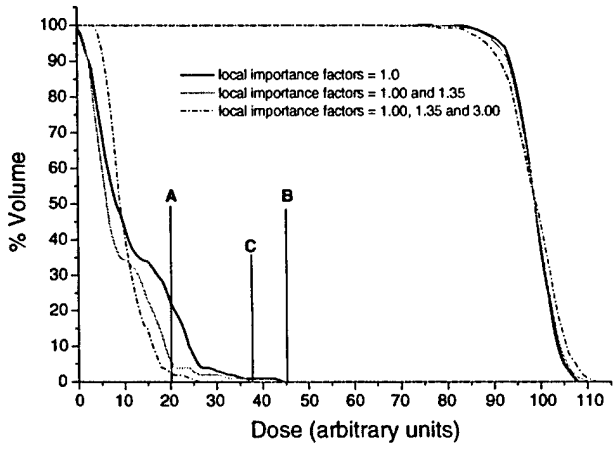

Figure 3. DVHs corresponding to three optimization runs, with different values of the local importance factors. Dose is normalized to the mean target dose.

importance factors, the number of voxels that received a dose exceeding the tolerance level was greatly reduced. These voxels can now be found only at the boundary region with the PTV, as represented by open circles in figure 2.

Further decrease of the fractional volume in the dose range A and C (see figure 3) was sought in our attempt to improve the dose to the CSV. Therefore we assigned a new local importance value of 3.0 to the voxels labelled with open circles in figure 2 and then repeated the above procedure. The importance factors of the remaining voxels were kept at the same

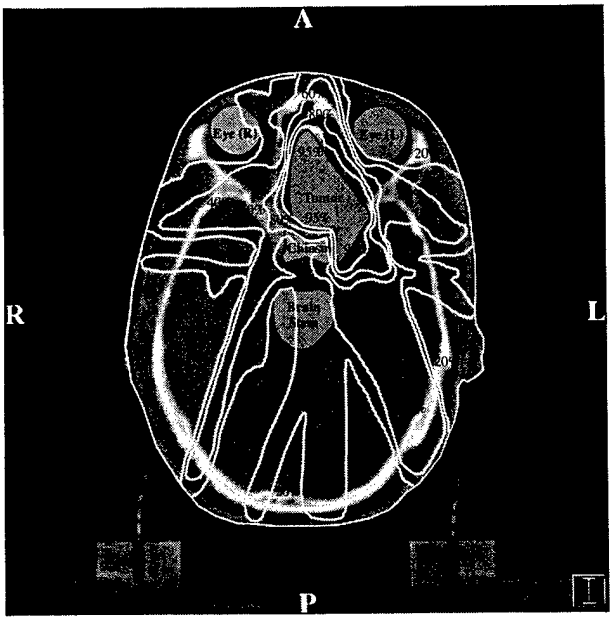

Figure 4. A transverse slice showing the anatomical structures delineated for the nasopharynx tumour and the corresponding optimized dose distribution for local importance factors of unit value. The doses are normalized to the mean target value.

values that were used in the previous optimization (i.e. 1.35 for the voxels labelled by the plain dots and 1.0 for the voxels that are not labelled by circles or dots). The DVHs of the new plan corresponding to this distribution of the importance factors are shown as dotted lines in figure 3. The maximum dose of the CSV drops by 20 dose units compared to the initial optimization result. The increased importance values for the CSV voxels lead to an increased dose inhomogeneity within the target. This is not surprising because of the trade-off nature of the problem. The important point here is that, when local importance factors are used, the trade-off is accentuated at a regional level and our control over the shapes of the final DVHs is greatly enhanced.

3.2. The nasopharynx tumour case

The second test case was a nasopharynx tumour. The prescription dose to the tumour was 60 Gy, and the tolerance doses were 10 Gy for the eyes, 35 Gy for the brain stem and 45 Gy for the optic chiasm, respectively. Nine beams were placed at the following angular positions: 10°, 80°, 120°, 160°, 180°, 200°, 240°, 270° and 355°. The size of the pencil beam defined at the isocenter was 0.5 cm.

A reasonable plan was obtained with the following set of structure-specific importance factors: 0.40 for the tumour, 0.32 for the right eye, 0.10 for the left eye, 0.04 for the brain stem 0.04 for the optic chiasm and 0.1 for the normal tissue, respectively. Figure 4 shows the resulting isodose distribution in a transverse slice of the skull. In this case, we found that the 95% isodose line covers acceptably well the PTV. The DVHs of the optimized plan are plotted with plain lines in figure 5.

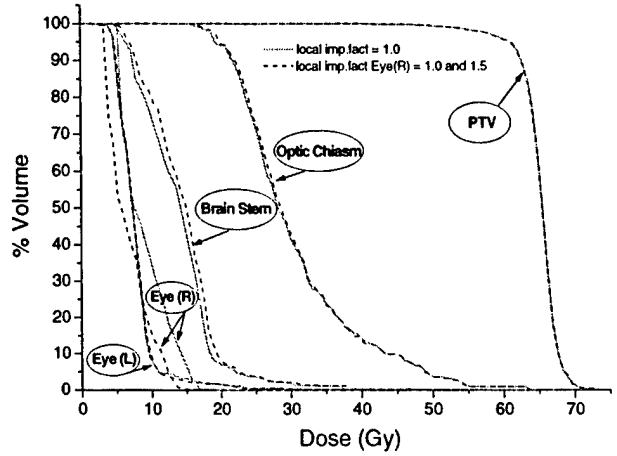

Figure 5. DVHs for plans optimized with unit value local importance factors (the plain lines) versus optimized using higher value of local importance factors for the right eye (the dashed lines).

In a first instance we were concerned with lowering the dose to the right eye. We located the voxels with a dose exceeding the 10 Gy tolerance level and increased their importance from 1.0 to 1.5. The beam profile optimization was performed again and the resulting DVHs are shown with dashed lines in figure 5. The results show no degradation of the target coverage and a significant reduction of the dose to the right eye accompanied by a reduction in the maximum dose by almost 5 Gy. While the DVH curve for the other eye remains the same, an insignificant degradation is observed for the brain stem and optic chiasm.

As an exercise, we further tried to increase the values of the local importance factors to 1.5 for those voxels receiving a dose higher than 10 Gy in both eyes. The dashed curves in figure 6 represent the corresponding DVHs of various structures after dose optimization. As in the previous case, the dose–volume characteristics of both eyes are improved significantly. Interestingly, the dose homogeneity in the PTV is also improved slightly. Only the dose to the optic chiasm unambiguously deteriorates in this case.

In order to understand the planning tool more extensively, we tested whether any improvement could be achieved in the optic chiasm dose after the significant improvement was made in sparing the two eyes. From figure 6 it is seen that 15% of the optic chiasm receives a dose greater than 40 Gy. We wondered whether this volume could be lowered and whether the maximum optic chiasm dose could be reduced, and if yes, at what cost. For this purpose, we found the overdosed voxels in the optic chiasm and assigned them with a new importance value of 1.4. The importance factor distributions in both eyes and other structures were kept the same as in the previous case. The DVHs corresponding to this new arrangement of the importance factors are plotted in figure 7. While the optic chiasm DVH was significantly improved, the dose inhomogeneity within the tumour increased. In addition, the level of improvement in the eyes resulted from the last trial has decreased, even though it did not go back to the original plan shown as the plain curves in figure 7. This result suggests that the order in which the critical structures are considered in the dose-tuning process may play a role. If a critical structure is closely located to the target, the boundary region is usually in the overlap area of several beamlets coming from different beams. In general, the dose in this type of structures is more strongly correlated with that of other structures. It is also instructive

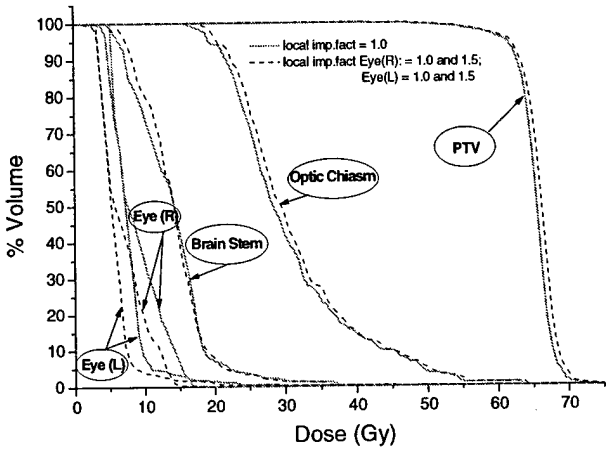

Figure 6. DVHs for plans optimized with unit value local importance factors (the plain lines) versus optimized using higher value of local importance factors for both the eye structures (the dashed lines).

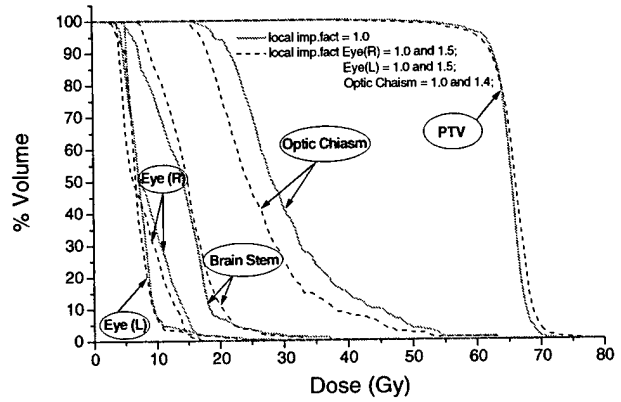

Figure 7. DVHs for plans optimized with unit value local importance factors (the plain lines) versus optimized using higher value of local importance factors for both the eye structures and the optic chiasm (the dashed lines).

to point out that the whole dose–volume curve of the optic chiasm was improved in figure 7 instead of only the dose bins above 40 Gy. This revealed the role of correlation between different voxels within the same structure, which is most pronounced for a structure like optic chiasm because of its small volume.

The above planning procedure is fairly straightforward. After an IMRT plan is obtained using a conventional inverse planning procedure, the system is already in the vicinity of the optimal solution. The plan at this point is usually at a stage of 'mostly satisfactory' except that one or a few sub-volumes in the target or some sensitive structures are overdosed/underdosed. The focus of using local importance factors is directed towards meeting the clinical goals for these disadvantaged regions. Because of the strong correspondence between the regional

dose and the local importance factor, we found that one or two trials are typically sufficient to improve the DVH shape of a structure and to come up with a better compromise solution. Even when the DVHs of the multiple structures need to be modified, we found that the process is not unmanageable, at least not as bad as it appears. One could proceed to change the local importance factors of different structures sequentially or simultaneously. Given the rapid advancement in computer hardware, the computing here should be made easier and easier with years to come.

4. Conclusions

An interactive DVH-based optimization tool for IMRT treatment planning is presented. The most important feature of the new planning environment is the introduction of voxel-dependent importance factors as an effective means for modifying the local doses and for adaptive planning. The system allows us to differentially fine-tune the shapes of the DVH curves of various structures according to clinical requirements and provides an invaluable tool to 'paint' and 'sculpt' IMRT dose. This new mechanism has been implemented in an existing inverse planning system. Application of the new planning technique to two test cases showed that the tool can significantly improve the plans obtained using currently available inverse planning techniques and affords a flexible means to meet diverse clinical needs. Upon clinical implementation we anticipate that the tool will have widespread application and make it possible to maximally utilize the efficacy of the IMRT technique.

Finally we mention that using variable local importance factors is not the only way to accomplish a voxel-dependent penalty scheme. Similar control could also be achieved by using a 'tunable' voxel-dependent objective function. This work is still in progress and will be reported elsewhere.

Acknowledgments

This work was supported in part by a Research Scholar Grant Award from the American Cancer Society and research grants from the Whitaker Foundation, the US Department of Defense and the Information Technology Systems and Services of Stanford University.

References

Bortfeld T 1999 Optimized planning using physical objectives and constraints *Semin. Radiat. Oncol.* **9** 20–34

Bortfeld T, Burkelbach J, Boesecke R and Schlegel W 1990 Methods of image reconstruction from projections applied to conformation radiotherapy *Phys. Med. Biol.* **35** 1423–34

Cho P S, Lee S, Marks R J II, Oh S, Sutlief S G and Phillips M H 1998 Optimization of intensity modulated beams with volume constraints using two methods: cost function minimization and projections onto convex sets *Med. Phys.* **25** 435–43

Cotrutz C, Kappas C, Theodorakos Y, Makris C and Mohan R 1998 Development in a Windows environment of a radiation treatment planning system for personal computers *Comput. Methods Progr. Biomed.* **56** 261–72

Cotrutz C, Lahanas M, Kappas C and Baltas D 2001 A multiobjective gradient-based dose optimization algorithm for external beam conformal radiotherapy *Phys. Med. Biol.* **46** 2161–75

Gopal R and Starkschall G 2001 Plan space: representation of treatment plans in multidimensional space *Med. Phys.* **28** 1227

Mageras G S and Mohan R 1993 Application of fast simulated annealing to optimization of conformal radiation treatments *Med. Phys.* **20** 639–47

McGary J E 2001 Corvus optimization algorithm and IMRT planning process *3-D Conformal and IMRT: Physics & Clinical Applications* ed J A Purdy, J R Palta, E B Butler and C A Perez (Madison, WI: Advanced Medical Publishing) pp 263–75

Morrill S M, Lam K S, Lane R G, Langer M and Rosen I I 1995 Very fast simulated reannealing in radiation therapy treatment plan optimization *Int. J. Radiat. Oncol. Biol. Phys.* **31** 179–88

Olivera G H, Shepard D M, Reckwerdt P J, Ruchala K, Zachman J, Fitchard E E and Mackie T R 1998 Maximum likelihood as a common computational framework in tomotherapy *Phys. Med. Biol.* **43** 3277–94

Rosen I I, Lam K S, Lane R G, Langer M and Morrill S M 1995 Comparison of simulated annealing algorithms for conformal therapy treatment planning *Int. J. Radiat. Oncol. Biol. Phys.* **33** 1091–9

Spirou S V and Chui C S 1998 A gradient inverse planning algorithm with dose–volume constraints *Med. Phys.* **25** 321–33

Togane D, Hamilton R J, Boyer A L and Xing L 1998 Dose volume histogram based optimization for intensity modulated radiation therapy *Med. Phys.* **25** A118

Webb S 1989 Optimization of conformal radiotherapy dose distributions by simulated annealing *Phys. Med. Biol.* **34** 1349–70 (Erratum: 1990 *Phys. Med. Biol.* **35** 297)

Wu Q and Mohan R 2000 Algorithms and functionality of an intensity modulated radiotherapy optimization system *Med. Phys.* **27** 701–11

Wu X and Zhu Y 2001 An optimization method for importance factors and beam weights based genetic algorithms for radiotherapy treatment planning *Phys. Med. Biol.* **46** 1085–99

Xing L and Chen G T Y 1996 Iterative algorithms for inverse treatment planning *Phys. Med. Biol.* **41** 2107–23

Xing L, Li J G, Donaldson S, Le Q T and Boyer A L 1999a Optimization of importance factors in inverse planning *Phys. Med. Biol.* **44** 2525–36

Xing L, Li J G, Pugachev A, Le Q T and Boyer A L 1999b Estimation theory and model parameter selection for therapeutic treatment plan optimization *Med. Phys.* **26** 2348–58

A Comprehensive Method of Breast-Conserving Radiation Therapy using Forward Multiple-Segment Planning and Step-and-Shoot Delivery

L. Xing[1], Ph.D., T. Pawlicki[1], Ph.D., L. Yuen[1], C.M.D., S. Crooks[1], Ph.D., J. Dugan[2], B.S., C. Li[2], Ph.D., F. Halberg[2], M.D., C. Cotrutz[1], Ph.D., J. Lehmann[1], Ph.D., Vivek Mehta, M.D., Sarah S. Donaldson, M.D., G. Luxton[1], Ph.D., A. L. Boyer[1], Ph.D., D. R. Goffinet[1], M.D.

[1]Department of Radiation Oncology, Stanford University School of Medicine, Stanford, California 94305-5304

[2]Department of Radiation Oncology, Marin Cancer Institute, Greenbrae, CA 94904

Address correspondence to:

Lei Xing, Ph.D.
Department of Radiation Oncology
Stanford University School of Medicine
300 Pasteur Drive
Stanford, CA 94305-5304

Phone: (650) 498-7896
FAX: (650) 498-4015
E-mail: lei@reyes.stanford.edu

Submitted to *Journal of Clinical Medical Physics.*

Purpose: To establish the multiple segment radiation therapy (MSRT) as a general technique for the treatment of breast cancer, to demonstrate its superiority over the standard opposed tangential-field (OTF) technique, and to illustrate why forward planning is more efficient than beamlet-based inverse planning approach for breast irradiation.

Methods and Materials: The patient setup and target definition were the same as that used in the standard OTF treatment. The MSRT treatment plan was obtained using a conventional 3D planning system with manual trial-and-error forward planning method. The approach utilized additional multileaf collimator (MLC) segments stacking on top of the original OTF to improve the dose distribution. The aperture and weight of the added segment were chosen in such a way that the dose was most uniform in the breast target. After the plan was completed, the static MLC fields of each gantry angle were concatenated together for step-and-shoot delivery. An algebraic method was used to minimize the MLC transmission in the delivery process. As a standard quality assurance (QA) procedure, the fluence map and MU of each field were independently checked before a patient treatment. Ten patients with early-stage breast tumors were planned with the MSRT and the treatment planning results were compared with those using OTF.

Results: The MSRT plans significantly improved target dose uniformity in comparison with the standard OTF plans. The overall planning and treatment delivery overhead of the MSRT was found to be minimum. Our results for ten breast cases revealed that the maximum target dose could easily be reduced from 109%~117% to 106% to 112%. The volume receiving high dose irradiation in the breast target was also markedly reduced. It was also possible to use MSRT to reduce the dose to the ipsilateral lung/heart.

Conclusions: The current IMRT planning, delivery, and QA deviate significantly from the conventional approach and requires additional steps in the treatment process. MSRT bridges the gap, both conceptually and operationally, between the conventional and IMRT treatments. The underlying reason for this method to be a viable choice is that the initial OTF plan have already brought the system to the vicinity of optimal solution. As a result, it is often sufficient to add 1-3 segments to substantially improve the dose distribution. For breast cancer, MSRT is a natural extension of standard treatment and improves the dosimetry without paying excessive overhead associated with the current IMRT. It does not rely on an inverse planning system, nor require

explicit delineation of the breast target. Furthermore, each segment is a standard field and conventional dose calculation and checking methods can be used for QA of MSRT.

Key Words: breast cancer, treatment planning, IMRT, step-and-shoot, MLC.

I. INTRODUCTION

Radiation therapy is accepted as an effective treatment modality in the management of both invasive and non-invasive breast cancer [1-4]. Conventional breast radiotherapy utilizes two opposed tangential photon beams with either uniform or wedged shaped fluence profiles. A certain volume of the ipsilateral lung and, in the case of the left breast, a small volume of the heart is inevitably included in the tangential fields, resulting in high radiation doses to this part of the lung and heart. For large size breast, the technique is frequently incapable of producing homogeneous dose distribution in the target volume. Consequently, breast irradiation has been associated with a number of potential complications, including radiation induced pneumonitis, cardiac toxicity, rib fracture, arm edema, severe breast or chest wall fibrosis, and soft tissue or bone necrosis, and radiation induced secondary cancer [4]. Adjuvant treatment with chemotherapy may further aggravate these effects.

Many approaches have been proposed to improve the current opposed tangential-field (OTF) treatment which aims at achieving more homogeneous dose distributions in the breast target volume and limit radiation dose to normal structures to reduce cardiac and pulmonary toxicity. Karlsson and Zackrisson [5,6] and Jansson et al. [7] proposed the use of matched electron and photon beams to reduce dose to the underlying structures. The medial part of the breast is treated with an electron beam, which is matched to two opposed photon beams used to treat the most lateral part of the breast. However, high dose inhomogeneity was seen in the matched region between the electron and photon beams. As was demonstrated in recent theoretical and experimental studies by Li et al. [8,9], the matching was improved by using intensity-modulated photon beams because of effective penumbra broadening. A drawback of the approach is that the beam setup and treatment procedure becomes less straightforward. Smitt et al. [10] examined the potential of fan-beam IMRT for breast cancer. While the volumes of the ipsilateral lung and the heart that received high doses were smaller as compared to the conventional plans, it was found that significantly larger volume of the two structures as well as the contralateral lung and the contralateral breast received low doses. Williams et al. [11] studied the feasibility of using multiple (3-7) intensity-modulated beams for breast cancer. The technique can treat the breast target as well as the nodal sites with a single set of intensity modulated radiation therapy (IMRT) fields, simplifying thus the treatment when the regional lymph nodes (supraclavicular, axillary

and internal mammary nodes) are involved and eliminating the potential overdosing/underdosing caused by matching the supraclavicular/axillary field with the tangential fields. But the adjacent sensitive structures are exposed to low, or moderate or even high doses of radiation because of the exiting and scattered photons. This is similar to that seen in breast cancer treatment using fan-beam IMRT [10] and cone-beam IMRT with multiple beams [8,9]. The increase in the volumes of normal structures receiving a low dose of radiation is detrimental to the clinical application of these techniques. Breast irradiation using modulated electron radiotherapy (MERT), which attempts to achieve conformal dose distributions by intensity- and/or energy-modulation of an electron beam, has also been proposed [12]. While it is straightforward to simulate MERT on a computer, there are a number of serious engineering and physics problems that must be overcome before its practical implementation.

Tangential field treatment using intensity-modulated fields offers a viable choice for breast cancer treatment [13]. This technique has been recently evaluated on 10 breast patients and notable improvement in the doses to critical structures was achieved. Compared with standard OTF plans, there is a significant reduction in the dose to the coronary artery region (for patients treated to the left breast), the mean dose to the contra-lateral breast, and the ipsilateral lung and soft tissue volumes receiving more than prescribed dose. The dose homogeneity within the target volume was also improved (~8%), especially in the superior and inferior regions of the breast. Similar results were also reported by McCormick [14], Chang et al.[15], Donovan et al [16], Kestin et al. [17], Lo et al [18], and van Asselen et al. [19].

While the dosimetric advantage of IMRT with opposed tangential beam configuration for breast cancer is clear, an important question is how to efficiently implement the technique in a busy clinical environment. The current IMRT planning and treatment process deviates significantly from the conventional approach and requires additional steps in planning, delivery and quality assurance [15,20-23]. When applied to breast irradiation, the current beamlet-based IMRT has two additional limitations:

(1) Inverse planning is a computer based decision-making method that derives the optimal beamlet weights by starting from a set of desired doses prescribed to the target and sensitive structures. In order to use an inverse planning system to generate a treatment plan, one must explicitly delineate the tumor volume, where high doses of radiation are required, and

define the sensitive structures, where dose avoidances are desired. This adds a large amount of extra work to physicians. The conventional approach of target definition, where the breast treatment volume is inherent by borders that are placed on by the clinician, is much more convenient and efficient.

(2) Inverse planning system obtains the solution by optimizing an objective function. The hardware limitations are usually not considered in the plan optimization process. A major limitation is the maximum spread of the MLC leaves, which restricts the maximum achievable field width without cartridge movement. Currently, the maximum field spread is 14.5cm in Varian accelerators. Other vendors have similar constraints. For large-sized breast patient with a field width (in anterior-posterior direction) close to this limit, we found that, a tangential treatment field was often split into two intensity-modulated sub-fields for delivery when an inverse planning system was used for planning. This is primarily because of the irregular fluence maps resulted from inverse planning dose optimization and the lack of human intelligence of the leaf sequencing algorithm embedded in the treatment planning system. An implicit feature of MSRT is that the MLC and jaw setting constraints have been taken into account during the manual treatment planning process and there is no disintegration of the dose optimization and the MLC leaf sequencing in the planning process. For a given jaw setting, the planning system would not allow for any MLC configuration that violates the machine constraints to happen at any stage of the planning process. It thus ensured that all the MLC segments were deliverable with a single step-and-shoot delivery upon completion of the MSRT plan.

In this paper we establish a variant of IMRT, multiple segment radiation therapy (MSRT) [27-29], for breast cancer treatment and illustrate its utility by using several clinical cases. While a few research groups have reported the use of MSRT for breast treatment [20,22,24-26], the focus of this work is on developing a clinically practical procedure and providing intuitive explanation on why forward planning with multiple segment delivery is more advantageous than the conventional IMRT. We address several untouched clinical issues related to the technique, including the use different types of wedges (physical or dynamic), field width problem, incorporation of MLC transmission into the step-and-shoot delivery, and QA. We have applied the technique to ten clinical cases and our results indicated that the MSRT markedly improved breast irradiation and provided superior dose distributions needed to reduce radiation side effects

and complications. The technique is especially valuable for radiation treatment of large-breasted women, where it is difficult to achieve homogeneous target dose distribution.

II. METHODS AND MATERIALS

II.1 CT data acquisition and target definition

Five right-sided and five left-sided breast cancer patients with invasive carcinomas of the breast, who had previously undergone lumpectomy, were selected for the study. The patients underwent computed tomography (CT) in the conventional treatment position supported by an Alpha Cradle immobilization device (Smithers Medical Products, Tallmadge, Ohio). Radiopaque markers were placed on the patients' chest to indicate the medial and lateral borders of the palpable breast tissue and the location of the lumpectomy scar. All ten breast patients underwent MSRT planning for the whole breast.

The radiation-sensitive structures included the left and right lungs, the heart, and the contralateral breast. For this study, the contours of the skin, target volume and the sensitive structures were outlined using the segmentation tools provided by the virtual simulation workstation (AcQSim™, Philips Medical System, Cleveland, OH). It is, however, not required to outline the structures in general MSRT treatment, similar to that in the routine OTF breast irradiation. The tangential fields were determined by the routine virtual simulation procedure performed on an AcQSim workstation. The fields may be adjusted at the stage of treatment planning according to the actual treatment objective for each patient with considerations concerning tumor bed coverage, in-field lung and cardiac volume, if left breast irradiation. Figure 1a shows an example of the OTF setup for the treatment of a left breast cancer patient. A flash region of 2 cm was used in the anterior field boarder to account for patients' respiration motion and setup uncertainty.

II.2 Treatment planning

Treatment planning was done with a 3D treatment planning system (FOCUS™, Computerized Medical System, St. Louis, MO). A uniform dose of 4,500 cGy or 5,040 cGy was

prescribed to the target volume in 180-cGy fractions. For comparison, three plans were generated for each patient. One was the standard opposed OTF plan and the other two were the MSRT plans with different constraints. Standard plans involved a medial and lateral tangential field with 6 or 15 MV photon energy. A wedge filter was used in the lateral direction. When a physical wedge was used, we avoided placing it in the medial field to reduce the scatter dose to the lung/heart and the contra-lateral breast. In this case, both fields were modulated with multiple segments (MSRT-B). The segmented fields in the lateral direction were delivered concurrently with the physical wedge in place. For treatment involved dynamic wedge(s), a slightly different approach was used and this will be described in Section II.3. All plans were obtained through manual trial-and-error process.

The MSRT planning started with a standard OTF plan. In most cases for treating breast cancer with single one plane dimensional wedging, there would be high does superiorly and inferiorly. After the initial wedged plan was obtained, we proceeded to introduce an additional MLC field segment to one or both beam directions to boost the "cold" region(s) under the guidance of dose distributions in the plane perpendicular to the incident beam direction. For MSRT-B, multiple segment modulation was allowed for both beams. All segments in the lateral beam were planned and delivered with the physical wedge in place. Figures 1d-1i show the three segments of the lateral and the medial fields for a MSRT-B treatment. The weights and MLC apertures of the segments were adjusted manually to achieve a uniform dose distribution. Our experience indicated that, for intermediately complex cases, it was often sufficient to introduce one or two additional segments to the original opposed tangential fields. For complex cases, two or three additional segments were frequently used. A segment with ipsilateral lung or heart blocked by MLC (the third segment in either medial or lateral MRST field) was also helpful in reducing the dose to these structures.

II.3 MSRT plan with dynamic wedge

In the MSRT-B treatment described above, both lateral and medial fields were modulated by multiple segments. Upon the completion of the MSRT-B planning, the sequential MLC shapes from the same gantry angle were stacked together for step-and-shoot delivery (see Sec. II.4). For the lateral field, the multiple segments were delivered with a physical wedge in place. If dynamic

wedge is to be employed for treatment, the above planning and delivery procedure needs be modified.

The complication with dynamic wedge based MSRT arises from the interplay between the MLC leaf movement and the dynamic jaw motion when the two means of beam modulations are employed simultaneously. In reality, there are two ways to proceed. The first one is to plan the treatment using the MSRT-B scheme described in Sec. II.2 and then deliver the segmented MLC fields and the dynamic wedge field separately. If this scheme is to be used, each segment is an MLC-shaped uniform field which must not be modified by the wedge filter. This is different from the delivery based on a physical wedge, where the fluence of each segment was modified by a physical wedge (unless one chooses to deliver the wedged field and the multiple segments separately). The major disadvantage of this approach was that it doubled the number of delivery fields and prolonged the treatment. To facilitate the treatment, we restricted one of the incident beam to be modulated with only dynamic wedge and the other beam with only MLC-shaped segmented fields (MSRT-S). This approach enabled us to take advantage of the MSRT treatment yet avoiding the separated delivery of the dynamic wedge field and the multiple segmented fields. However, one should note that a wedge field is 1D compensation in nature and, by restricting one of the fields to be modulated only by the dynamic wedge, we did not taking full advantage of the 2D compensation of MLC-based beam modulation. The overall treatment planning procedure for MSRT-S was similar to that described in the Section II.2. In figure 2 we show an example of such a treatment with three segments in the medial direction and a 30° enhanced dynamic wedge in the lateral direction.

II.4 Step-and-shoot delivery

The MLC movement trajectories (or leaf sequences) were known upon the completion of MSRT plan and there was no need for a leaf sequencing algorithm to convert an optimal fluence map into MLC sequences. The static MLC file of each segment was exported as an ASCII file from the FOCUS treatment planning system. For each gantry angle, the segmented fields were stacked together to form a step-and-shoot delivery using a simple software tool, developed in-house, which reads in each individual MLC segment and exports the step-and-shoot delivery file according to the MLC manufacturer's specifications of the file structure. In addition, a step-and-shoot delivery file for portal verification was also generated (see Sec. II.5). The step-and-shoot

files must have correct CRC (computer redundancy check) code attached at the end of the file in order to be executable by the MLC workstation. The subroutine generating CRC code was implemented into the in-house software.

A step-and-shoot delivery is perhaps the simplest scheme from the delivery and QA points of view. In this modality, MLC leaf movements and dose deliveries are done at different instances [30-33]. A leaf sequence file consists of alternatives of dose-only and motion-only instances. Figure 3 shows an example, which corresponds to the delivery of the MSRT-B treatment outlined in Fig. 1. In figure 3 f_k and af_k are the fractional MU of the k^{th} instance and the accumulated fractional MU, respectively. If the treatment planning system has already considered the MLC transmission in treatment plan, we have

$$f_k = MU_k / MU, \qquad (1)$$

where MU_k ($k=1, 2, 3, \ldots$) are the monitor units of the k-th segment from the treatment planning system and $MU = \sum_k MU_k$ is the total MU of the field.

Equation (1) was applied directly to the treatment plan obtained using FOCUS 3D planning system since the MLC transmission has been already taken into account in the dose calculation of each segment. Otherwise, it is desirable to take the MLC transmission into account during the delivery process. The influence of MLC transmission can be compensated by adjusting the values of $\{f_k\}$ in the step-and-shoot delivery file. A general method of incorporating the MLC transmission into the step-and-shoot delivery has been established [34,35]. Assuming that the average MLC transmission coefficient is α, the transmission fluence of a segment with fractional monitor unit of f_k is given by $MU(1-f_k)\alpha$. To the first order approximation, the $\tilde{f}_k$ used in the MLC leaf file should be obtained by minimizing $F = \sum_k (\tilde{f}_k - f_k)^2$, where f_k is given by Eq. (1). It has been shown in Ref. [35] that this offers an effective way to compensate the MLC transmission for the step-and-shoot delivery.

For Varian's accelerators, the upper and lower jaws are fixed during the whole step-and-shoot delivery process. At a given segment, some pairs of leaves may need to be closed. In order to avoid unnecessary exposure from the ends of a pair of closed leaves, it is desirable to move the leaf ends to a position under the lower jaw protection, as shown in the third segment in Fig.

2c. Otherwise, a large amount of leakage (~30%)[36-38] will be resulted in the region of closed leaf ends.

II.5 Quality assurance

Quality assurance is of practical importance. MSRT is modality in between a conventional conformal radiation therapy and IMRT. The patient specific pre-treatment QA of MSRT consisted of two integral parts: MU and fluence map checks. We used an in-house MU calculation program to independently check the MU settings [39]. The MU setting of each segment could also be easily checked using a manual calculation procedure. But this does not check the functionality of the software module that concatenates the individual MLC segments together for step-and-shoot delivery. After a MLC leaf sequence file was obtained, we used the file as input and re-computed the fluence map using a software described in an earlier publication [22]. This independent calculation ensured that the step-and-shoot MLC files were executable and generated the intended fluence map.

III. RESULTS

For intermediate or large sized breast patients, a standard OTF plan is frequently incapable of generating homogeneous dose distribution. MSRT affords an effective way to improve the dose distribution. Ten patients with various breast sizes have been studied using MSRT. In Table 1 we summarize the treatment plans obtained using the standard OTF technique, MSRT-B, and MSRT-S. Minimum, maximum, and mean doses in the breast target volume and critical structures are given for each treatment plan. For these cases, the prescribed dose was specified to a point ~3 cm anterior to the isocenter and it was desired that the 100% isodose curve to cover the breast target volume. For comparison, we have scaled the prescription dose of all treatment plans to 5,040 cGy. The hot spots of the standard OTF plans in the breast volume ranged from 109% to 118% when normalized to the prescription dose. These plans represented typical clinical cases that fell into the category of intermediately complicated or complicated cases.

Figure 1 shows the standard setup of the opposed fields (top row) and the segmented fields in the medial (middle row) and lateral (bottom row) direction of an MSRT-B treatment for the

first patient listed in Table I. Figure 2 shows the same setup obtained with an MSRT-S treatment technique, in which the lateral field was generated using a 30° dynamic wedge. The isodose distributions in the central transverse section and in a plane perpendicular to the incident beams for the standard OTF, MSRT-B, and MSRT-S treatments are plotted in figure 4, and the corresponding cumulative dose-volume histograms (DVHs) are displayed in figure 5. As can be seen from figures 4 and 5, the dose inhomogeneity in the target volume was significantly reduced with both MSRT-B (figure 4b) and MSRT-S (figure 4c) techniques, as well as reduction in the high dose to the ipsilateral lung and heart when compared with the OTF plan. The target maximum dose was reduced from 118% to 112% for the MSRT-B plan, and to 112% for the MSRT-S plan. Furthermore, the target volume receiving high dose irradiation was significantly reduced. In order to include the medial breast tissue into the radiation field, ~10% of the heart volume and the left lung were included in the tangential fields. As thus, a significant fraction of the heart and lung receiving high radiation dose. The high doses to the heart was reduced by almost 6% using MSRT-B technique as a result of adding one additional segment in each incident beam (figures 1f and 1i), together with ~5% improvement in the maximum target dose in the target volume. The heart volume and ipsilateral lung volumes receiving high dose irradiation were also markedly reduced for MSRT-B treatment. As can be seen from figures 4 and 5, the MSRT-S also showed moderate improvement in the lung/heart doses in comparison with the standard OTF plan.

In Table II we list the MU setting of each segment of the MSRT-B and MSRT-S plans for the patient discussed above. In addition, the MU values from the independent calculation are also presented. We have also recomputed the fluence map based on the MLC leaf sequences and compared it with the intended fluence map for each beam. The independent fluence maps were found to be the same as the intended maps from the planning system.

IV. DISCUSSION

There are two aspects in conformal radiation treatment planning: conformance of a certain dose to the target volume and the dose uniformity inside the target. For simple beam configurations (eg., OTF, AP/PA), the dose conformation to the target volume is usually realized through beam shaping based on the initial MLC segments. In this case, a field-in-field technique obtained by

adding a few segments to the original incident beams is often a viable choice to significantly improve the target dose uniformity. Breast irradiation using OTF belongs to this category of treatments. The dose conformance here is realized by the proper choice of the initial tangential (wedged) fields. The main purpose of introducing additional segments is to improve the dose homogeneity inside the target volume and/or to spare the sensitive structure(s) located along the path of the beams. Previous studies and our results clearly showed the dosimetric advantage of the MSRT for breast treatment.

MSRT is a convenient scheme of IMRT. For breast irradiation, MSRT is superior over IMRT for a few reasons. First, it is possible to obtain a MSRT treatment plan through a manual procedure using a conventional 3D treatment planning system. In practice, when the isodose curve shaping can be accomplished by MLC shaping of the initial segments, a manual forward planning is a competitive approach to inverse planning. In inverse planning, an objective function is constructed based on general physical/dosimetric or biological considerations and is defined as a global quantity [41]. In constructing an objective function, the voxel-dependent local information is "compressed" into a global quantity. Hence, one loses, to a certain extent, control over them. When a desired dose distribution is not attainable, a compromised solution is found using the algorithm's ranking. In reality, the compromised distribution may not necessarily be what the planner wants and several trial-and-error adjustment of prescription and relative importance factors of different anatomical structures may be needed to obtain a clinically sensible plan. For a simple beam configuration, the inverse planning approach may not necessarily be more efficient than a manual MSRT planning with the aperture weights and shapes adjusted in a trial-and-error fashion. After all, the final dose distribution has to be evaluated by the planner in either inverse or forward method. The manual planning is more direct in fine-tuning the doses in the target when isodose shaping is already achieved with the initial segments.

For a simple beam configuration, *a priori* knowledge can be incorporated into a manual forward planning process more efficiently as compared with computerized inverse planning. The feedback mechanism (or the trial-and-error) is more natural and straightforward. Based on the empirical experience, a planner can quickly find a suitable wedge filter to lead him/her to the vicinity of an optimal solution. The planner can then fine-tune the dose distribution with additional segmented field(s). The whole planning process was found not much more complex

than the standard OTF planning process. Note that a wedged field in MSRT planning represents a "hidden" intensity modulated field. It would require at least ten segmented fields to produce a wedged field. Plus the added segments, the "effective" modulation in MSRT should be comparable to that of beamlet-based IMRT. The use of a wedge filter in planning provides a way for us to take a "shortcut" to find the optimal solution. Of course, the forward planning is efficient only when the number of system variables is not large and when the optimal solution is not "far" from the conventional OTF solution. The types of clinical cases that can potentially benefit from the proposed method include, but not limited to, tangential breast irradiation, AP/PA or oblique-field treatment of lung and Hodgkins disease.

We emphasize that the MSRT planning does not require explicit delineation of the target volume and sensitive structures. This is another major advantage of MSRT over the current IMRT inverse planning approach, in which one must outline the breast target slice-by-slice in order for the automated inverse planning algorithm to perform dose optimization. Clinically, there exists a class of radiation treatment where the target volume is often defined on radiographic films or empirically without explicit delineation for the target. MSRT provides a natural solution to improve the dose distribution of this type of treatment.

IMRT represents a major deviation from conventional radiation therapy. Currently, IMRT with inverse planning is still in its early stage of clinical implementation and much educational training in planning, QA and the overall process are needed to bring the new modality into routine clinical practice. MSRT, on the other hand, combines the useful features of conventional radiation therapy and intensity-modulation and bridges the "gap" between what seemingly to be two different processes. It affords a valuable educational mechanism to familiarize the staff with IMRT and makes it possible to evolve gradually instead of going through a paradigm change in planning, delivery, and QA. MSRT provides thus a timely solution to improve not only breast irradiation but also the clinical implementation of IMRT. At the implementation level, each segment in MSRT is a conventional field and the dose calculation can be done using standard methods developed over the years in 3D conformal radiation therapy. In addition, there is no need for a leaf sequencing algorithm since the MLC sequences are known upon the completion of the MSRT plan.

V. CONCLUSION

Despite the well-appreciated fact that intensity-modulation could lead to significantly improved dose distributions in breast irradiation, its clinical implementation has been hindered by the deficiencies in the current inverse planning system and by the lack of a comprehensive treatment procedure. This is evidenced by the fact that very few institutions are using IMRT routinely for breast cancer treatment. A clinical challenge in IMRT breast treatment is how to modulate breast irradiation without increasing the treatment complexity. In this work we have described MSRT treatment of breast cancer in details and demonstrated its utility using several examples. Two different delivery schemes (MSRT-B and MSRT-S) have been discussed to meet the requirements of different clinical environments. We have also attempted to illustrate the pros and cons for the forward and inverse planning techniques. We pointed out that when dose conformance can be realized using MLC beam shaping devices, the addition of a few extra segments could often improve the dose distribution significantly. In this case, the manual forward planning technique is a competitive approach in comparison with computerized inverse planning. MSRT is particularly efficient in incorporating prior and posterior knowledge and physical constraints into the treatment planning process. In addition, it allows us to take advantage of intensity-modulation without changing the conventional procedure of patient setup and tumor volume definition and even without relying on an inverse planning system. It is thus a more natural way to evolve from conventional radiation therapy to the more sophisticated IMRT treatment. MSRT is likely to be beneficial for any radiation treatment where a simple beam configuration is used and where it is difficult to achieve a homogeneous dose distribution within the target volume.

ACKNOWLEDGEMENT

We thank David Y. Yang, J. Kung and M. Murphy for useful discussion on how to incorporating the MLC leaf transmission into a step-and-shoot delivery. This work was supported in part by Research Grants from the Department of Defense (BC996645), the American Cancer Society, and the Whitaker Foundation.

Table 1

Doses for ten breast cases. Five left breasts (#1-5) and five right breasts (#6-10) were studied. Results of three different treatment techniques, including standard tangential-field treatment, MSRT-B, and MSRT-S, are listed here. The breast size is defined by the dimension of the medial field (the first number is the inferior-superior dimension and the 2nd one measures the distance in the posterior-anterior direction), and the distance between the entrance points of the medial and the lateral fields.

Patient	Breast size	Standard plan					MSRT-B					MSRT-S				
#	(cm^3)	D^T_{max}	D^T_{min}	D^T_{ave}	D^L_{max}	D^H_{max}	D^T_{max}	D^T_{min}	D^T_{ave}	D^L_{max}	D^H_{max}	D^T_{max}	D^T_{min}	D^T_{ave}	D^L_{max}	D^H_{max}
1	13.0x20.6x26.7	5932	3235	5212	5494	5312	5653	3247	5240	5342	4989	5639	3240	5177	5464	5296
2	9.5x22.0.x19.1	5692	3497	5155	5314	4501	5536	3465	5111	5232	4140	5521	3344	5147	5220	4492
3	14.0x19.0x24.1	5861	3593	5236	5363	4658	5630	3579	5117	5122	4452	5500	3479	5074	4985	4015
4	8.0x16.5x17.7	5513	3738	5028	4867	4408	5369	3783	5047	4847	4427	5462	3742	5162	5109	4676
5	10.0x19.2x16.8	5686	4497	4886	5467	4908	5421	4639	4792	5203	4824	5385	3452	4948	5235	4828
6	9.0x20.0x21.1	5703	3940	5230	5101	*	5532	3939	5195	5015	*	5542	3948	5214	5081	*
7	8.0x18.2x17.0	5590	4066	5111	5172	*	5408	4053	5082	5099	*	5402	3809	5105	5057	*
8	7.0x14.0x17.9	5630	4175	5113	5542	*	5433	4125	5043	5345	*	5502	4205	5148	5387	*
9	8.5x19.0x19.0	5838	4027	5185	5257	*	5471	4005	5120	5207	*	5545	4018	5148	5236	*
10	9.0x17.5x20.2	5799	3823	5217	5424	*	5535	3808	5148	5268	*	5522	4044	5155	5258	*

Table 2 Parameters of MSRT-B and MSRT-S treatment of a left breast case. For MSRT-B, three segments were used in each incident beam direction. The MU setting of each segment was provided by the FOCUS treatment planning system. The fractional MU, f_k, of the *k-th* segment was obtained using $f_k = MU_k / \sum_k MU_k$.

Tx technique	MSRT-B						MSRT-S			
Beam direction	Medial field			Lateral field			Medial field			Lateral field
Wedge filter	None			30° physical wedge			None			30° enhanced dynamic wedge
Segment	1	2	3	1	2	3	1	2	3	1
Segment MU	96	11	7	183	10	9	76	31	6	143
Independent cal.	97	11	7	178	10	9	73	32	6	147
f_k	0.8431	0.0980	0.0588	0.9056	0.0500	0.0444	0.6733	0.2772	0.0495	1.0000

Figure Caption

Figure 1. Standard tangential field arrangement for treatment of a left breast cancer patient (top row). The middle and bottom rows are the MLC shapes of the three segments of the medial and lateral MSRT fields, respectively. A physical wedge of 30° was used in the lateral field.

Figure 2. MLC shapes of the medial field (a-c) of a MSRT-S plan. The lateral field (d) in the MSRT-S treatment is a 30° enhanced dynamic wedge field.

Figure 3. Instances in a step-and-shoot delivery scheme for the medial and lateral MSRT fields shown in figure 1. Here af_k represents the accumulated fractional MU at a given instance and varies from zero to unity. Subtraction of the two consecutive segments gives the fractional MU delivered when the system goes from one instance to the subsequent one. For convenience, the fractional MU, f, of each segment are specified for each segment (a "step" instance plus a "shoot" instance makes a segment).

Figure 4. Comparison of the isodose distributions of the treatment plans of the left-sided breast case using the tangential field technique (a), MSRT-B (b), and MSRT-S (c). Target volume includes the whole breast and the internal mammary nodes. Isodose levels are shown at 110%, 100%, 90%, 70%, 50%, 30%, and 10%.

Figure 5. Dose-volume histograms for the targets and normal structures for the treatment plans of the left-sided breast cancer patient shown in Fig. 4. The build-up region of 0.5cm is excluded from the breast tissue. Dash-dotted lines: OTF plan. Dashed lines: MSRT-B plan. Solid lines: MSRT-S plan.

References

1. Fisher B, Redmond C, Poisson R, et al: Eight-year results of a randomized clinical trial comparing total mastectomy and lumpectomy with or without irradiation in the treatment of breast cancer [published erratum appears in N Engl J Med 1994 May 19;330(20):1467] [see comments]. Comment in: N Engl J Med 1989 Sep 7;321(10):689-90. New England Journal of Medicine 320:822-8, 1989

2. Harris JR, Hellman S, Henderson IC, et al: Breast Diseases. Philadelphia, PA, J.B. Lippincott Co., 1991

3. Rutqvist LE, Pettersson D, Johansson H: Adjuvant radiation therapy versus surgery alone in operable breast cancer: long-term follow-up of a randomized clinical trial. Radiotherapy & Oncology 26:104-10, 1993

4. Dobbs HJ: Radiation therapy for breast cancer at the millennium. Radiotherapy & Oncology 54:191-200, 2000

5. Karlsson M, Zackrisson B: Matching of electron and photon beams with a multi-leaf collimator. Radiotherapy & Oncology 29:317-26, 1993

6. Zackrisson B, Arevarn M, Karlsson M: Optimized MLC-beam arrangements for tangential breast irradiation. Radiotherapy & Oncology 54:209-12, 2000

7. Jansson T, Lindman H, Nygard K, et al: Radiotherapy of breast cancer after breast-conserving surgery: an improved technique using mixed electron-photon beams with a multileaf collimator. Radiotherapy & Oncology 46:83-9, 1998

8. Li JG, Xing L, Boyer AL, et al: Matching photon and electron fields with dynamic intensity modulation. Medical Physics 26:2379-84, 1999

9. Li JG, Williams SS, Goffinet DR, et al: Breast-conserving radiation therapy using combined electron and IMRT technique. Radiotherapy & Oncology 56:65-71, 2000

10. Smitt MC, Li SD, Shostak CA, et al: Breast-conserving radiation therapy: potential of inverse planning with intensity modulation. Radiology 203:871-6, 1997

11. Williams SS, Xing L, Boyer AL, et al: Intensity modulated treatment of breast cancer with inclusion of supraclavicular and internal mammary lymph nodes. International Journal Radiation Oncology, Biology, Physics 42:370, 1998

12. Hyodynmaa S, Gustafsson A, Brahme A: Optimization of conformal electron beam therapy using energy- and fluence-modulated beams. Medical Physics 23:659-66, 1996

13. Hong L, Hunt M, Chui C, et al: Intensity-modulated tangential beam irradiation of the intact breast. International Journal of Radiation Oncology, Biology, Physics 44:1155-64, 1999

14. McCormick B, Hong L, Chui C, et al: Breast IMRT: The potential for treatment improvement with intensity modulation in left-breast disease. International Journal of Radiation Oncology, Biology, Physics 48:298, 2000

15. Chang SX, Deschesne KM, Cullip TJ, et al: A comparison of different intensity modulation treatment techniques for tangential breast irradiation. International Journal of Radiation Oncology, Biology, Physics 45:1305-14, 1999

16. Donovan EM, Johnson U, Shentall G, et al: Evaluation of compensation in breast radiotherapy: a planning study using multiple static fields. International Journal of Radiation Oncology, Biology, Physics 46:671-9, 2000

17. Kestin LL, Sharpe MB, Franzier RC, et al: Intensity-modulation to improve dose uniformity with tangential breast radiotherapy: initial clinical experience. International Journal of Radiation Oncology, Biology, Physics 48:1559-1568, 2000

18. Lo YC, Yasuda G, Fitzgerald TJ, et al: Intensity modulation for breast treatment using static multi-leaf collimators. International Journal of Radiation Oncology, Biology, Physics 46:187-94, 2000

19. van Assen B, Raaijmakers CPJ, Hofman p, et al: An improved breast irradiation technique using three-dimensional geometric information and intensity modulation. Radiotherapy & Oncology 58:341-347, 2001

20. Burman C, Chui CS, Kutcher G, et al: Planning, delivery, and quality assurance of intensity-modulated radiotherapy using dynamic multileaf collimator: a strategy for large-scale implementation for the treatment of carcinoma of the prostate. International Journal of Radiation Oncology, Biology, Physics 39:863-73, 1997

21. Low DA, Li Z, Klein EE: Verification of milled two-dimensional photon compensating filters using an electronic portal imaging device. Medical Physics 23:929-38, 1996

22. Xing L, Li JG: Computer verification of fluence maps in intensity modulated radiation therapy. Medical Physics 27:2084-92, 2000

23. Xing L, Curran B, Hill R, et al: Dosimetric verification of a commercial inverse treatment planning system. Physics in Medicine & Biology 44:463-78, 1999

24. Wang X, Spirou S, LoSasso T, et al: Dosimetric verification of intensity-modulated fields. Medical Physics 23:317-27, 1996

25. Low DA, Harms WB, Mutic S, et al: A technique for the quantitative evaluation of dose distributions. Medical Physics 25:656-61, 1998

26. Tsai JS, Wazer DE, Ling MN, et al: Dosimetric verification of the dynamic intensity-modulated radiation therapy of 92 patients. International Journal of Radiation Oncology, Biology, Physics 40:1213-30, 1998

27. Fraass BA, Kessler ML, McShan DL, et al: Optimization and clinical use of multisegment intensity-modulated radiation therapy for high-dose conformal therapy. Seminars in Radiation Oncology 9:60-77, 1999

28. Xiao Y, Galvin J, Hossain M, et al: An optimized forward-planning technique for intensity modulated radiation therapy. Medical Physics 27:2093-9, 2000

29. Klein EE, Low DA, J.W. S, et al: Differential dosing of prostate and seminal vesicales using dynamic multileaf collimation. International Journal of Radiation Oncology, Biology, Physics 48:1447-1456, 2000

30. Bortfeld T, Boyer AL, Schlegel W, et al: Realization and verification of three-dimensional conformal radiotherapy with modulated fields. International Journal of Radiation Oncology, Biology, Physics 30:899-908, 1994

31. Svensson R, Kallman P, Brahme A: An analytical solution for the dynamic control of multileaf collimators. Physics in Medicine & Biology 39:37-61, 1994

32. Ma L, Boyer AL, Xing L, et al: An optimized leaf-setting algorithm for beam intensity modulation using dynamic multileaf collimators. Physics in Medicine & Biology 43:1629-43, 1998

33. Boyer A, Xing L, Xia P: Beam shaping and intensity modulation in modern technology of radiation oncology. Madison, WI, Medical physics publishing, 1999

34. Dirkx ML, Heijmen BJ, van Santvoort JP: Leaf trajectory calculation for dynamic multileaf collimation to realize optimized fluence profiles. Physics in Medicine & Biology 43:1171-84, 1998

35. Kung J, Murphy M, Xing L: An algebraic method to incorporate collimator leakage into step-and-shoot leaf sequences for intensity-modulated radiation therapy. Medical Physics 28:submitted, 2001

36. Klein EE, Tepper J, Sontag M, et al: Technology assessment of multileaf collimation: a North American users survey. International Journal of Radiation Oncology, Biology, Physics 44:705-10, 1999

37. LoSasso T, Chui CS, Ling CC: Physical and dosimetric aspects of a multileaf collimation system used in the dynamic mode for implementing intensity modulated radiotherapy. Medical Physics 25:1919-27, 1998

38. LoSasso T, Chui CS, Ling CC: Comprehensive quality assurance for the delivery of intensity modulated radiotherapy with a multileaf collimator used in the dynamic mode. Medical Physics 28:2209-2219, 2001

39. Xing L, Chen Y, Luxton G, et al: Monitor unit calculation for an intensity modulated photon field by a simple scatter-summation algorithm. Physics in Medicine & Biology 45:N1-7, 2000

40. Chen Y, Xing L, Luxton G, et al: A multi-purpose quality assurance tool for MLC-based IMRT., ICCR. Heidelberg, Germany, Springer-Verlag, 2000, pp 371-373

41. Xing L, Li JG, Pugachev A, et al: Estimation theory and model parameter selection for therapeutic treatment plan optimization. Medical Physics 26:2348-58, 1999

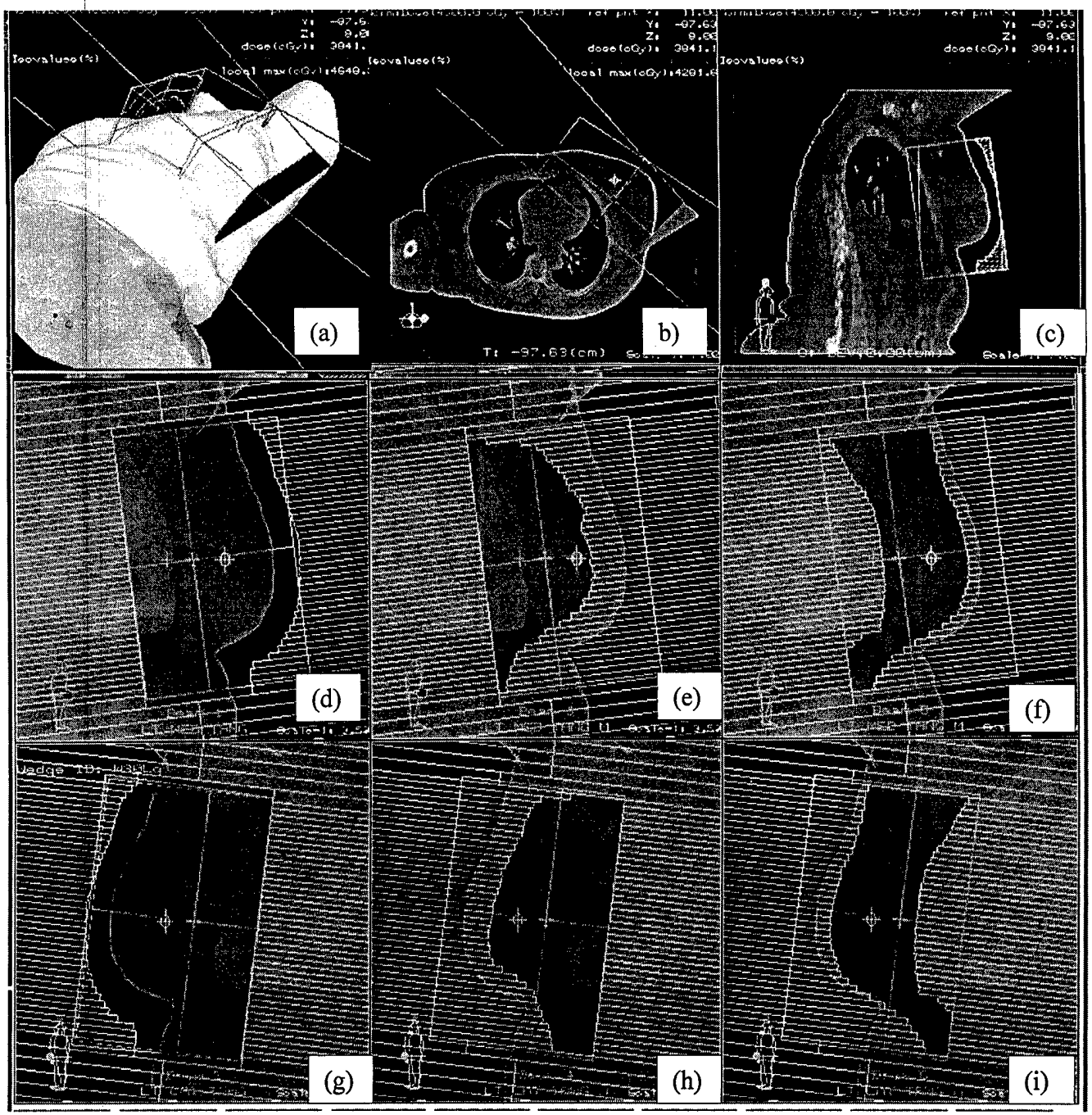

Fig. 1

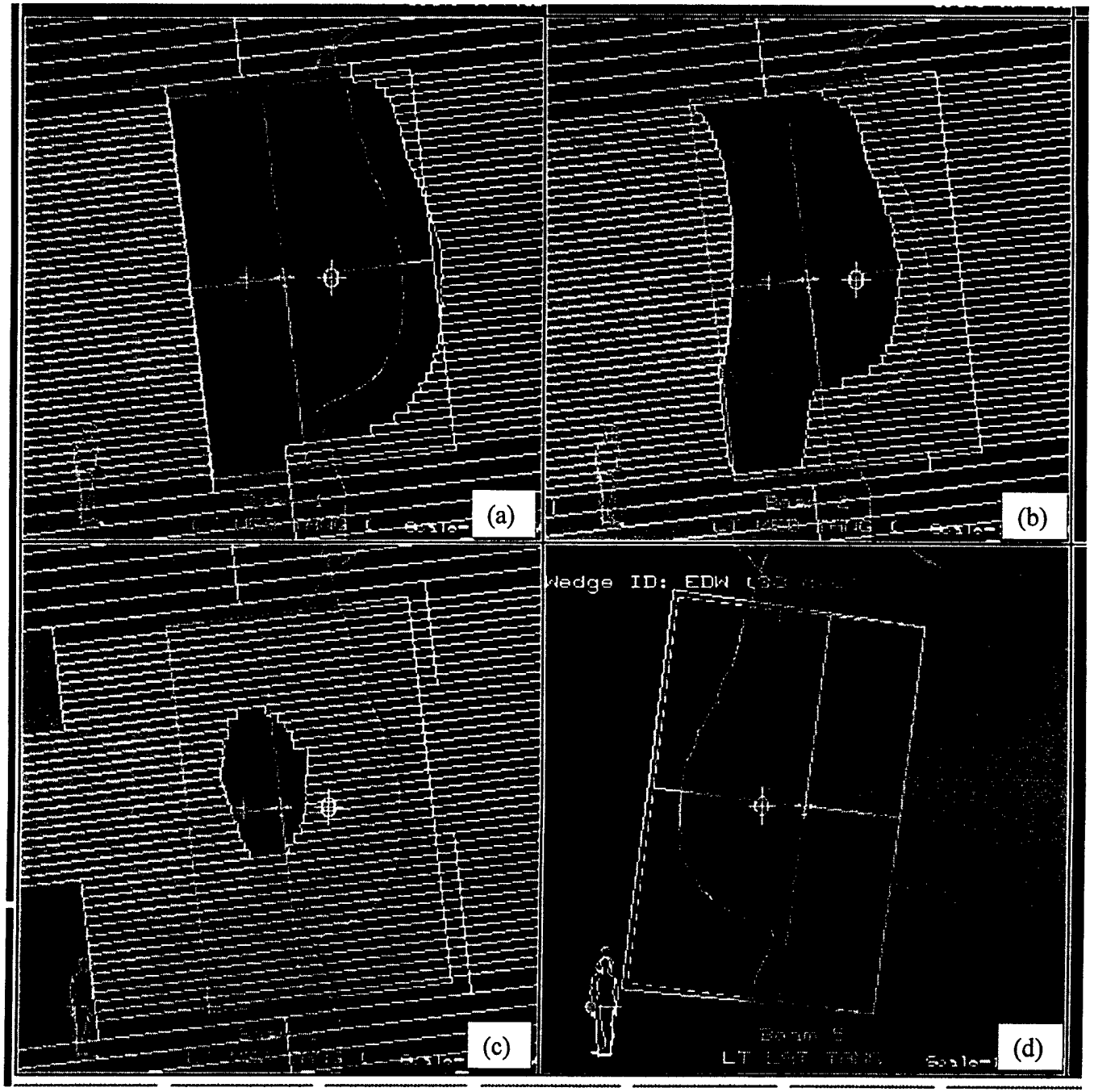

Fig. 2

Step-and-shoot Delivery

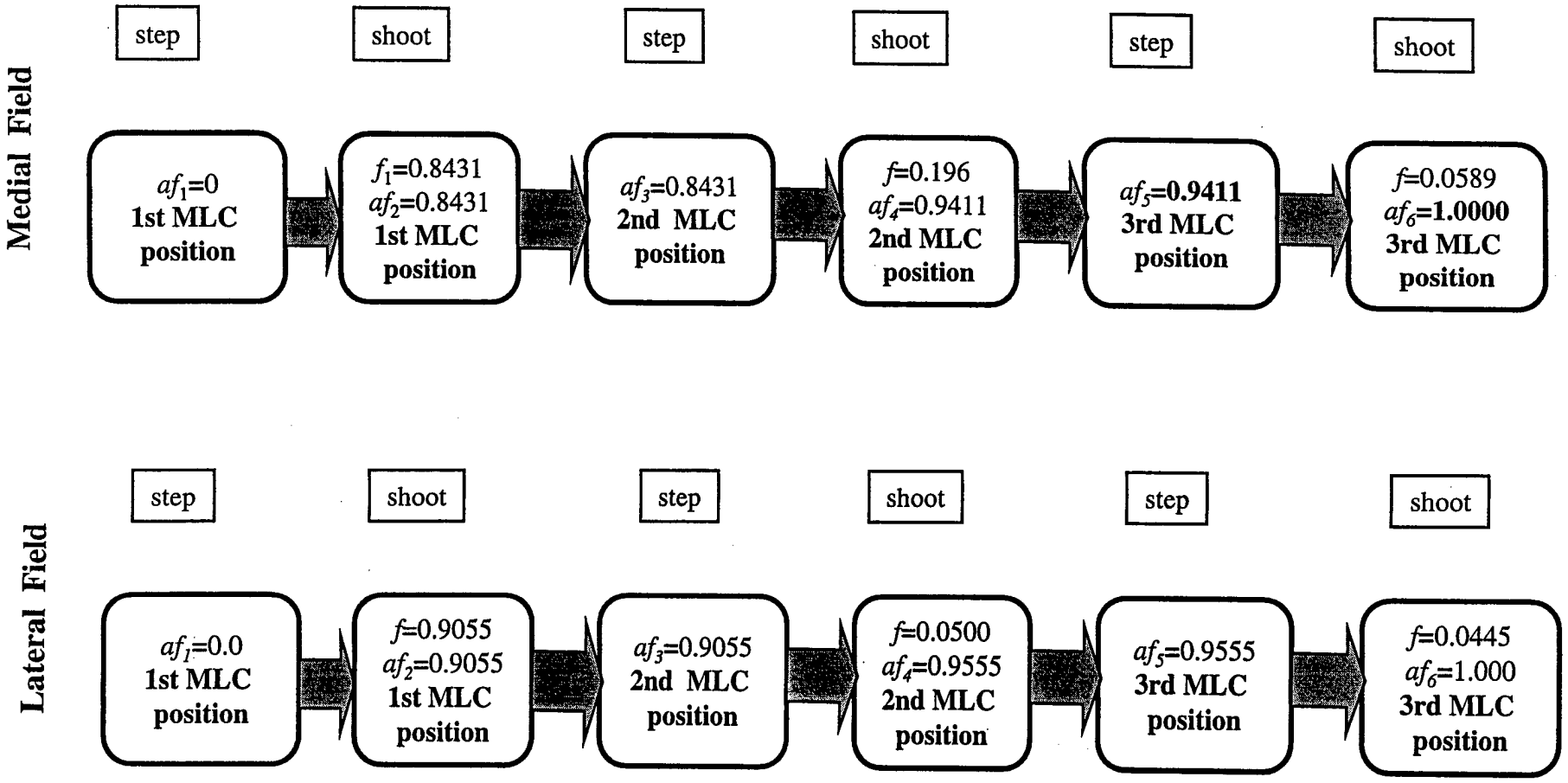

Fig. 3

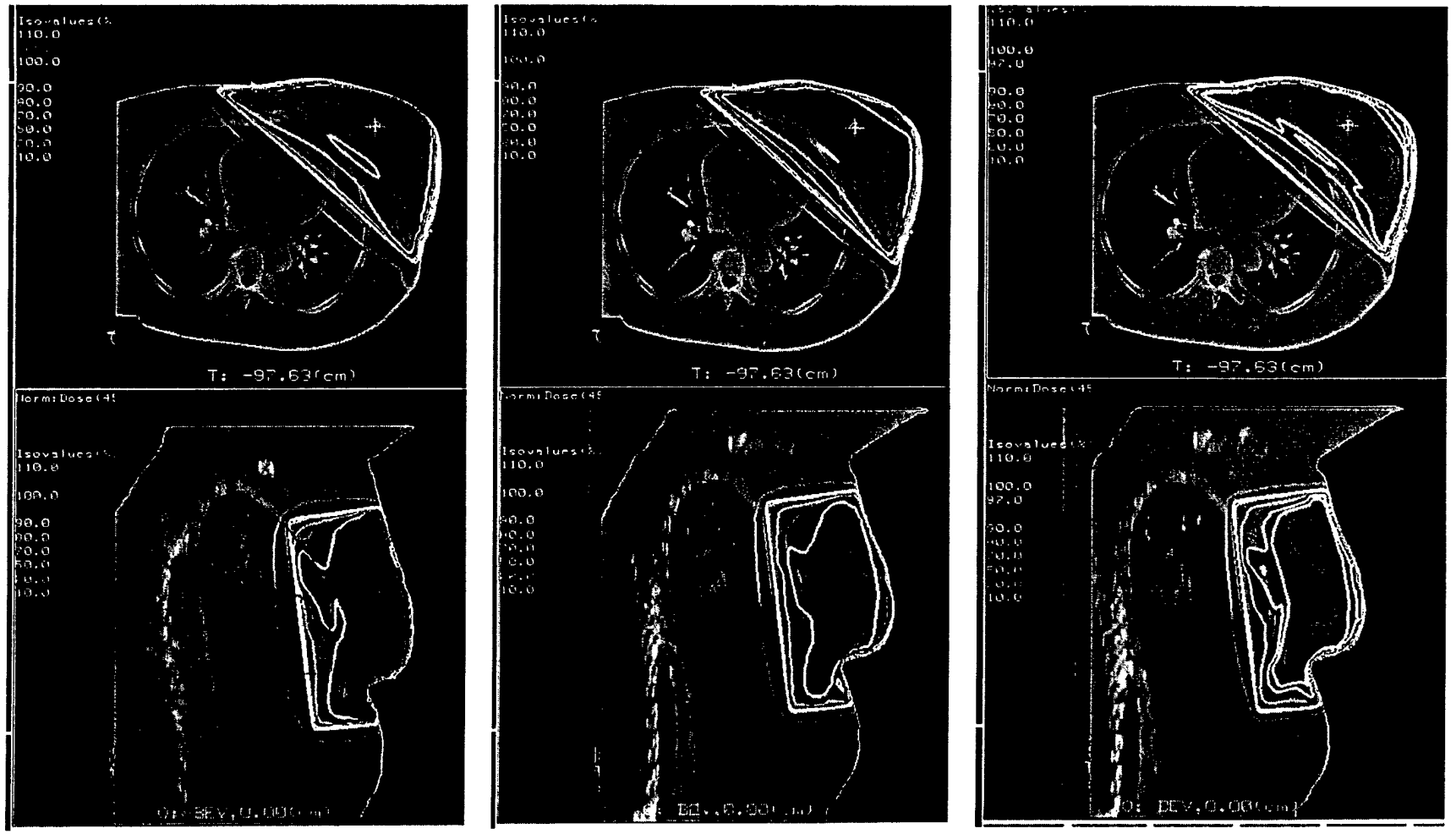

(a) (b) (c)

Fig. 4

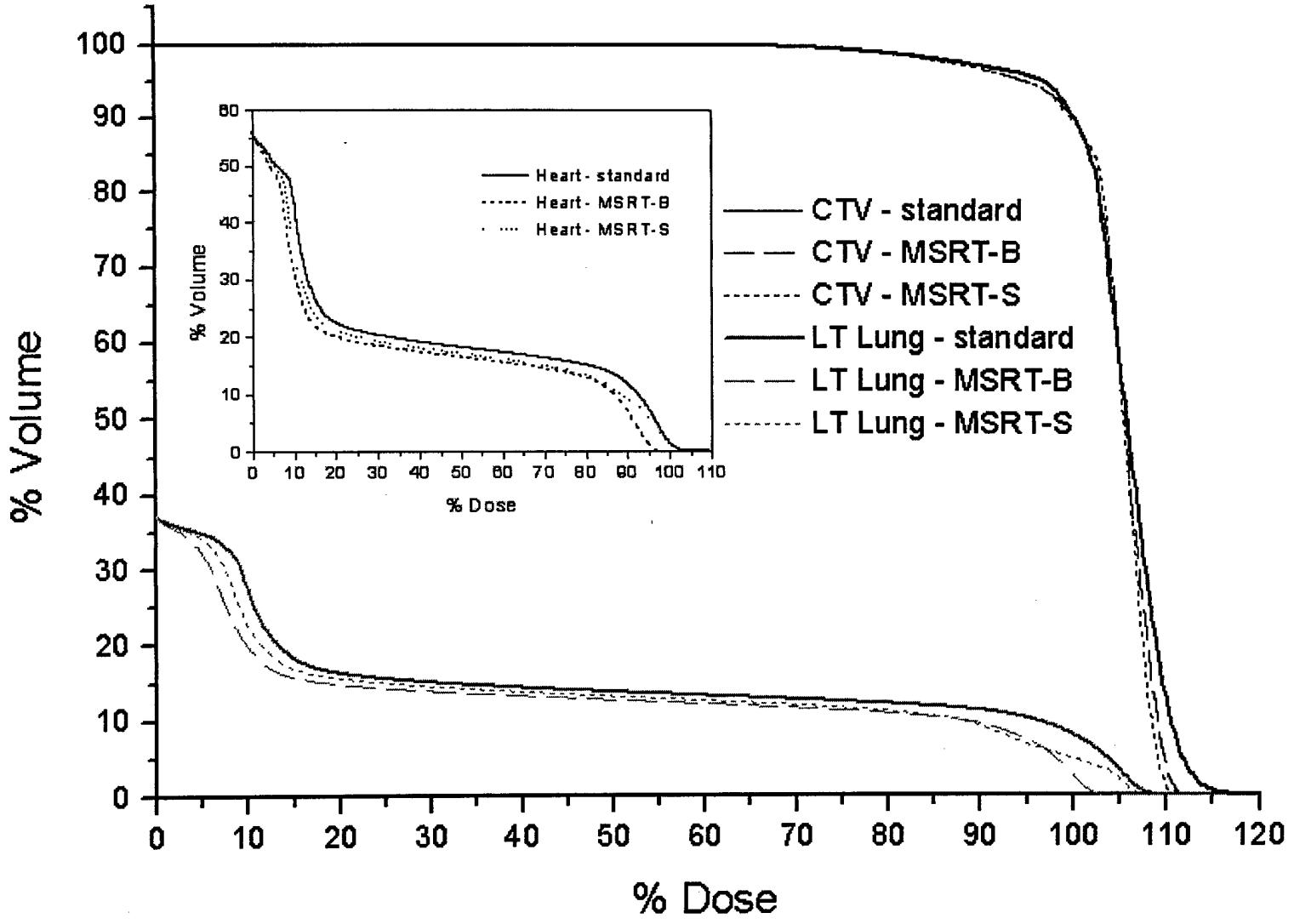
% Volume
% Dose
CTV - standard
CTV - MSRT-B
CTV - MSRT-S
LT Lung - standard
LT Lung - MSRT-B
LT Lung - MSRT-S
Heart - standard
Heart - MSRT-B
Heart - MSRT-S
% Volume
% Dose

Fig. 5

Incorporating prior knowledge into beam orientation optimization in IMRT

Andrei Pugachev, M.S. and Lei Xing[a)], Ph.D.

Department of Radiation Oncology, Stanford University School of Medicine,

Stanford, California 94305-5304, USA

[a)]Author to whom correspondence should be addressed.

Stanford University School of Medicine
Department of Radiation Oncology
300 Pasteur Drive
Stanford, CA 94305-5304

E-mail: lei@reyes.stanford.edu
Phone: (650) 498 7896
Fax: (650) 498 4015

Submitted to: International Journal of Radiation Oncology, Biology, Physics

Purpose: Selection of beam configuration in currently available IMRT treatment planning systems is still based on trial-and-error hunting. Computer beam orientation optimization has potential to improve the situation but its practical implementation is hindered by the excessive computing time associated with the calculation. The purpose of this work is to provide an effective means to speed up the beam orientation optimization by incorporating *a priori* knowledge of the system and to demonstrate the utility of the new algorithm for beam placement in IMRT.

Methods and Materials: Beam orientation optimization was performed in two steps. First, the quality of each possible beam orientation was evaluated using a beam's-eye-view dosimetrics (BEVD) developed in our previous study. A simulated annealing algorithm was then employed to search for the optimal set of beam orientations, taking into account the BEVD scores of different incident beam directions. During the calculation, sampling of gantry angles was weighted according to the BEVD score computed prior to the optimization. A beam direction with a higher BEVD score had higher probability to be included into the trial configuration, and *vice versa*. The inclusion of the BEVD weighting in the stochastic beam angle sampling process made it possible to avoid spending valuable computing time unnecessarily at "bad" beam angles. Simultaneous iterative inverse treatment planning algorithm (SIITP) was used for beam intensity profile optimization during the optimization process. The BEVD-guided beam orientation optimization was applied to an IMRT treatment of paraspinal tumor. The advantage of the new optimization algorithm was demonstrated by comparing the calculation with the conventional scheme without the BEVD weighting in the beam sampling.

Results: The BEVD tool provided a useful guidance for the selection of the potentially good directions for the beams to incident and was utilized to guide the search for the optimal beam configuration. The BEVD-guided sampling improved both optimization speed and convergence of the calculation. A comparison of several five-field IMRT treatment plans obtained with and without BEVD-guidance indicated that the computational efficiency was increased by a factor of ~10.

Conclusion: Incorporation of BEVD information allows for development of a more robust tool for beam orientation optimization in IMRT planning. It enables us to more effectively utilize

the angular degree of freedom in IMRT without paying the excessive computing overhead and brings us one step closer toward the goal of automated selection of beam orientations in a clinical environment.

Key words – IMRT, inverse planning, intensity modulation, optimization, beam orientation

Introduction

Beam configuration may have significant influence on IMRT dose distribution and an individualized beam configuration is frequently needed to achieve the best possible treatment [1, 2]. Clinically, beam orientations are usually selected based on trial-and-error search. Considerable effort may be required to come up with a set of acceptable beams. The final results may strongly depend on the planner's experience and understanding of the planning system. An ideal solution is to incorporate the beam orientation optimization into the planning system to automate the beam placement process. With currently available techniques, unfortunately, this would take a prohibitive amount of computing time even on a high-end workstation. Generally speaking, in order to optimize beam configuration, one can add the degree of freedom of beam angles to the objective function and optimize them together with the beamlet weights. While this does not pose any conceptual challenge, the search space is greatly enlarged because of the coupling between beam profiles and beam configuration [1, 3-8]. Improving the computational efficiency is a key to having a clinically practical beam orientation optimization tool.

A stochastic algorithm used for beam orientation optimization involves testing a large number of beam configurations. In the current algorithms, the beam orientations are sampled randomly and, for every sampled beam configuration, the beam profiles must be optimized in order to obtain the value of the objective function for determining whether the trial should be accepted or not. In practice, some beam directions are better/worse than others and this information is available through an independent evaluation based on the system's geometric and dosimetric information [2, 9, 10]. Incorporation of this type of prior knowledge can potentially make the angular search more intelligent and greatly facilitate the calculation. The prior knowledge here acts like a filter that prescreens the search space by identifying the potential "good" and "bad" gantry angles. In this way, the simulated annealing algorithm can "heavily" sample the region where the potential for a beam to be placed is high and avoid spending valuable computing time exploring the beam configurations that are less likely to be the optimal solution.

We have recently introduced a beam's eye view dosimetrics (BEVD) to rank the beam orientations [2, 9]. The central point of the technique is that the figure of merit of a beam

direction should be measured by what that beam could achieve dosimetrically without exceeding the dose constraints of the system. Application of the BEVD technique to several model systems and clinical cases clearly showed its advantage in IMRT [2, 9]. In this study, we points out that the BEVD represents the prior knowledge of the system and provide a computationally intelligent algorithm for beam orientation optimization. The calculation was performed in two steps. First, the BEVD score was evaluated for every possible beam orientation. The simulated annealing optimization of beam orientations then followed under the guidance of BEVD score. In this algorithm, the probability of a beam orientation being sampled depended on the corresponding BEVD score. The new optimization scheme was tested using clinical cases and the results indicated that this approach significantly reduced the computational time and greatly facilitated the IMRT beam orientation selection process.

Methods and Materials

BEVD as a priori knowledge for beam orientation optimization

Relative merit of a single beam can be obtained prior to beam orientation optimization. An appealing approach is along the line of the beam's eyes view (BEV), which was originally used in 3D treatment planning as an interactive tool to assist the oncologists to define radiation portal entry angles that exclude critical structures while fully encompassing the target volume [2, 9, 11]. The binary beam orientation scoring was further improved by the introduction of BEV volumetrics [12-15]. The volume of normal structures intersected by a specified aperture/portal direction was calculated for all possible incident directions, permitting the planer to evaluate quantitatively the relative merit of a given portal field. In this approach, the good beam directions were those minimizing the volume of normal tissue intersected.. While the technique worked well for conventional 3D radiation therapy, radical modifications must be made for it to be suitable for IMRT.

Generally speaking, an intensity modulated beam which intercepts a large volume of sensitive structure(s) is not necessarily a bad beam. The dose tolerances of the involved sensitive structures should also be considered when constructing a metric for measuring the

quality of incident beam directions (note that the BEV volumetrics approach is based *purely* on the geometric information of the patient). We have recently derived a BEVD that ranks a beam direction by what the beam could achieve dosimetrically without violating the dose constraint of the system. To compute the BEVD score of a given gantry angle, a ray tracing is performed for each involved beamlet and the sensitive structure(s) along the path of the beamlet is located. The maximum achievable weight of a beamlet, which depends on the tolerance(s) and location(s) of the sensitive structure(s), determines the width of the radiation "window" of the beamlet. The score of the beam is calculated according to [2, 9]

$$S_i = \frac{1}{N_T} \sum_{n \in \text{Target}} \left(\frac{d_{ni}}{D_T^P} \right)^2, \qquad (1)$$

where d_{ni} is the maximum dose delivered to the voxel n by the beam from the direction indexed by i, N_T is the number of voxels in the target, and D_T^P is the target prescription dose.

The BEVD score described above is obtained under the assumption of a single incident beam. It is capable to identify potentially "good" and "bad" directions and can be used as a useful guidance for beam placement in either manual planning or computer optimization. The optimal beam configuration for an IMRT treatment balances the BEVD score and the beam interplay due to the overlap of radiation fields. In the following, we describe how to utilize the BEVD information to facilitate the beam orientation optimization calculation.

BEVD-guided beam orientation optimization

For simplicity only coplanar beams were considered in this paper. Non-coplanar beams could be included into the search space similarly by adding the degree of freedom of couch angle [1, 2, 16]. Beam orientation was specified by the gantry angle varying from 0° to 360° in 5° increment. All calculations were done on a Silicon Graphics O_2 R5000 workstation (Silicon Graphics, Inc., Mountain View, CA) using the PLUNC treatment planning system (University of North Carolina, Chapel Hil, NC).

System variables were divided into two groups: gantry position and beam profile (beamlet weights). Simulated annealing [17-20] was used for beam orientation optimization and the simultaneous iterative inverse treatment planning algorithm (SIITP) for beam intensity profile optimization [21, 22]. However, the beam profile optimization could also be done using

other existing inverse planning algorithms [23-26]. A quadratic dose-based objective function defined by

$$F = \sum_i w_i \left(D_i - D_i^p\right)^2 \qquad (2)$$

was used in this study, where D_i is the calculated dose value in voxel i, D_i^p is the desired dose and w_i is the structure-specific the importance factor. The values of the importance factors were determined empirically [27-31]. D_i^p was the prescribed dose for the target and zero for sensitive structures. The zero prescription dose to the sensitive structures ensured that the optimization continuously improved the dose to the sensitive structures when there was room for improvement, instead of stopping at *a priori* non-zero value.

In previously reported algorithms, the gantry angles underwent random changes to explore different combinations of beam orientations. The corresponding dose distribution was then calculated and the objective function evaluated. The trial beam configuration was accepted with the probability

$$P = \begin{cases} 1 & \text{If } \Delta F < 0 \\ \exp(-\dfrac{\Delta F}{T}) & \text{Otherwise} \end{cases}, \qquad (3)$$

where ΔF is the change of the objective function and T the system temperature. The temperature was gradually lowered according to an exponential cooling schedule. Typically, 3,000~5,000 sets of beam orientations were sampled in the optimization of coplanar beams to find the solution. The conventional approach is brute-force in nature. Given a patient, the geometric characteristics and dose tolerances of sensitive structures are known. The angular search space can be pre-ranked using BEVD and used to assist the optimization process. Ideally, the integration of BEVD into beam orientation optimization algorithm should be done in two steps. First, we use the BEVD information to prescreen the search space to eliminate the "bad" gantry angles. A computer optimization is then used to individualize the beam orientations by searching the reduced solution space. While conceptually simple, the situation is more complicated here. The issue is that the BEVD score is obtained under the assumption of a single incident beam. Therefore, it reflects only one facet of the beam configuration selection problem. The final beam configuration also depends on the interplay between the incident beams due to the overlap of radiation fields. The optimal beam configuration needs to

balance between the BEVD scores and the beam interplay. Even though less likely from the perspective of the BEVD, a beam direction with a low but non-zero BEVD score may show up in the final solution if it is angularly well separated from others. In other words, our prior BEVD knowledge about the angular space is "fuzzy" and incomplete. The goal here is to develop a formal and robust approach to incorporate the partial information into the beam orientation optimization.

We used the BEVD score to construct a prior "probability density function" and modified the beam sampling used during the simulated annealing. The strategy was to assign a higher sampling probability to a beam direction with a high BEVD score, and *vice versa*. The overall calculation process is outlined in Fig. 1, along with the conventional simulated annealing algorithm. The starting temperature was chosen to be higher than the largest value of the objective functions calculated for several sets of randomly sampled beam orientations. A trial beam configuration was introduced by assigning a random angular variation to a randomly selected beam in the system. The value of the corresponding BEVD-based probability function [see Eq. (4) in the next paragraph for definition] was computed to decide whether the trial should be rejected right away or should be further checked by the simulated annealing acceptance probability defined in Eq. (3). In order to evaluate the value of Eq. (3), the beam profiles of the trial beam configuration must be optimized. Because of the pre-screening of the BEVD probability density function, we avoided spending valuable computing time on those trials that were less likely to be the final solution. The temperature was gradually lowered according to an exponential cooling schedule, which was the same as that in conventional simulated annealing algorithm. The stopping temperature was determined by monitoring the objective function as a function of the temperature change.

In the above we have introduced a BEVD probability density function to pre-screen the trial beam configurations. While our requirement on the general behavior of the BEVD probability density function is clear, its specific form is a matter of experimenting. We found that fast convergence was achieved when the probability was proportional to the square of the BEVD score. That is,

$$P(\theta) = \left(\frac{BEVD(\theta)}{BEVD_{MAX}} \right)^2, \qquad (4)$$

where $BEVD(\theta)$ is the score corresponding to the gantry angle θ and $BEVD_{MAX}$ is the normalization factor equal to the maximum value of the score function. Several other expressions, including linear and cubic forms, were tested. Even though they all lead to the same optimal solution and speeded up the conventional simulated annealing calculation, the level of improvement was less significant than that from Eq. (4). It is possible to incorporate any other type of information available about the relative value of beam orientations, such as entropy measure [10], into the sampling probability (4).

An IMRT treatment of paraspinal tumor was used here to illustrate the usefulness of prior knowledge of the system in facilitating IMRT planning. Five 15 MV photon beams were used for the treatment. To assess the computational efficiency, the convergence behavior of the new algorithm was compared with that of the conventional simulated annealing calculation. To demonstrate the improvement in plan quality, the results of the BEVD-guided optimization were compared with an IMRT plan obtained with five equiangular spaced beams. The DVHs for the target and the sensitive structures as well as the dose distributions were used for the evaluation of the treatment plans.

Results

The BEVD-guided beam orientation optimization was applied to a five-field IMRT treatment of paraspinal tumor. The prescribed doses and importance factors of different structures are given in table 1. In figure 2 we show the BEVD score as a function of gantry angle. This calculation was performed prior to beam orientation optimization calculation and the result depended only on the patient's geometric information and dosimetric tolerances of the involved sensitive structures. Because of the dosimetric restriction of the liver and the long radiological path for the photon to reach the target, the angles between 260° and 360° are considered as disadvantageous region in terms of target irradiation, as reflected by the lower BEVD scores. The BEVD has a distinct peak at 225°. The optimal beam angles from the BEVD-guided beam orientation optimization are listed in table 2. It is interesting to note that one of the optimal gantry angles (220°) is located very near the highest BEVD score (225°) in

the final optimized solution. Furthermore, there is no beam located in the angularly disadvantageous region (between 260° and 360°) identified by BEVD.

The conventional simulated annealing algorithm generated the same beam configuration as listed in table 1 for four out of five independent runs, but with much longer computing time. To assess the improvement in computing efficiency, we studied the convergence behavior of the BEVD-guidance optimization in parallel to the conventional simulated annealing optimization. Two tests were done. First, we set the temperature in the simulated annealing to zero and compared the performance of the beam orientation optimizations with and without incorporation of BEVD knowledge. When the temperature is set to zero, only trial configurations with lower objective function are accepted in both cases and the system only moves toward downhill direction. However, this calculation cannot be replaced by a gradient search since the latter does not allow the system to "tunnel" through the barriers of a "bumpy" objective function. The evolution of the objective function as a function iteration step is shown as the dashed line in figure 3. The solid line shows the convergence of the system when the BEVD was incorporated into the sampling using the algorithm described in the last section. The step-wise decrease of the objective function reflects the "tunneling" effect of computational process. With the guidance of BEVD score, the performance of the modified simulated annealing algorithm was improved significantly. The objective function reached its minimum in approximately 360 iterations. Whereas it took much more iterations for the conventional brute-force simulated annealing to reach convergence, and one of them did not converge even if we let the calculation continued up to 5,000 iterations. The result indicated that the incorporation of prior BEVD knowledge does not only increase the calculation speed, but also provide us with an significantly improved chance of success in searching for the optimal solution even when the simulated annealing cooling schedule is not well designed.

The next level of test involved a comparison of the BEVD guided optimization and the conventional simulated annealing optimization with an exponential cooling schedule. Figure 4 shows the objective function as a function of iteration step for the two types of calculations. In each case, an averaging was taken over five independent runs to reduce the "noisy" behavior of the evolution of the objective function. Comparing figures 3 and 4, it can be seen that switching on the annealing in both cases speeds up the convergence and decreases the number of iterations required for the system to reach the ground state. From figure 4 it is seen that the

simulated annealing with BEVD guided sampling outperformed the standard simulated annealing significantly. All five BEVD-guided optimization calculation reached the global minimum within 300 iterations. With 400 iterations, only one out of five runs of standard simulated annealing was able to get close to the ground state with the value of objective function near the BEVD-guided calculation. All other four simulations lead to sub-optimal solutions with much higher objective function values with 400 iterations.

For comparison, in figure 4 we also plotted the value of the objective function (dashed horizontal line) for a five-field IMRT plan with equally angled beams listed in table 2. The dose distribution corresponding to the five equally angled beams is shown in figure 5a. The improvement in dose distribution after BEVD-guided optimization is shown in figure 5b. Figure 6 shows comparison of DVHs of the plans obtained using the equiangular spaced beam configuration and the BEVD-guided optimization. Whereas the target DVH was improved slightly, the fractional dose-volume of the spinal cord, kidney, and liver were all lowered by moderate to significant amounts. Considering the large volumes of the kidney and liver and the reduction in radiation doses, the improvement should be considered as clinically significant.

On average, it took slightly more than two hours for the SGI O_2 workstation to carry out 300 iterations. However, with state-of-the-art computer hardware available now on the market and improved programming it is likely that the calculation efficiency will be enhanced to a level where BEVD-guided beam orientation becomes practically achievable in a clinical environment. In addition to the plan presented here, we have performed BEVD-guided beam orientation optimization for a few nasopharyngeal cases. Similar reduction in computing time was observed while reliable results were obtained. Due to the similarity of the findings, we will not repeatedly present them here.

Discussion

In this study we have proposed to incorporate the BEVD information into beam orientation optimization algorithm to guide the angular search. The BEVD ranking is a single beam score function available prior to inverse treatment planning. Generally speaking, an intensity modulated beam which intercepts one or more sensitive structures is not necessarily a

bad beam. In reality, it is the dose and/or dose-volume that determine the damage to a sensitive structure. The BEVD score measures the dosimetric capability of a given beam direction. While not providing the optimal beam configuration because of the neglect of beam interplay, it points out where are the potentially good and bad directions for beam placement and represents prior partial knowledge of the system. This is supported by our optimization results presented in the last section. Indeed, all the beams showed up in the final optimal solution have reasonable BEVD scores and in particular, one of the beams appears very near the peak position of the BEVD function. Even in a sub-optimal solution resulting from the conventional simulated annealing calculation, none of the beams took a position in the disadvantageous region of the BEVD function.

We have shown that the incorporation of the valuable BEVD information greatly facilitated the beam orientation optimization. The proposed approach here is different from other beam orientation optimization algorithms, for example those described in Refs. [32, 33] in that the available information is utilized. Instead of adding to the objective function used to evaluate the "fitness" or "energy" of a trial configuration, we use the BEVD at the step of designing the trial configuration. In our calculations, the gantry angles were sampled according to a simulated annealing algorithm with consideration of BEVD. During an iteration step, the angle of an arbitrarily chosen beam was varied by a random amount. The trial was pre-screened by the BEVD according to Eq. (3). Instead of performing beam profile optimization for every trial beam configuration, we performed the conventional simulated annealing calculation (optimizing beam profiles and computing the corresponding value of the objective function) only for those trials that passed the pre-screening, as depicted in figure 1. The pre-screening allowed us to eliminate those beam configurations that were less likely to be the candidates for the optimal solution and saved a large amount of computing time. Application of the technique to clinical cases clearly showed its advantage. It reduced the sampling rate for those angles that were less likely to appear in the final solution and saved a large amount of computing time.

The inclusion of BEVD makes the computation more intelligent and can bring the system to the vicinity of the optimal solution more rapidly. As a result, the BEVD-guided beam orientation optimization not only speeds up the calculation, but also improves the convergence behavior of the conventional simulated annealing calculation. Because of the introduction of

the prior BEVD knowledge, the beam orientation optimization becomes almost independent of the annealing schedule used for simulated annealing. This is clearly seen from a comparison of the results presented in figures 3 and 4. On the other hand, the conventional simulated annealing algorithm is a brute-force calculation and relies heavily on the annealing schedule. Theoretically, a simulated annealing algorithm is guaranteed to find the global minimum of a multi-dimensional function provided that the cooling is slow enough. But the rate of convergence is low and the calculation could be trapped in a local minimum with any practically achievable number of iterations [19, 34]. Indeed, this problem showed up in our system: one of five runs did not converge to the best solution when the conventional simulated annealing (with 5,000 iterations) was employed. The limited convergence was also observed in beam profile optimization when a simulated annealing was used [35]. This phenomenon did not occur in our BEVD-guided simulated annealing calculation. We found that the solution obtained by the modifed algorithm was always equal or better than that of the conventional simulated annealing judged by the value of objective function. Therefore, the BEVD-guided calculation is more robust and has significant practical implication. Mathematically, this result is not surprising because the prior BEVD knowledge provided a certain degree of artificial intelligence to the system and assisted the optimization.

The inclusion of the redundant information into the plan selection process represents a major "leap" in theory from the conventional approaches. The technique proposed here can be categorized into the general Bayesian decision-making theory [19, 36]. The BEVD function serves as *a priori* probability density function. The role of the BEVD is similar to the "noise spectrum" in a statistical system, which represents our prior knowledge of radiation therapy and indicates our "bias" on the values of the system variables. In image analysis and many other fields of science and engineering, it has proven extremely useful to include the prior knowledge of the system into the estimation process [19, 36]. By utilizing the partial information of the system variables, one can effectively search the solution space and eliminate some unnecessary uncertainties in the estimation process. It is in this sense that the proposed formalism is superior to the conventional simulated annealing method. Generally speaking, it is a fundamental rule of estimation theory that the use of prior knowledge will lead to a more accurate estimation. The significant reduction in computing time is, one the other hand, specific to our system because of elimination of invoking beam profile optimization repeatedly.

Conclusion

While the beam configuration plays an important role in IMRT treatment, its selection in clinical treatment planning is still based on trial-and-error and considerable effort may be required to come up with a set of acceptable beams. In this paper we described a novel beam-orientation optimization algorithm in which the BEVD ranking information was utilized as *a priori* knowledge to guide the search in angular space. The inclusion of the BEVD weighting in the stochastic beam angle sampling process makes the search process more intelligent and efficient. The technique was applied to an IMRT treatment of paraspinal tumor and several nasoparyngeal IMRT treatments. The results clearly showed its potential in facilitating IMRT planning. The algorithm improved both the calculation speed and the convergence behavior of the beam orientation optimization and puts us one step closer to patient-specific optimization involving angular variables in routine clinical environment.

Acknowledgements

We would like to thank our colleagues at Stanford University, Artur L. Boyer, Sarah S. Donaldson, Gary Luxton, Todd Pawlicki, Steven Crooks, Cristian Cotrutz, Sandeep Hunjan, Jun Lian, and David Y. Yang for many useful discussions. This work was supported in part by a Research Scholar Grant Award from the American Cancer Society and Research Grants from the Whitaker Foundation, the US Department of Defense and the Information Technology Systems and Services of Stanford University.

	Relative importance factors	Target prescription and sensitive structure tolerance doses
GTV	1.0	1.0
Spinal cord	1.0	0.6
Liver	0.01	0.4
Kidney	0.02	0.4
Skin	0.001	1.0

Table 1. Relative importance factors and dose tolerances.

Equiangular spaced beam orientations					
Gantry angles	40°	110°	180°	255°	325°
Optimized beam orientations					
Gantry angles	110°	145°	180°	220°	250°

Table 2. Beam orientations used in equiangular treatment and the treatment with beam orientation optimization.

Legends

Figure 1. A. Flow chart of the conventional simulated annealing beam orientation optimization algorithm. B. Flow chart of the BEVD-guided simulated annealing sampling algorithm.

Figure 2. BEVD score as a function of the gantry angle.

Figure 3. The objective function *vs.* iteration step with the temperature set to zero during the optimization process. Dashed and solid lines correspond to the simulated annealing performed with standard sampling and the BEVD-guided sampling, respectively.

Figure 4. The objective function *vs.* iteration step for simulated annealing with the exponential cooling schedule. Dashed and solid lines correspond to the simulated annealing performed with standard sampling and the BEVD-guided sampling, respectively. Horizontal dashed line indicates the objective function value of an IMRT plan with five equiangular beams.

Figure 5. (a) The dose distribution of an IMRT paraspinal treatment with five equiangular spaced beams. (b) The dose distribution of the IMRT paraspinal treatment with five beams obtained using the BEVD-guided beam orientation algorithm.

Figure 6. Target and sensitive structure DVHs of the IMRT treatment plans for a paraspinal tumor. The dashed curves and solid curves correspond to the plans with five equiangular spaced beams and five beams obtained using BEVD-guided optimization.

References:

1. Pugachev A, Li JG, Boyer AL, Hancock SL, Le QT, Donaldson SS and Xing L, Role of beam orientation optimization in intensity-modulated radiation therapy. *International Journal of Radiation Oncology, Biology, Physics* **50**(2): 551-60, 2001.
2. Pugachev A and Xing L, Pseudo beam'-eye-view as applied to beam orientation selection in intensity-modulated radiation therapy. *International Journal of Radiation Oncology, Biology, Physics* **51**(5): 1361-1370, 2001.
3. Stein J, Mohan R, Wang XH, Bortfeld T, Wu Q, Preiser K, Ling CC and Schlegel W, Number and orientations of beams in intensity-modulated radiation treatments. *Medical Physics* **24**(2): 149-60, 1997.
4. Bortfeld T and Schlegel W, Optimization of beam orientations in radiation therapy: some theoretical considerations. *Physics in Medicine & Biology* **38**(2): 291-304, 1993.
5. Rowbottom CG, Oldham M and Webb S, Constrained customization of non-coplanar beam orientations in radiotherapy of brain tumours. *Physics in Medicine & Biology* **44**(2): 383-99, 1999.
6. Sailer SL, Rosenman JG, Symon JR, Cullip TJ and Chaney EL, The Tetrad and Hexad - Maximum Beam Separation As a Starting Point For Noncoplanar 3d Treatment Planning - Prostate Cancer As a Test Case. *International Journal of Radiation Oncology, Biology, Physics* **30**(2): 439-446, 1994.
7. Sherouse GW, A Mathematical Basis For Selection of Wedge Angle and Orientation. *Medical Physics* **20**(4): 1211-1218, 1993.
8. Soderstrom S and Brahme A, Which is the most suitable number of photon beam portals in coplanar radiation therapy? . *International Journal of Radiation Oncology, Biology, Physics* **33**(1): 151-9, 1995.
9. Pugachev A and Xing L, Computer assisted beam orientation selection in IMRT. *Physics in Medicine and Biology* **46**: 2467-2476, 2001.
10. Soderstrom S and Brahme A, Selection of suitable beam orientations in radiation therapy using entropy and Fourier transform measures. *Physics in Medicine and Biology* **37**(4): 911-924, 1992.
11. Pugachev A and Xing L, Computer Assisted Selection of Beam Energy and Orientations in IMRT. *International Journal of Radiation Oncology, Biology, Physics* **51**(3): 74, 2001.

12. Chen GT, Spelbring DR, Pelizzari CA, Balter JM, Myrianthopoulos LC, Vijayakumar S and Halpern H, The use of beam's eye view volumetrics in the selection of non-coplanar radiation portals. *International Journal of Radiation Oncology, Biology, Physics* **23**(1): 153-63, 1992.

13. Myrianthopoulos LC, Chen GT, Vijayakumar S, Halpern HJ, Spelbring DR and Pelizzari CA, Beam's eye view volumetrics: an aid in rapid treatment plan development and evaluation. *International Journal of Radiation Oncology, Biology, Physics* **23**(2): 367-75, 1992.

14. McShan DL, Fraass BA and Lichter AS, Full integration of the beam's eye view concept into computerized treatment planning. *International Journal of Radiation Oncology, Biology, Physics* **18**(6): 1485-94, 1990.

15. McShan DL, Kessler ML and Fraass BA, Advanced interactive planning techniques for conformal therapy: high level beam descriptions and volumetric mapping techniques. *International Journal of Radiation Oncology, Biology, Physics* **33**(5): 1061-72, 1995.

16. Meyer J, Mills JA, Haas OC, Burnham KJ and Parvin EM, Accommodation of couch constraints for coplanar intensity modulated radiation therapy. *Radiotherapy & Oncology* **61**(1): 23-32, 2001.

17. Webb S, Optimisation of conformal radiotherapy dose distributions by simulated annealing. *Physics in Medicine & Biology* **34**(10): 1349-70, 1989.

18. Rosen, II, Lam KS, Lane RG, Langer M and Morrill SM, Comparison of simulated annealing algorithms for conformal therapy treatment planning. *International Journal of Radiation Oncology, Biology, Physics* **33**(5): 1091-9, 1995.

19. Winkler G, *Image analysis, random field and dynamic Monte Carlo methods*. Springer-Verlag, Berlin, 1995.

20. Li J, Boyer A and Xing L, Clinical Implementation of Wedge Filter Optimization in 3D Radiotherapy Treatment Planning. *Radiotherapy & Oncology* **53**: 257-264, 1999.

21. Xing L and Chen GTY, Iterative algorithms for Inverse treatment planning. *Physics in Medicine & Biology* **41**(2): 2107-23, 1996.

22. Xing L, Hamilton RJ, Spelbring D, Pelizzari CA, Chen GT and Boyer AL, Fast iterative algorithms for three-dimensional inverse treatment planning. *Medical Physics* **25**(10): 1845-9, 1998.

23. Wu Q and Mohan R, Algorithms and functionality of an intensity modulated radiotherapy optimization system. *Medical Physics* **27**(4): 701-11, 2000.

24. Olivera GH, Shepard DM, Reckwerdt PJ, Ruchala K, Zachman J, Fitchard EE and Mackie TR, Maximum likelihood as a common computational framework in tomotherapy. *Physics in Medicine & Biology* **43**(11): 3277-94, 1998.

25. Rosen, II, Lane RG, Morrill SM and Belli JA, Treatment plan optimization using linear programming. *Medical Physics* **18**(2): 141-52, 1991.

26. Cho PS, Lee S, Marks RJ, 2nd, Oh S, Sutlief SG and Phillips MH, Optimization of intensity modulated beams with volume constraints using two methods: cost function minimization and projections onto convex sets. *Medical Physics* **25**(4): 435-43, 1998.

27. Mohan R, Wang X, Jackson A, Bortfeld T, Boyer AL, Kutcher GJ, Leibel SA, Fuks Z and Ling CC, The potential and limitations of the inverse radiotherapy technique. *Radiotherapy & Oncology* **32**(3): 232-48, 1994.

28. Xing L, Li JG, Donaldson S, Le QT and Boyer AL, Optimization of importance factors in inverse planning. *Physics in Medicine & Biology* **44**(10): 2525-36, 1999.

29. Xing L, Li JG, Pugachev A, Le QT and Boyer AL, Estimation theory and model parameter selection for therapeutic treatment plan optimization. *Medical Physics* **26**(11): 2348-58, 1999.

30. Cotrutz C, Lahanas M, Kappas C and Baltas D, A multiobjective gradient-based dose optimization algorithm for external beam conformal radiotherapy. *Physics in Medicine & Biology* **46**(8): 2161-75, 2001.

31. Gopal R and Starkschall G, Plan space: Representation of treatment plans in multidimensional space. *Medical Physics* **28**(6): 1227, 2001.

32. Rowbottom CG, Nutting CM and Webb S, Beam-orientation optimization of intensity-modulated radiotherapy: clinical application to parotid gland tumours. *Radiotherapy & Oncology* **59**(2): 169-77, 2001.

33. Haas OC, Burnham KJ and Mills JA, Optimization of beam orientation in radiotherapy using planar geometry. *Physics in Medicine & Biology* **43**(8): 2179-93, 1998.

34. Deasy JO, Multiple local minima in radiotherapy optimization problems with dose-volume constraints. *Medical Physics* **24**(7): 1157-61, 1997.

35. Llacer J and Deasy J, Multiple extrema in inverse radiation therapy planning. *Physics in Medicine and Biology* : submitted, 2001.

36. Winkler RL, *An Introduction to Bayesian Interference and Decision*. Holt, Rinehart & Winston, Inc., New York, 1972.

A. Simulated annealing optimization

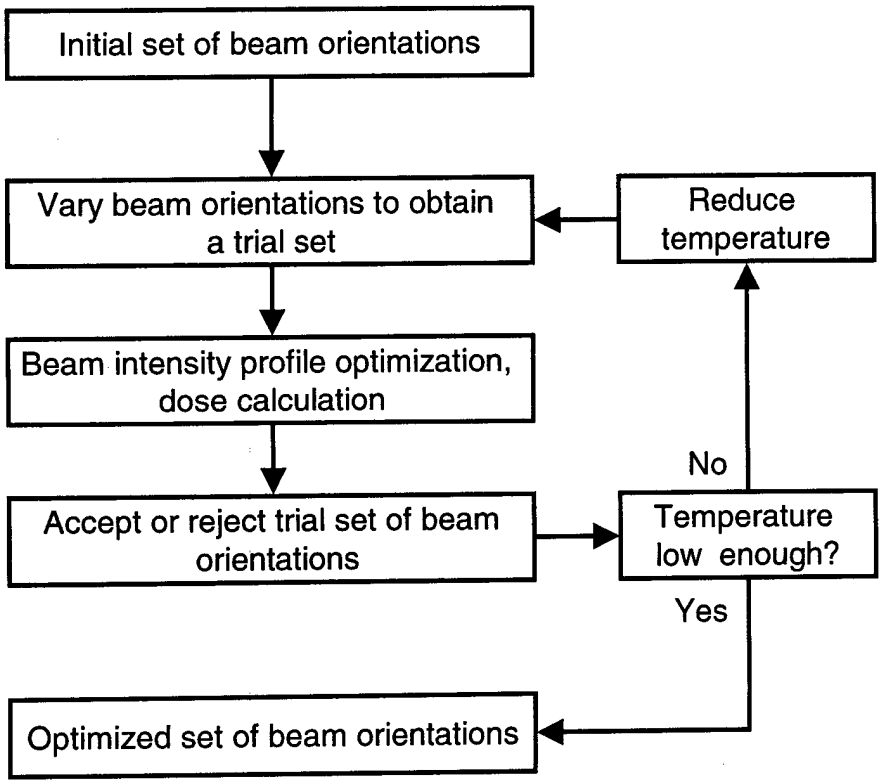

B. Beam orientation sampling

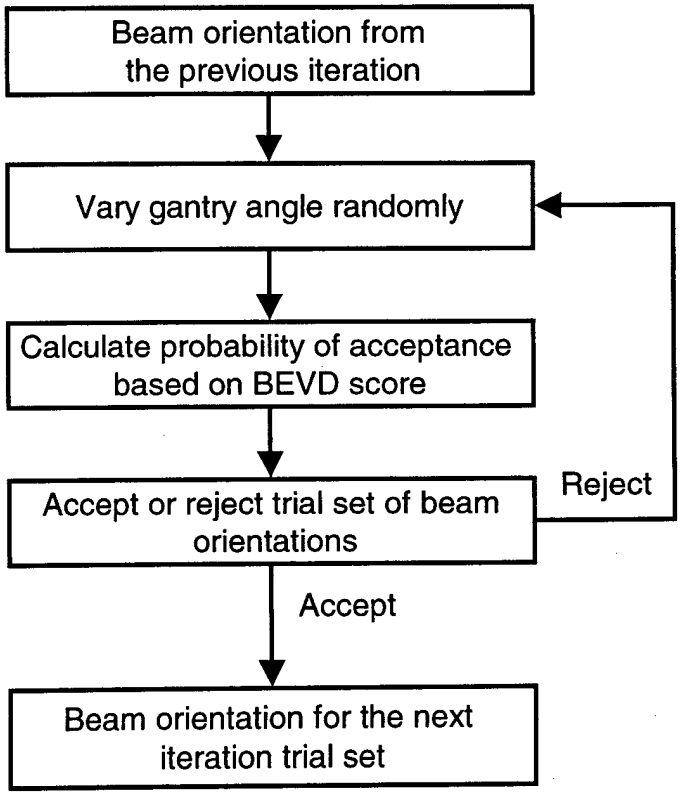

Fig. 1

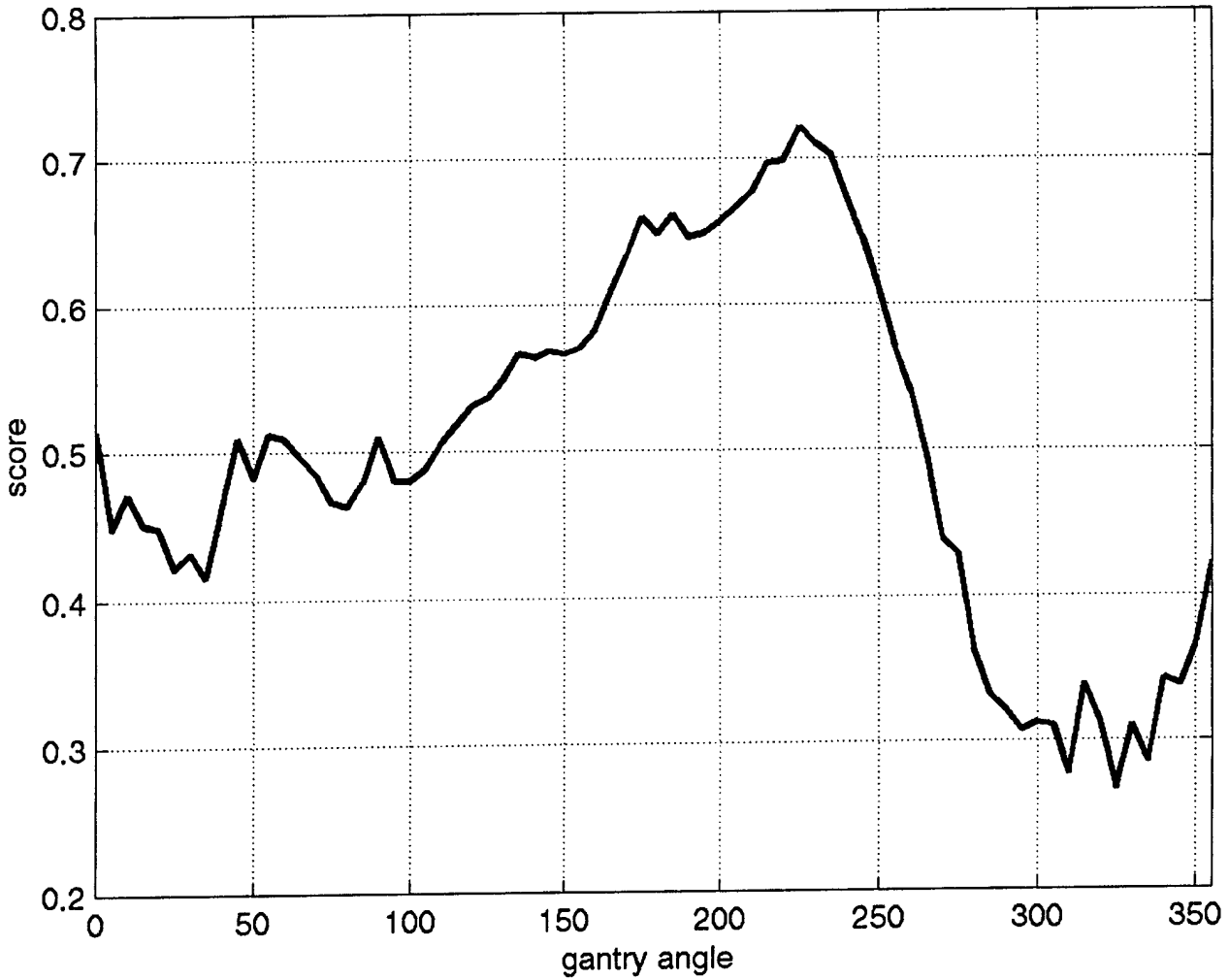
0.8
0.7
0.6
0.5
0.4
0.3
0.2
score
0
50
100
150
200
250
300
350
gantry angle

Fig. 2

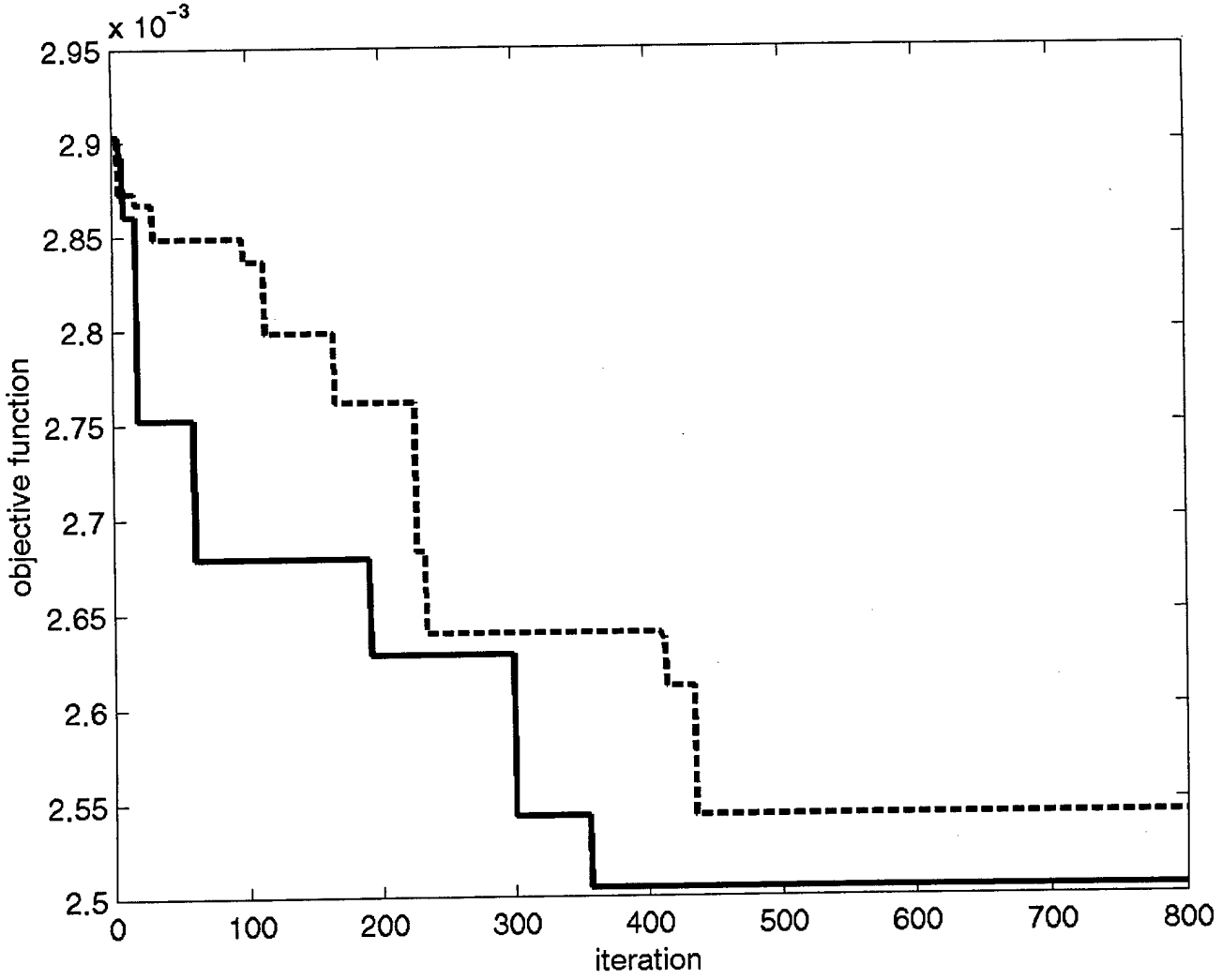
x 10^-3
2.95
2.9
2.85
2.8
2.75
2.7
2.65
2.6
2.55
2.5
objective function
0
100
200
300
400
500
600
700
800
iteration

Fig. 3

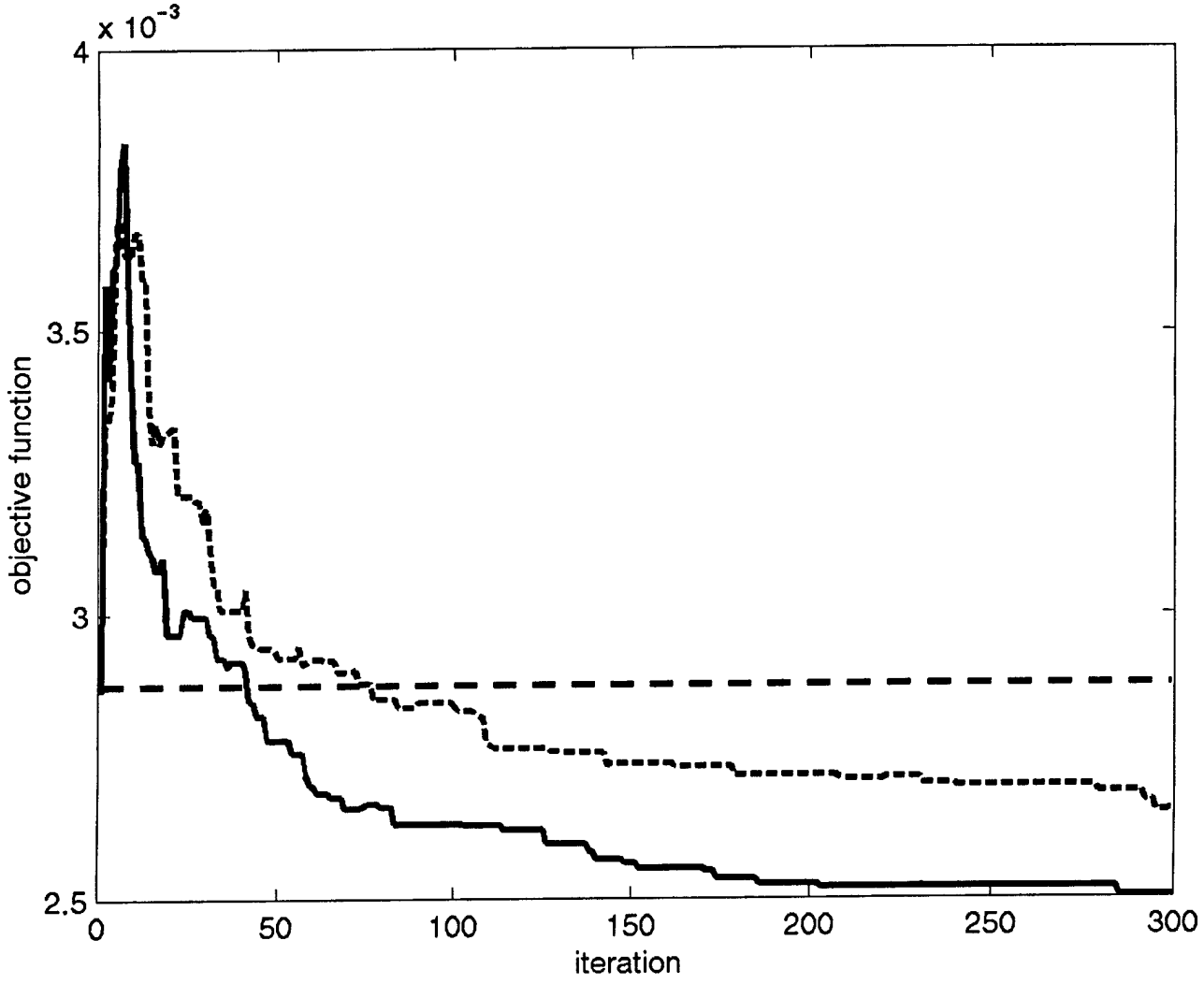
x 10^-3
4
3.5
3
2.5
objective function
0
50
100
150
200
250
300
iteration

Fig. 4

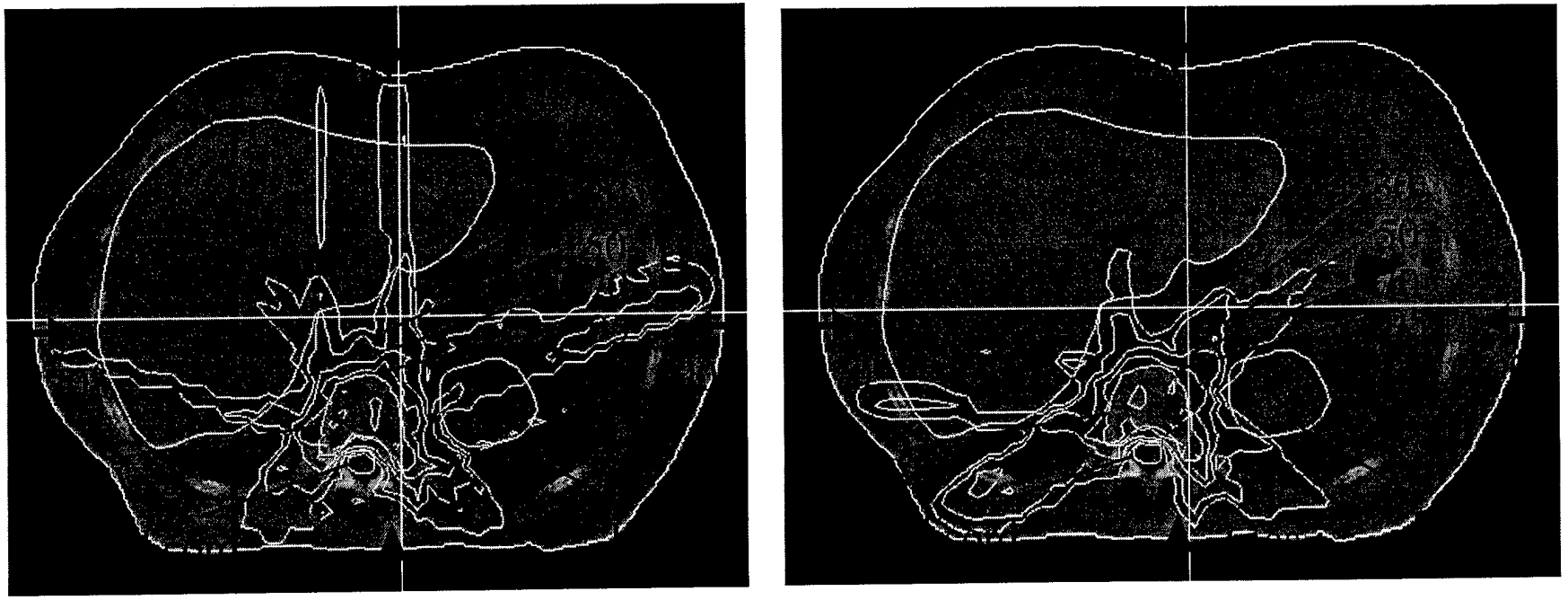

Fig. 5

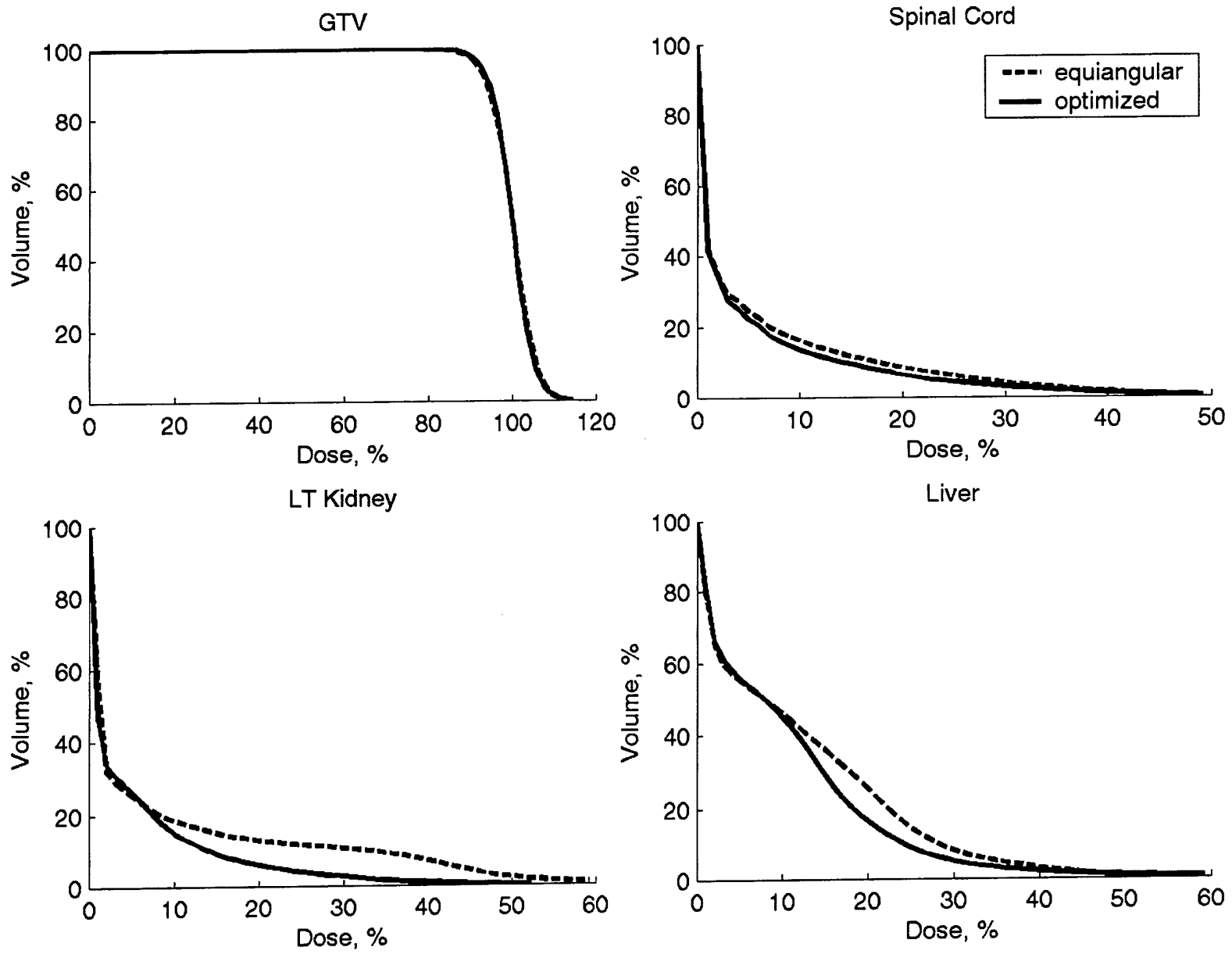
GTV
Volume, %
Dose, %
Spinal Cord
equiangular
optimized
LT Kidney
Liver

Fig. 6

IMRT dose shaping with regionally variable penalty scheme

Cristian Cotrutz , Ph.D. and Lei Xing[(a)], Ph.D.

Department of Radiation Oncology, Stanford University School of Medicine,
300 Pasteur Drive, Stanford CA 94305-5304, USA

Short Title: IMRT dose shaping

[a)]Author to whom correspondence should be addressed.

Stanford University School of Medicine
Department of Radiation Oncology
300 Pasteur Drive
Stanford, CA 94305-5304

E-mail: lei@reyes.stanford.edu
Phone: (650) 498 7896
Fax: (650) 498 4015

Submitted to: Medical Physics

ABSTRACT

A commonly known deficiency of currently available inverse planning systems is the difficulty in fine-tuning the final dose distribution. In practice, it is not uncommon that just a few unsatisfactory regions in the planning target volume (PTV) or an organ at risk (OAR) prevent an IMRT plan from being clinically acceptable. The purpose of this work is to introduce a mechanism for controlling the regional doses after a conventional IMRT plan is obtained and to demonstrate its clinical utility. Two types of importance factors are introduced in the objective function to model the tradeoffs of different clinical objectives. The first is the conventional structure-dependent importance factor, which quantifies the inter-structure tradeoff. The second type is the voxel-dependent importance factor which "modulates" the importance of different voxels within a structure. The planning proceeds in two major steps. Firstly a conventional inverse planning is performed, where the structure-dependent importance factors are determined in a trial-and-error fashion. The next level of planning involves fine-tuning the regional doses to meet specific clinical requirements. To achieve this, the voxels where doses need to be modified are identified either graphically on the isodose layouts, or on the corresponding DVH curves. The importance value of these voxels is then adjusted to increase/decrease the penalty at the corresponding regions. The technique is applied to two clinical cases. It was found that both tumor hot spots and critical structure maximal doses can be easily controlled by varying the regional penalty. One to three trials were sufficient for the conventionally optimized dose distributions to be adjusted to meet clinical expectation. Thus introducing the voxel-dependent penalty scheme provides an effective means for IMRT painting and sculpting of the dose distributions.

Key words: IMRT, dose optimization, importance factors, inverse planning.

I.- INTRODUCTION

Treatment planning requires the calculation of a set of parameters for the delivery of a certain radiation dose to the tumor. If IMRT is to be used, the number of physically feasible plans is huge, and efforts have been focused on the determination of the beamlet weights for pre-selected beam energies and beam configurations. Inverse planning is often used to derive the beam parameters with an objective function as the ranking criterion. Many attempts have been made in trying to construct clinically relevant objective functions, in linear, quadratic, and non-linear forms. They can be classified as dose-based[1-11] and biological-based models [12-14]. The former is concerned with accurate dose distributions and the latter argues that optimization can be guided by estimates of biological effects on considered tissues. In principle, the biologically based models are most relevant for plan ranking. However, the dose-response function of various structures is not sufficiently understood. At this point, the dose-based approach is still widely employed in practice whereas biological models are more often used for research. This is also evidenced by the fact that all commercial IMRT planning systems have chosen dose-based ranking as the starting point.

There exist many algorithms for inverse planning. In all cases, the optimizations are reported to be successful. To a large extent, the success is of a mathematical nature. Indeed, while investigating a few commercial IMRT planning systems at Stanford, we found that the plans computed by what are called optimization systems are not always within the expectation of the planner and that several trial-and-error adjustments of the system parameters might be required to achieve a clinically acceptable plan. Given a patient, the obtained plan can vary widely from one planer to the next, even within a department. Furthermore these IMRT treatment plans are often sub-optimal for patient treatments. If IMRT is to have a genuine and broad impact on radiation therapy, a more adaptable and "intelligent" inverse planning must be developed.

In our opinion, the underlying reason for the inverse planning to be an intractable process lies in the existence of multiple free parameters (e.g., the prescribed doses to the target and sensitive structures, the importance factors of various structures, beam orientations) in the current IMRT dose optimization formalisms, and the lack of a more explicit relation between these parameters and the final dose distribution. The determination of these parameters is essentially a "guessing" game and multiple trial-and-errors are often needed. The influence of the free parameters on the final solution is not known until the optimization is performed.

With the development of fast inverse planning algorithms and the advancement of computer technology, it is possible to computationally determine an optimal set of importance factors[15] or even to establish a computational environment in which the importance factors are adjusted interactively during the optimization process[16]. While facilitating the planning process, this approach is still not intuitive and transparent because of the implicit relation between the final plan and the parameters. On one hand, our plan selection decision-making is based on the visual evaluation of the isodose distribution or DVHs. On the other hand, in order to modify the dose at a region or to change the shape of a DVH curve, we need to go back to the beginning of plan optimization process and modify some parameters whose role to the dose in the region of interest is known only vaguely. In reality, it is this vagueness or ambiguity that makes the inverse planning process difficult to control and tedious. If we proceed along the above procedure, the best we can achieve is to lower/increase the overall dose to a structure. Therefore, lack of control over the local doses within a structure has been considered as one of the major problems in inverse planning.

The question that we ask here is: knowing the region(s) that is "hot" or "cold" for a given solution, or knowing the part of a DVH curve that we wish to modify, is it possible to directly identify the responsible parties in the parameter space and then vary them accordingly so that the dose distribution is improved toward our expectation? When this process is realized manually (that is, visually identifying the "hot" or "cold" regions on isodose plots or identifying the unsatisfactory part of a DVH curve using a computer mouse), it provides us with a natural adaptive planning environment. Toward establishing such an interactive planning environment, we introduce a new inverse-planning scheme in which the importance factors are defined on a voxel specific basis rather than on an anatomical structure basis. The new scheme provides an adaptive mechanism to fine-tune the local doses and enables us to adaptively search for plans that otherwise would be unreachable.

This paper is organized as follows. In Sec. II we provide some background knowledge on the modeling of the tradeoff strategies in inverse planning and summarize the useful features of the voxel-dependent tradeoff scheme. Issues related to the implementation of the voxel-dependent penalty scheme are also described. To demonstrate the utility of the new inverse-planning scheme, we have applied it to study two clinical cases. The results will be summarized in Sec. III along with some in-depth discussion. We conclude in Sec. IV.

II.- METHODS AND MATERIALS

In inverse planning, dose optimization is performed under the guidance of an objective function, which is defined as a global quantity derived from general physical considerations. Because the clinical objectives are usually multifaceted and potentially incompatible with one another, a set of structure-dependent importance factors[14,17,18] is often incorporated in the objective function to parameterize the trade-off strategies. After an "optimal" plan is computed for a trial set of importance factors, there are generally two types of dose modifications that may be needed in the target volume or a sensitive structure. One is the overall dose in a structure and the other is the dose in one or more sub-volumes of a structure. The former modification is generally handled by the trial-and-error adjustments of structure-specific importance factors. The latter situation occurs quite frequently in clinical IMRT planning and is problematic. In practice, it is not uncommon that just a few unsatisfactory regions of the target volume or a sensitive structure prevent an optimized plan from being clinically acceptable. For instance, in a prostate IMRT treatment, one may wish to control more freely the dose to the urethra and perhaps the dose at the prostate-rectum boundary. Unfortunately, with the structure-specific importance factors, the system is under-determined and the best we can do is to adjust the structure specific importance that influence not only the dose in the region of concern, but also in other part of the system.

The key to enhance the degree of controllability over the regional doses is to establish a more effective link between the local dosimetric behavior of the system and the system variables. These types of system variables, however, are not defined within the currently available inverse planning systems. Parameters, such as importance factors and prescription doses are structure specific, and thus cannot be used to effectively control the doses on a sub-structural level. To solve this dilemma, we introduce voxel-dependent importance factors into the inverse planning as a means to control the intra-structural tradeoffs and describe a manual planning method in which the local importance factors are adaptively modified to meet our clinical requirements. With the use of the voxel-based penalty scheme, the regional penalty will not depend only on the dose discrepancy between prescription and calculated doses but also on the local importance information, which is based on *a priori* or *a posteriori* knowledge.

To proceed along the line described above, we write the importance factor at a voxel n as a product of two factors, an overall factor specific to the structure σ, r_σ, and a voxel dependent

component describing the relative weighting of different voxels inside the structure, r_n. The r_σ's parameterize the overall tradeoff strategy of different structures, whereas r_n's characterize the inner-structural weightings. The conventional quadratic objective function now reads:

$$F = \sum_{\sigma=1}^{n_\sigma} \left[\frac{1}{N_\sigma} \sum_{n=1}^{N_\sigma} r_\sigma \cdot r_n \cdot [D_c(n) - D_0(n)]^2 \right] \qquad (1)$$

where N_σ represents the total number of voxels of a structure, $D_0(n)$ is the prescription dose and $D_c(n)$ is the calculated dose at each iteration. The dose calculation algorithm has been described in Ref. [19]. While a quadratic objective function is used in this work, the methodology of using voxel-dependent importance factors to fine-tune an IMRT dose distribution is quite general and can be integrated to enhance the performance of any existing inverse planning algorithms.

The overall planning process is schematically presented in figure 1. The first step is the conventional inverse planning, where all r_n's are set to unity and r_σ's are adjusted in the traditional trial-and-error fashion. For a given set of $\{r_\sigma\}$, the beam profiles are optimized using a gradient search algorithm[18]. Upon the completion of conventional IMRT dose optimization, we usually reach a point near the clinically acceptable solution and the remaining is to fine-tune the regional doses according to clinical requirements. This is where local importance factors are "switched-on" and start playing a role. The two types of improvements commonly needed at this stage are: (1) to increase/decrease the doses in one or a few particular sub-volumes of the target or a sensitive structure; and (2) to differentially modify the fractional volume or number of voxels falling into one or a few DVH dose bins of the target or a sensitive structure. For the former type of fine-tuning, we visually inspect the isodose layouts and outline with a computer mouse the region(s) where dose(s) needs to be modified. In the latter situation, we graphically locate the interval(s) on the DVH curve(s) and then the voxel indices associated with the selected dose bins are identified. In either case, once the region(s) of interest (ROI) is identified, the next step is to increase/decrease the local importance factors of the involved voxels to drive the doses of the ROI toward our clinical expectation. Obviously, increasing the values of the local importance factors will increase the penalty level at the considered voxels and the resulting dose distribution will better comply with the prescription of the region, and *vise versa*. The amount of change in the local importance factors is empirical and we usually proceed by assigning a value of 15~100%

higher/lower than their previous ones after the corresponding voxels are identified. For every change in the importance factors, the dose is re-optimized and the plan is then re-evaluated. The fine-tuning process proceeds in an iterative fashion, as shown in figure 1. The adjustment of the local importance factors can be performed sequentially or simultaneously for a few structures. According to our experience, one to three iterations are often sufficient to significantly improve the conventional inverse planning solution.

III.- RESULTS & DISCUSSION

The technique proposed for IMRT dose shaping was tested using a prostate case and a paraspinal tumor case. Several clinically relevant scenarios were investigated and the results are summarized as follows.

III.1. Six-Field IMRT Treatment of a Prostate Cancer

The first study involved a prostate cancer. The sensitive structures relevant to this study included rectum, bladder and femoral heads. The IMRT treatment used six co-planar beams with gantry angles of 0, 55, 135, 180, 225 and 305 degrees in IEC convention. Using the conventional inverse planning procedure we obtained a set of optimal structure specific importance factors that are listed in Table 1, along with the relative prescription doses used for the optimization. The DVHs of the structures involved in the conventional inverse plan are shown in Figure 2(a)-(e) in gray solid lines.

III.1.1. DVH-based fine-tuning of prostate underdosage

Inspecting the target DVH shown in Fig. 2a, we noticed that a fairly large fraction of the prostate volume receives a dose less than 88% of the prescription. Assuming that our clinical objective is to increase the fractional prostate volume receiving a dose less than 88% (shown between the two vertical lines in Figure 2a), two successive fine-tunings were performed. In the first attempt, based on the DVH data, we identified the responsible voxels and assigned to them a higher importance, r_n=2.0. The black solid lines in figure 2 show the optimization results after this trial. The second attempt was made to further improve the prostate coverage. For this purpose, we re-identified the voxels that were still under dosed (below 88%) after the first trial and further increase the importance of the newly identified voxels to 3.0. The results after re-optimization are shown as dotted lines. Figures 2(b)-(e) show the effect of increasing

the local importance factors on the DVHs of the involved sensitive structures. As can be seen from Fig. 2, by using the local importance factors we were able to fine-tune the target doses flexibly. For instance, the prostate volume covered by the 85% isodose curve was increased by 5% after the two trials. In Figure 3 we show the 85% isodose lines corresponding to the three optimized plans. The isodose line corresponding to the plan obtained with the largest voxel-based importance factors has the best target coverage and this is most distinct at the left posterior part of the prostate target.

A noticeable fact is that the bladder and rectum suffered minor but practically insignificant changes when the local importance factors in prostate were increased. The differences in the femoral head doses might be important, especially in the left one, where approximately 40% more of its volume got irradiated as the prostate dose coverage was improved. Physically, this effect was produced by the intensity increase in a set of beamlets in the left anterior beam (gantry angle 55 degree). This phenomenon is interesting and reminds us that, in dose optimization, there is generally no net gain. That is, the improvement in the dose to a structure is often accompanied by the dosimetrically adverse effect(s) at other points in the same or different structures. The important point to note is that from the clinical point of view, some dose distributions are more acceptable than others and our goal is to find the solution that most improves the plan, with a clinically insignificant or acceptable sacrifice. In order to achieve this, it is necessary to have a direct control degree over the regional doses. In this sense we believe that the hereby-proposed method of dose shaping is valuable.

III.1.2. Dose layout-based fine-tuning of hot spots in the prostate target

The second scenario considered here was the reduction of a hot spot within the prostate target. Inspecting the target DVH shown in figure 2a, it is seen that there is a small number of voxels in the prostate that receive a dose higher than 106%. This is more clearly seen in the dose layout shown in Fig. 4, where two hot spots are found. Assuming that our clinical objective now is to reduce the doses to these two hot spots, particularly to the one near the center of the prostate. For this purpose, we graphically identified the hot regions and then assigned a higher importance (r_n=2.0 in the first attempt, and 3.0 in the 2nd attempt) to the corresponding voxels. Figure 5 shows the isodose distribution after two trials. The hot spot near the urethra disappeared and the size of the other hot spot was reduced significantly. This improvement is also evident in the DVH shown in figure 6(a). The gray curves in figures 6(a)-(e) correspond to the conventionally optimized plan (r_σ = 1.0) while the plans obtained by introducing voxel-

importance factors are shown with black solid lines (r_n = 2.0) and dotted lines (r_n = 3.0), respectively. As the value of r_n increases, the role of the selected voxels becomes more important, forcing the system to satisfy the dosimetric requirements at the selected voxels. Similar to the precedent scenario, the DVHs of bladder and rectum remained practically unchanged after the dose shaping. The major difference occurred at the left femoral head.. As expected, in order to reduce the doses to the hot regions of the conventional plan, the intensity of the beamlets affecting both the femoral heads and the prostate (the hot regions) became smaller. Accordingly, the dose to the intervening femoral head was reduced. This is opposite to the effect described in Sec. III.1.1, where the goal was to reduce the underdosage in the prostate. Nevertheless, the improvements in both cases were accomplished without violating the constraint of the left femoral head.

III.2. Five-field IMRT treatment of a paraspinal tumor

The method described in this paper was also applied to a challenging IMRT boost treatment of a metastatic tumor at the tenth vertebra body with the spinal cord adjacent to it (figure 7). We planned a dose distribution that covered the tumor volume as uniformly as possible, while trying to spare the spinal cord, liver and kidney. The target dose was 16 Gy. A concern for this case was the dose to the spinal cord because the patient had already been treated with conventional techniques without cord sparing. In this study, five 6MV non-equally spaced coplanar beams (95, 140, 175, 225 and 275 degrees--respecting the IEC convention) were used for the treatment. The structure specific importance factors and the prescription doses are shown in Table 2. The DVHs of the conventional IMRT plan are plotted with gray lines in figure 8.

As the patient was treated previously, one of the clinical concerns was the dose to the spinal cord. To reduce the maximum spinal cord dose, we identified the corresponding voxels that received doses in the 60-70% interval (marked with vertical lines in figure 8) and assigned them with a higher importance, r_n=3.0. After re-optimization we obtained the DVHs shown by the black solid lines in figure 8. While the maximum spinal cord dose was reduced by 10% and the DVHs of the other two structures (liver and kidney) suffered only slightly. The tumor coverage becomes worse than that of the conventional optimized plan, as a consequence of reducing the spinal cord dose. This is similar to the scenario discussed in Sec. III.1.1.

We would like to emphasize here that the IMRT solution space is greatly enlarged when voxel-based importance factors are permitted. In fact, the conventional planning scheme with

uniform importance factors is a special case of the voxel-dependent importance scheme. The voxel-based planning scheme allows us to obtain solutions that would be otherwise non-attainable. To give an example, we used the conventional inverse planning regime to reduce the spinal cord dose by simply increasing the overall importance of the spinal cord. For fair comparison, we have attempted to make the tumor DVH the same as for the plan fine-tuned by modulating local importance factors (e.g., dotted lines in figure 8). The two sets of DVHs are shown in figure 8 along with the original IMRT plan. In general, the voxel-based planning scheme produced a solution that follows more closely our expectation, that is, to differentially reduce the fractional cord volume that receives a dose higher than 60% of the prescription. This is reflected by two things: (1) for the same tumor coverage, the reduction of the maximum spinal cord dose is greater in the plan obtained using voxel dependent importance factors; and (2) in comparison to the new plan with structure specific importance (dotted line), the DVH curve obtained using voxel-based importance factors deviated less from the original plan (black solid line) in the part that is specified (implicitly) not to change.

IV.- CONCLUSIONS

Inverse planning is at the foundation of IMRT and its performance critically determines the success of an IMRT treatment. Unfortunately, the currently available IMRT dose optimization formalism is deficient and the solutions resulting from the so-called "optimization" systems are often sub-optimal or even not optimal at all. Considerable effort may be required to compute a clinically acceptable plan and the final results may strongly depend on the planner's experience and understanding of the planning system. We have proposed and demonstrated an interactive inverse-planning scheme with voxel-dependent importance factors. The approach offers the planner an effective tool to fine-tune an IMRT dose distribution and makes the dose optimization process more tractable and controllable. While the local penalty was varied by the local importance factors, in practice we believe that it is also possible to achieve the same or similar effect by other means, *e.g* by changing the form of the penalty function. Finally, we mention that the inverse planning formalism proposed in this paper is quite broad and has many co-lateral applications. With minor modifications, the technique should be directly applicable to improve the dose optimization in many other radiation therapy modalities, such as prostate implantation, gamma knife, micro-MLC based stereotactic radiosurgery, and other variants of IMRT, such as tomotherapy, intensity modulated arc therapy, hybrid treatment of IMRT with electron or brachytherapy.

ACKNOWLEDGEMENTS

We wish to thank Drs. Steven Hancock, Sarah Donaldson, Quynh-Thu Le, Christopher King, Arthur Boyer and Gary Luxton for many useful discussions on the subject. This work was partly supported by a Research Scholar Award from the American Cancer Society (RSG-01-022-01-CCE) and a research grant from the Department of Defense (BC996645).

REFERENCES

[1]T. Bortfeld, J. Burkelbach, R. Boesecke and W. Schlegel, "Methods of image reconstruction from projections applied to conformation radiotherapy," Physics in Medicine & Biology **35** (10), 1423-34 (1990).

[2]S. Webb, "Optimisation of conformal radiotherapy dose distributions by simulated annealing [published erratum appears in Phys Med Biol 1990 Feb;35(2):297]," Physics in Medicine & Biology **34** (10), 1349-70 (1989).

[3]S. M. Morill, R. G. Lane, J. A. Wong and Rosen, II, "Dose-volume considerations with linear programming optimization," Medical Physics **18** (6), 1201-10 (1991).

[4]Rosen, II, R. G. Lane, S. M. Morrill and J. A. Belli, "Treatment plan optimization using linear programming," Medical Physics **18** (2), 141-52 (1991).

[5]L. Xing and G.T.Y. Chen, "Iterative algorithms for Inverse treatment planning," Physics in Medicine & Biology **41** (2), 2107-23 (1996).

[6]S. V. Spirou and C. S. Chui, "A gradient inverse planning algorithm with dose-volume constraints," Medical Physics **25** (3), 321-33 (1998).

[7]G. H. Olivera, D. M. Shepard, P. J. Reckwerdt, K. Ruchala, J. Zachman, E. E. Fitchard and T. R. Mackie, "Maximum likelihood as a common computational framework in tomotherapy," Physics in Medicine & Biology **43** (11), 3277-94 (1998).

[8]Q. Wu and R. Mohan, "Algorithms and functionality of an intensity modulated radiotherapy optimization system," Medical Physics **27** (4), 701-11 (2000).

[9]T. Holmes and T. R. Mackie, "A comparison of three inverse treatment planning algorithms," Physics in Medicine & Biology **39** (1), 91-106 (1994).

[10]G Starkschall, A Pollak and CW Stevens, "Treatment Planning using a dose-volume feasibility search algorithm," Int J Radiat Oncol Biol Phys **49** (5), 1419-27 (2001).

[11]P. S. Cho, S. Lee, R. J. Marks, 2nd, S. Oh, S. G. Sutlief and M. H. Phillips, "Optimization of intensity modulated beams with volume constraints using two methods: cost function minimization and projections onto convex sets," Medical Physics **25** (4), 435-43 (1998).

[12]R. Mohan, G.S. Mageras, B. Baldwin, L.J. Brewster, G.J. Kutcher, S. Leibel, C.M. Burman, C.C. Ling and Z. Fuks, "Clinically relevant optimization of 3D conformal treatments," Medical Physics **19**, 933-944 (1992).

[13]A. Brahme, "Optimized radiation therapy based on radiobiological objectives," Seminars in Radiation Oncology **9** (1), 35-47 (1999).

[14]XH Wang, R Mohan, A Jackson, SA Leibel, Z Fuks and CC Ling, "Optimization of intensity-modulated 3D conformal treatment plans based on biological indices," Radiother Oncol **37** (2), 140-52 (1995).

[15]L. Xing, J. G. Li, A. Pugachev, Q. T. Le and A. L. Boyer, "Estimation theory and model parameter selection for therapeutic treatment plan optimization," Medical Physics **26** (11), 2348-58 (1999).

[16]L. Xing, J. G. Li, S. Donaldson, Q. T. Le and A. L. Boyer, "Optimization of importance factors in inverse planning," Physics in Medicine & Biology **44** (10), 2525-36 (1999).

[17]L. Xing, C. Pelizzari, F. T. Kuchnir and G. T. Chen, "Optimization of relative weights and wedge angles in treatment planning," Medical Physics **24** (2), 215-21 (1997).

[18]C. Cotrutz, M. Lahanas, C. Kappas and D. Baltas, "A multiobjective gradient-based dose optimization algorithm for external beam conformal radiotherapy," Physics in Medicine & Biology **46** (8), 2161-2175 (2001).

[19]C. Cotrutz, C. Kappas, Y. Theodorakos, C. Makris and R. Mohan, "Development in a Windows environment of a radiation treatment planning system for personal computers," Computer Methods & Programs in Biomedicine **56**, 261-72 (1998).

FIGURE CAPTIONS

Figure 1: Flow chart of the interactive inverse planning process with voxel-dependent importance factors.

Figure 2: DVHs of: Prostate (a); Bladder (b); Rectum (c); Right Femoral Head (d) and Left Femoral Head (e). The gray lines represent the conventional IMRT plan; the black solid and dotted lines correspond to plans optimized with regional importance factors of 2 and 3, respectively. These values were assigned for those voxels accounted within the vertical lines in 2a.

Figure 3: Isodose plot showing the 85% isodose lines of the three IMRT plans: the inner isodose corresponds to the conventional optimization and the outer lines to the optimizations performed with values of the regional importance factors of r_n=2 and r_n=3, respectively.

Figure 4: Dose distribution of the conventional prostate IMRT plan. Two hot spots of 106% are present within the prostate.

Figure 5: Prostate dose distribution after dose shaping by increasing the regional importance factors. The left 106% hot spot in Figure 4 disappeared completely while the size of the second one was reduced considerably.

Figure 6: DVHs of: Prostate (a); Bladder (b); Rectum (c); Right Femoral Head (d) and Left Femoral Head (e) for three IMRT plans. The gray lines represent the conventional plan; the black solid and dotted lines correspond to plans optimized with voxel importance factors of 2 and 3, respectively. These values were assigned for those voxels accounted within the 105-110% dose interval (vertical lines in figure 6a).

Figure 7: Isodose distribution of a paraspinal IMRT treatment plan.

Figure 8: Comparison of three IMRT plans: gray solid lines show the DVHs for a conventional IMRT plan which was subsequently re-optimized using regional importance factors (black solid lines). The third plan (dotted lines) is obtained conventionally, by raising the importance of the spinal cord structure, until the target DVH became similar to the re-optimized plan (black solid lines).

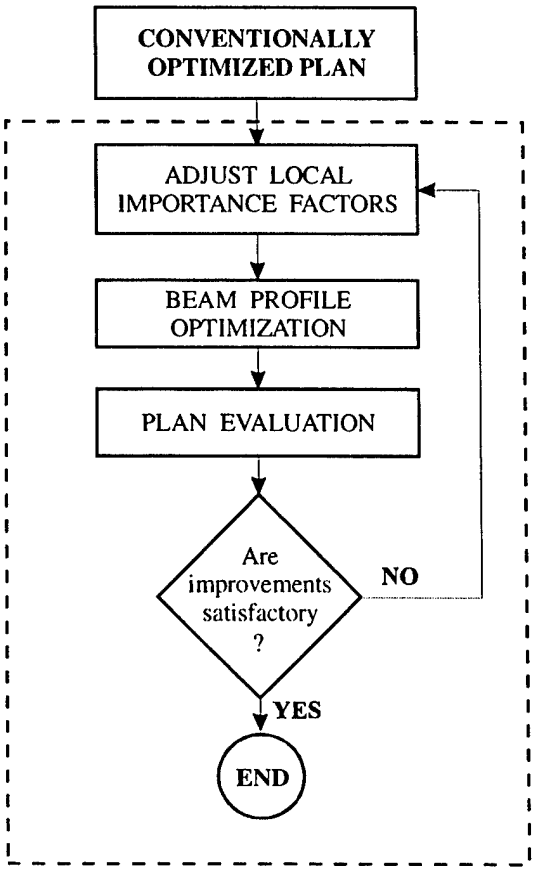
CONVENTIONALLY OPTIMIZED PLAN
ADJUST LOCAL IMPORTANCE FACTORS
BEAM PROFILE OPTIMIZATION
PLAN EVALUATION
Are improvements satisfactory ?
NO
YES
END

Figure 1

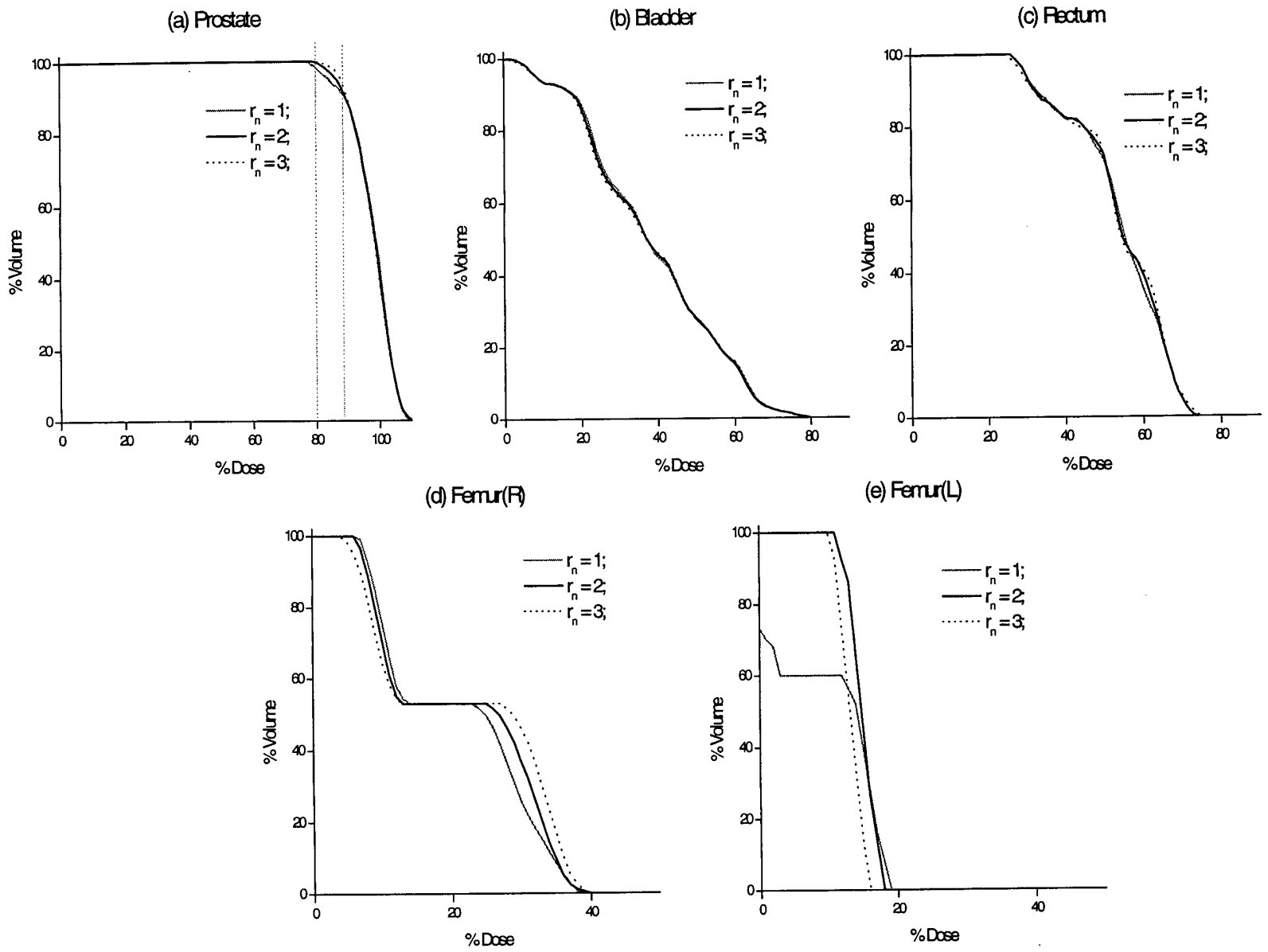
(a) Prostate
(b) Bladder
(c) Rectum
(d) Femur(R)
(e) Femur(L)
% Volume
% Dose
$r_n = 1$;
$r_n = 2$;
$r_n = 3$;

Figure 2

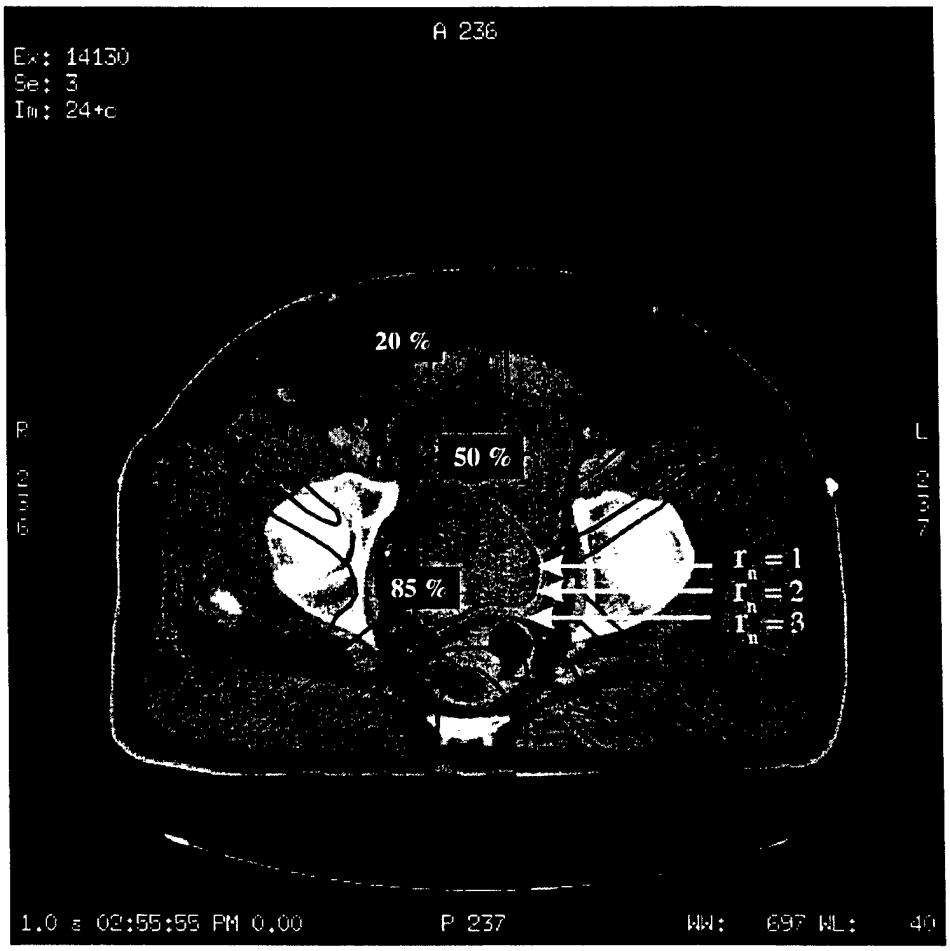
A 236
Ex: 14130
Se: 3
Im: 24+c
20 %
50 %
85 %
$r_n = 1$
$r_n = 2$
$r_n = 3$
P
L
1.0 s 02:55:55 PM 0.00
P 237
WW: 697 WL: 40

Figure 3

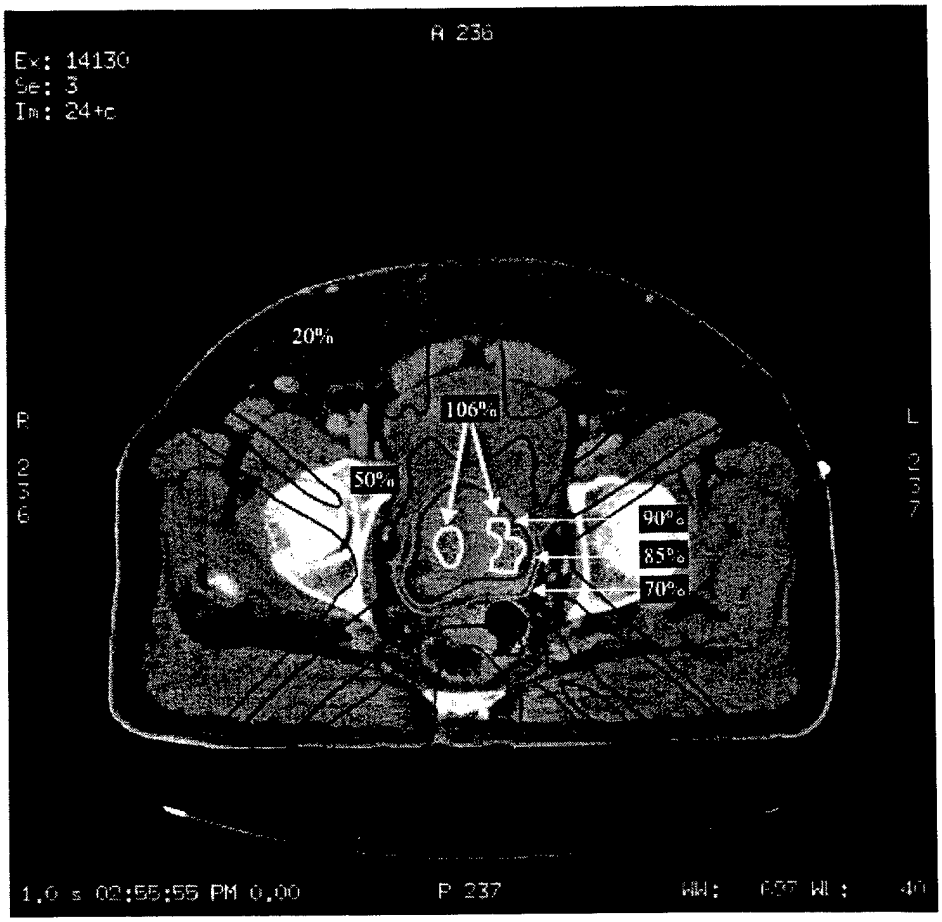
A 236
Ex: 14130
Se: 3
Im: 24+c
20%
106%
50%
90%
85%
70%
P
L
1,0 s 02:55:55 PM 0,00
P 237
WW:
WL :

Figure 4

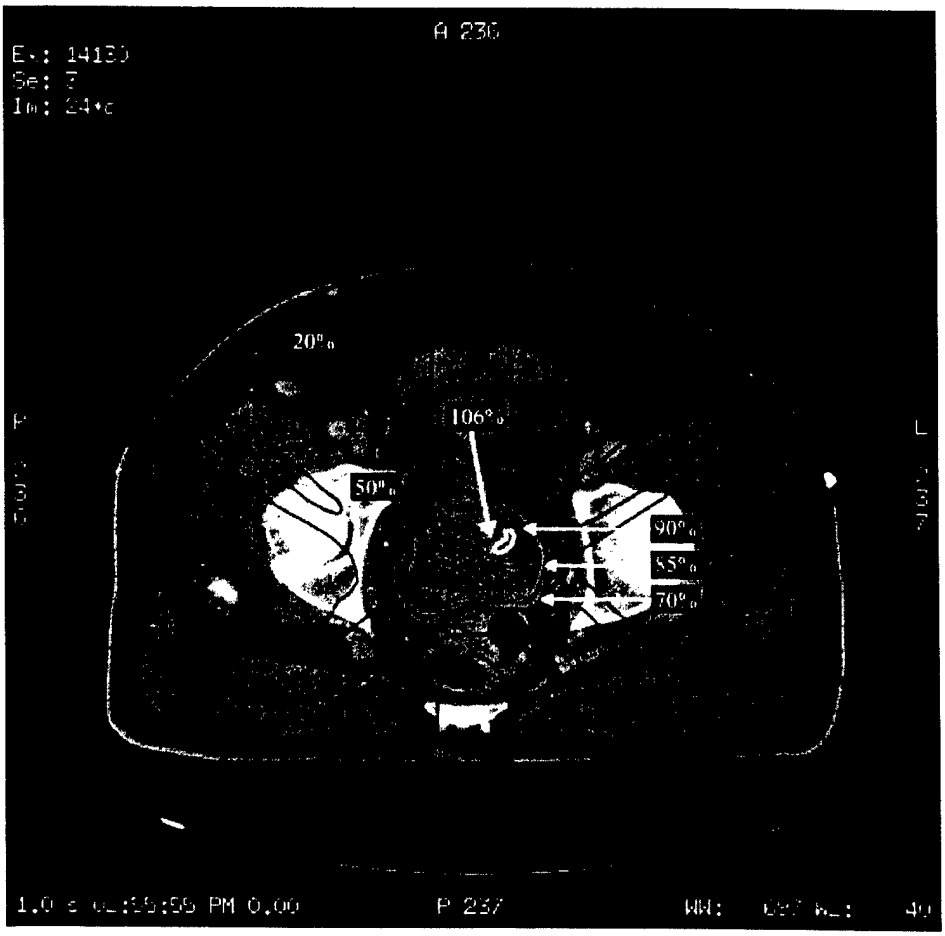

Figure 5

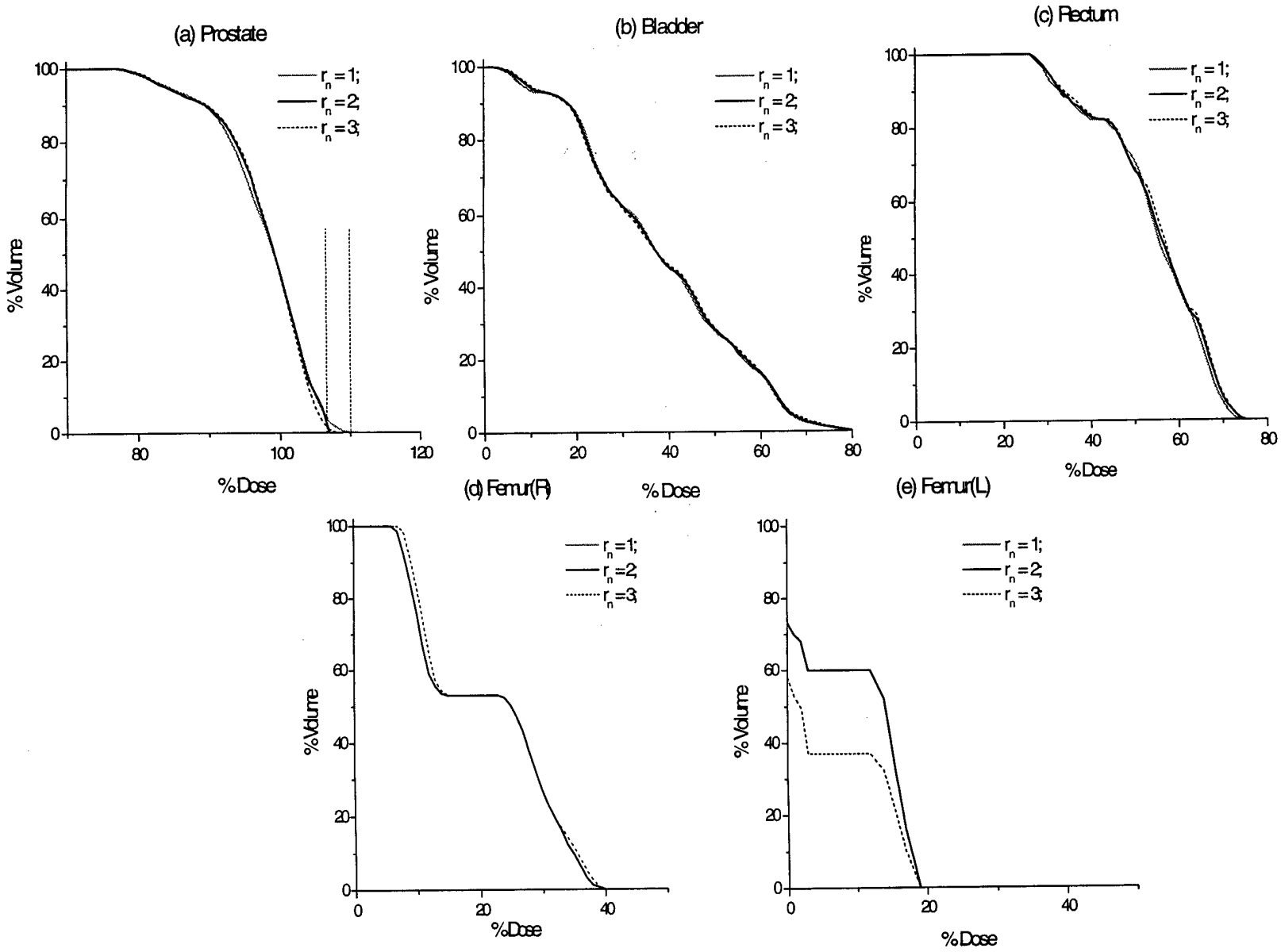
(a) Prostate
(b) Bladder
(c) Rectum
(d) Femur(R)
(e) Femur(L)
% Volume
%Dose
$r_n = 1$;
$r_n = 2$;
$r_n = 3$;

Figure 6

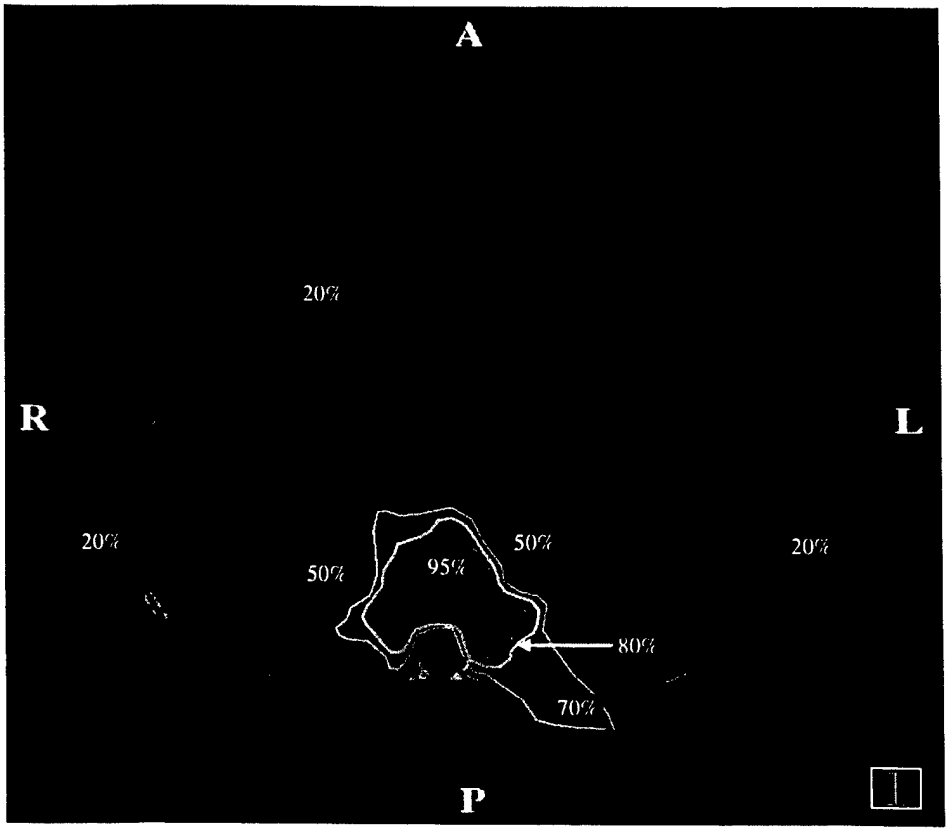

Figure 7

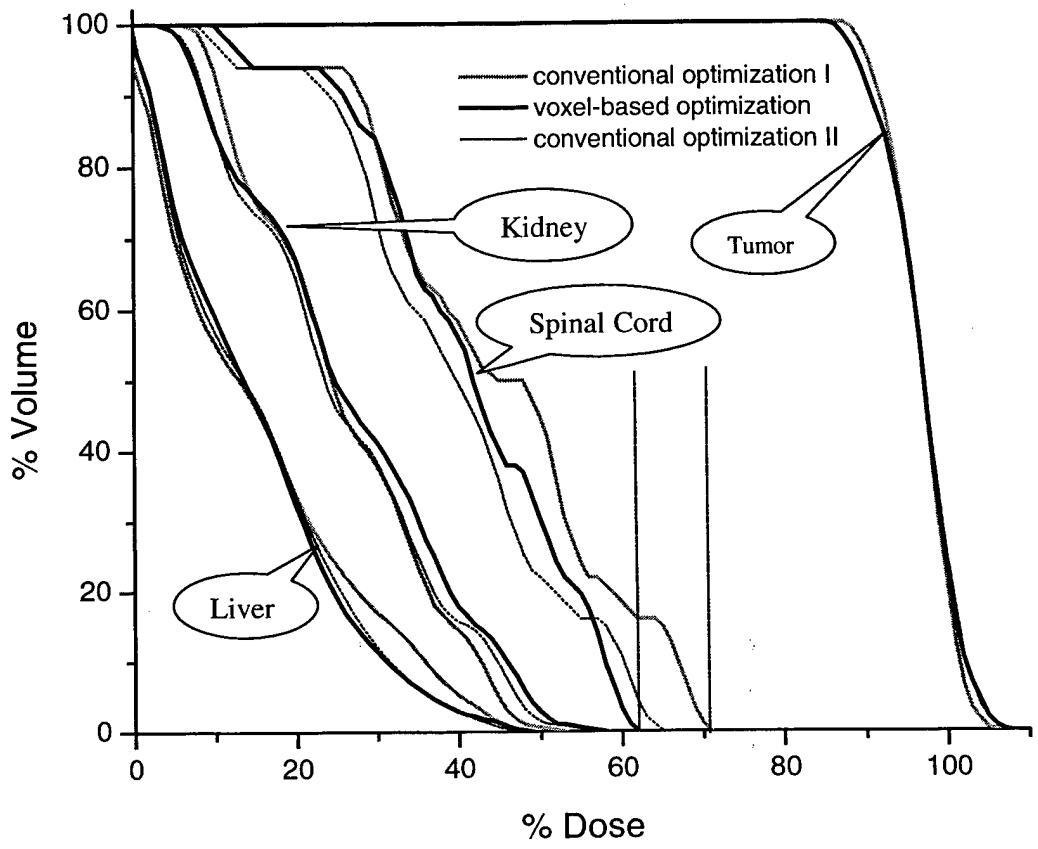
conventional optimization I
voxel-based optimization
conventional optimization II
Kidney
Tumor
Spinal Cord
Liver
% Volume
% Dose
0
20
40
60
80
100

Figure 8

Table I: Summary of the parameters used for obtaining the prostate conventional optimized plan.

	Relative importance factors	Target prescription and OAR tolerance doses
GTV	0.20	1.00
Bladder	0.05	0.60
Rectum	0.05	0.65
Femural Head (R)	0.05	0.45
Femural Head (L)	0.05	0.45
Tissue	0.60	0.60

Table II: Summary of the parameters used for obtaining the paraspinal tumor conventional optimized plan.

	Relative importance factors	Target prescription and OAR tolerance doses
GTV	0.860	1.00
Spinal Cord	0.030	0.30
Liver	0.005	0.40
Kidney	0.050	0.30
Tissue	0.055	0.75

Incorporating leaf transmission and head scatter corrections into step-and-shoot leaf sequences for IMRT

Yong Yang, Ph.D. and Lei Xing[a)], Ph.D.

Department of Radiation Oncology, Stanford University School of Medicine,

Stanford, CA 94305-5304

[a)] Author to whom correspondence should be addressed:

Department of Radiation Oncology
Stanford University School of Medicine,
300 Pasteur Drive, A0-40
Stanford, CA 94305-5304
Telephone: (650) 498-7896
Fax: (650) 498-4015
Email: lei@reyes.stanford.edu

Submitted to: International Journal of Radiation Oncology, Biology, Physics

Purpose: Leaf transmission and head scatter are two important factors that influence IMRT delivery and should be correctly taken into account when generating MLC leaf sequences. Significant discrepancies between the desired and delivered intensity profiles could otherwise be resulted. The purpose of this work is to propose a reliable algorithm to minimize the dosimetric effects caused by the two factors in step-and-shoot mode.

Methods and Materials: The goal of the algorithm is to minimize the difference between the desired fluence map and actually delivered fluence map. For this purpose, an error function, defined as the least-square difference between the desired and the delivered fluence maps, is introduced. The effects of transmission and head scatter are minimized by adjusting the factional MUs in the initial MLC leaf sequences, created by using the desired fluence map without inclusion of the contributions from the two factors. Computationally, a downhill simplex optimization method is used to minimize the error function with respect to the fractional MUs. A three-source model is used to evaluate the relative head scatter distribution for each segment at the beginning of the calculation. The algorithm has been assessed by comparing the dose distributions delivered by the corrected leaf sequence files and the theoretical predication, calculated by Monte Carlo simulation using the desired fluence maps, for an intuitive test field and several clinical IMRT cases.

Results: The deviations between the desired fluence maps and the ones calculated using the corrected leaf sequence files are less than 0.3% of the maximum MU for the test field and less than 1.0% for the clinical IMRT cases. The experimental data show that both absolute and relative dose distributions delivered by the corrected leaf sequences agree with the desired ones within 2.5% of the maximum dose or 2mm in high dose gradient regions. Compared with the results obtained by using the leaf sequences in which only the transmission or none of the two effects is corrected, significant improvements in the fluence and dose distributions have been observed.

Conclusions: Transmission and head scatter play important roles in the dosimetric behavior of IMRT delivery. A larger error may be resulted if only one factor is considered due to the opposite effects of the two factors. We noted that, the influence of the two effects is more pronounced in absolute dose than in the relative dose. The algorithm proposed in this work accurately corrects for these two effects in step-and – shoot delivery and provides a reliable tool for clinical IMRT application.

Key word: MLC, head scatter, step-and -shoot mode, leaf sequences, IMRT

Introduction

Intensity modulated radiation therapy (IMRT) can be effectively delivered using a multileaf collimator (MLC) either in segmental mode (SMLC, also called step-and-shoot mode)(1-4) or in dynamic mode (DMLC)(5-8). In the SMLC mode, each intensity-modulated beam is delivered by a sequence of segments of different shapes formed by the MLC leaves and the beam is off while the leaves move from one segment to another. In the DMLC mode, however, the intensity-modulated beam is delivered by the continuous movement of the leaves at variable speed while the beam is on. The advantage of DMLC is that it is able to deliver the desired intensity profile with a high fidelity and the advantage of SMLC is that it is relatively simple and easy to implement and verify (9).

An IMRT planning process usually includes two important steps. First, the best possible fluence maps, which are generally called the "desired intensity maps", are generated by the optimization module. The desired intensity maps are then converted into MLC leaf sequences (or MLC trajectories) as a function of monitor units (MU). Many leaf sequencing algorithms (1-8) have been developed to realize the second step, with the mechanical constraints, such as tongue-and-groove effects, collision constraints for adjoining leaf pairs, taken into account. However, most algorithms, especially the step-and-shoot algorithms, have assumed an ideal MLC and ignored the influence of MLC transmission and head scatter, which may lead to significant discrepancies between the desired and actually delivered intensity maps. Some recent studies (10–11) have indicated that these factors might cause a 5%-20% dosimetric error for a typical IMRT plan if they are not correctly accounted for.

The problem of correcting the effects of transmission and head scatter is less intractable for DMLC than for SMLC. When these effects are included, in general, the final working intensity profile (12) corresponding to the leaf sequences used for treatment is different from the desired one. In the case of dynamic delivery, since the working intensity profile is continuous, it can be updated iteratively to account for the effects of transmission and head scatter. At the end of the iterative calculation, the best working profile can be found and used to generate the final leaf sequences (12-16). In contrast, the same approach cannot be easily implemented in the SMLC mode since the working

intensity profile is discretized and cannot be updated in the iterative fashion. This has been discussed extensively by Chui et al (12). An effective method to correct the effects of transmission and head scatter for the SMLC mode is highly desirable.

The purpose of this work is to develop an effective algorithm to minimize the dosimetric influence of MLC leaf transmission and head scatter in SMLC delivery mode. In the next section we first summarize some theoretical aspects related to the MLC leaf sequencing and IMRT fluence map calculation, and in particular, the three-source model used for the calculation of relative head scatter distributions of MLC segments. We then introduce an error function, defined as the least-square difference between the desired and computed fluence maps, and formulate the problem into the minimization of the error function with respect to the fractional MUs in the MLC leaf sequence file. The algorithm is assessed using an intuitive test field and several clinical IMRT cases.

Methods and Materials

Head scatter

An algorithm based on a three-source model is used to calculate head scatter factor of a beamlet in each segment. In this algorithm, the photon radiation to the point of calculation is treated as from three effective sources: one source for the primary photons from the target and two extra-focal photon sources for the scattered photons from the primary collimator and the flattening filter, respectively. The scatter source intensity distributions, different source positions and the off-axis difference of the scatter radiation are taken into account in the calculation model. We assume that the primary source is a point source located at the rotational central axis of the collimator in the exit plane of the target and its source intensity does not change with the jaw settings. In addition, the extra-focal photon source for the scatter radiation from the primary collimator is represented by a planar annulus source and that for the scatter radiation from the flattening filter can be described by a planar disk source. Source parameters are determined by the data of Monte Carlo simulation (17) and by fitting the head scatter factors for the symmetric square fields, which were measured in air using a PWT Farmer 0.6 cm^3 ion chamber with a 3 mm-thick brass buildup cap for the Varian Clinic 2300C/D

15MV photon beam (Varian Oncology System, Palo Alto, CA). Head scatter factor is calculated by integrating the radiation contributed from areas (determined by the detector's eye view) in the two scatter sources (18). In addition, in order to reduce the calculation time and save computer memory, we use the head scatter factor of the centered beamlet in each opened leaf pair of a segment to represent the head scatter factors of all other beamlets in the same leaf pair of the segment, the errors arising from such approximation are less than 0.3% in most situations. However, the calculation time and required computer memory are greatly reduced.

To verify the accuracy of the algorithm for small irregular fields, head scatter factors were measured at different positions for several clinical segments. All the measurements were performed at isocenter plane using a film measurement technique proposed by LoSasso et al (10), in which Kodak XV2 film in ready pack was used and lead disks (6 mm in diameter and 3mm in thickness) were placed at measurement point upstream and downstream in contact with the film jacket to achieve sufficient buildup for 15 MV X rays. The calibration curve for the used films was determined by optical densities measured at d_{max}=3.0 cm for different MU irradiation in the field center of a 10×10 cm^2 field with SSD=100 cm in solid water. The optical densities of measurement points were converted to dose and head scatter factor was then obtained. All the measured data were normalized to unity for a symmetric 10×10 cm^2 field at the isocenter. We use the following formula to obtain head scatter factor for the beamlet *(i,j)* in a segment,

$$S_{c,m}(i,j) = \frac{D_m(i,j)}{D_m(10,10,isocenter)OAR(r)}, \qquad (1)$$

where $S_{c,m}(i,j)$ is the measured head scatter factor for the beamlet *(i,j)* in a segment, $D_m(i,j)$ is the dose measured at the center of beamlet *(i,j)*; $D_m(10,10,isocenter)$ is the dose measured at isocenter for reference field (symmetric 10×10 cm^2 field) ; r is the distance between isocenter and the center of beamlet *(i,j)*. OAR (r) is the primary off-axis ratio measured at isocenter plane for the center of beamlet *(i,j)* in air.

Calculation of fluence map

The fluence of a given IMRT field can be divided into a grid of beamlets (9). For an IMRT leaf sequence file with K segments, the delivered fluence map in isocenter plane, $\Phi(i, j)$, can be calculated by summing the contributions of all segments,

$$\Phi(i, j) = \sum_{k}^{K} f_k \varphi_k(i, j), \qquad (2)$$

where f_k is the fractional MU of the *k-th* segment in the leaf sequence file, $\varphi_k(i,j)$ is the fluence per unit MU from the *k-th* segment in the beamlet *(i,j)*. If we denote the boundary of the *k-th* segment by A_k and introduce a notation

$$\delta_{ij,A_k} = \begin{cases} 1 & beamlet(i, j) \in A_k \\ 0 & beamlet(i, j) \notin A_k \end{cases}, \qquad (3)$$

the fluence per unit from the *k-th* segment for beamlet *(i,j)* can be written as

$$\varphi_k(i, j) = S_{c,k}(i, j)\delta_{ij,k} + \alpha S_c^{'}(1 - \delta_{ij,k}), \qquad (4)$$

where $S_{c,k}(i, j)$ is the head scatter factor of the beamlet *(i,j)* in *k*th segment and is calculated by the three-source model described earlier, $S_c^{'}$ is the head scatter factor for the rectangular field defined by the jaws. For a Varian machine, $S_c^{'}$ is field-specific constant since the jaw settings do not change during the whole irradiation process of an IMRT field. In addition, we assume that all the beamlets in a rectangular field have the same $S_c^{'}$. Such an approximation is reasonable since $S_c^{'}$ is only involved in the transmission fluence calculation. α in Eq. (4) is the average transmission factor, representing the amount of radiation passing through the MLC leaves (on average) as a percentage of the radiation of an open field defined by the jaws. It can be measured using an ion chamber or films (10, 19). For our Varian Clinic 2300C/D 15MV photon beam, the average transmission factor is determined to be 1.74%.

Error function and minimization calculation

It is usually impossible to produce the exactly desired fluence map using step-and-shoot mode with realistic MLC and an optimum solution is desired. Our strategy is to minimize the difference between the desired fluence map and actually delivered fluence

map. For this purpose, an error function is constructed according to the least-square difference between the desired and the delivered fluence map, this is,

$$F = \sum_{i,j} [\Phi(i,j) - \Phi_d(i,j)]^2 , \qquad (5)$$

where $\Phi(i,j)$ and $\Phi_d(i,j)$ are the calculated and the desired fluences of beamlet *(i,j)*, respectively. In equation (5), only those beamlets with non-zero fluences in the desired intensity map are considered since we cannot physically produce a beamlet with zero fluence.

To proceed, we add a correction factor to the fractional MU of each segment. The effects of transmission and head scatter are minimized by iteratively adjusting the correction factors in the MLC leaf sequences. The corrected fractional MU of the *k-th* segment, $f_k^{'}$, can be expressed as,

$$f_k^{'} = f_k^0 - \Delta f_k , \qquad (6)$$

where f_k^0 is the fractional MU of the *k-th* segment in the leaf sequence file generated from the desired intensity profile without considering the transmission and head scatter and Δf_k is the correction factor for the *k-th* segment.

The calculation starts with the MLC leaf sequence file derived from the desired fluence map without considering the transmission and head scatter. The desired intensity maps come from the optimization module of a commercial treatment planning system (Corvus, NOMOS cooperation, Sewickley, PA) (20), and are outputted in the form of a grid of beamlet intensities. The initial leaf sequences are generated using the algorithm proposed by Bortfeld et al (1). But any other step-and-shoot leaf sequence algorithm can also be used here (2, 4, 21, 22). The procedure of the algorithm is shown in figure 1. A downhill simplex algorithm is employed to minimize the error function and search the optimum correction factors. The starting vertices for downhill simplex algorithm can be chosen randomly before the optimization process. In our work, from the initial uncorrected delivered fluence, a -1.0% correction of the total MU was added to the fractional MU of a segment each time while other correction factors remained as zero, thus M+1 vertices were generated and used as the starting vertices of the algorithm. The iteration process stops when the tolerance value or a preset maximum iteration number

was reached. In our calculation, the tolerance value was set as 0.00001 and the maximum iteration number was set to 8000.

Dosimetric verification

The algorithm was verified by an intuitive test field and some clinical IMRT fields of prostate treatments using the Varian Clinic 2300C/D 15MV photon beam. The dose distributions delivered by the leaf sequence files correcting for head scatter and transmission were measured using Kodak XV2 films at different depths in solid water phantom. In the measurements, radiographic films were placed in isocenter plane perpendicularly to the beam. The optical densities were converted to doses by the method described above. The absolute doses were also measured with a PWT Farmer 0.6cm^3 ion chamber in a relatively flat part of the intensity maps to normalize the relative dose distributions obtained by the film measurements. The measured results were compared with the theoretical prediction calculated by Monte Carlo simulation (23,24,25) using the desired fluence maps. The verification process is schematically illustrated in figure 2.

The intuitive test field consisted of five consecutive 2.0×10 cm^2 segments (Fig. 3) aiming to produce a 10×10 cm^2 uniform open beam. This type of an intuitive example is best suited for illustrating our algorithm since its absolute dose distribution can be easily determined. Three step-and-shoot leaf sequence files were generated: (1) no corrections for transmission and head scatter; (2) corrections for both transmission and head scatter; and (3) only correction for transmission. The leaf sequence files were used in the film measurements of the dose distributions in isocenter plane at depth 5.0cm in a solid water phantom. In addition, a measurement for a single-segment 10×10 cm^2 open field shaped by MLC with the same jaw settings was also performed.

IMRT fields from clinical prostate cases were also used to further test our algorithm. The plans were generated using CORVUS system. The dose distributions were measured in isocenter plane at depth 3.0cm in a solid water phantom. Three MLC leaf sequence files with different correction schemes similar to those described above were generated and delivered for each IMRT field. The dose distributions corresponding to these cases were measured and compared.

Results

Head scatter factor

Figure 4 shows the measured and calculated head scatter factors for square fields from 4 cm to 40 cm at isocenter for the 15MV beam. The line is the calculated values and the scattered solid circles represent the measured ones. The agreement between these two groups of data is within 0.3% for all measurement fields. Table I lists the measured and calculated head scatter factors for 8 different beamlets in four randomly chosen segments of a clinical prostate IMRT field (Two of the four segments are shown in Fig. 5.). The four measurement positions (the corresponding measurement results are listed in Table I) in these two segments are also labeled in Fig. 5. For all measured beamlets, the calculated results agree with the measurements within 0.8%.

Fluence maps

The first test was done by using a 10×10 cm^2 open beam. In this case, the desired intensity map for the test field was set to a uniform distribution of 30MU. Table II lists the incident intensity maps calculated by the different leaf sequence files: (1) both transmission and head scatter were ignored (Table II (a)); (2) only transmission was corrected (Table II (b)); and (3) both transmission and head scatter were corrected by our method (Table II (c)). The values listed in Table II are the absolute MUs for each beamlet. It could be easily obtained from Table II that the absolute intensity deviation between the calculated and the desired intensity map was about 1.2 MU (~ 4.0% of the desired intensity) if both head scatter and transmission were ignored, about -1.0 MU (~-3.3% of the desired intensity) if only transmission was corrected and less than 0.1 MU (~0.3% of the desired intensity) when both effects were corrected by our method.

A six-field prostate IMRT treatment was also used to assess our algorithm. The beam incident angles were 0°, 40°, 115°, 180°, 245° and 320° respectively in Varian's convention. The number of intensity level was set to 10 and the leaf sequences were generated using the Corvus planning system. The numbers of segments for the six fields were 16, 15, 12, 16, 13 and 13, respectively. In Table III (a), we show the desired intensity map for the field with gantry angle 0°. In Table III (b) to (d), we also show the

intensity maps calculated by using the uncorrected, corrected and only transmission corrected leaf sequence files. From Table III, we find that the maximum absolute MU differences between the calculated and desired intensity maps were about 1.5MU (~3.0% of the maximum MU in the field) if neither head scatter nor transmission was corrected and about -2MU (~-4.0% of the maximum MU in the field) if only transmission was corrected. The maximum differences between the relative intensity maps for these two situations were about 3% and 2%, respectively. After correcting for the transmission and head scatter using our algorithm, both the absolute and relative intensity maps were in agreement with desired ones within 1.0% of the maximum intensity of the field, except those beamlets whose desired intensity was zero. Table IV lists the obtained correction factors to the fractional MUs for the IMRT field. Similar results were also found for the other five fields of the case.

Dosimetric verification

Figure 6a and 6b show the measured relative and absolute dose profiles in the isocenter plane at depth 5cm in solid water for the test field along the midline of the 21st leaf pair. The dose profiles of the single-segment 10×10 cm^2 field are also shown as benchmark. Although there are almost no differences between the relative dose distributions, the discrepancies between the absolute dose distributions are quite large. The absolute dose without considering the head scatter and transmission is higher than that of single-segment 10×10 cm^2 field by about 1.2cGy (~3.8%). When only the transmission is corrected, the absolute dose profile is lower than that of single-segment 10×10 cm^2 field by about 1.1cGy (~-3.5%). Our leaf sequence file, which corrects for both head and transmission, generates a dose distribution very close to that of single-segment 10×10 cm^2 field (within 1.0% deviation).

The dose distributions calculated using Monte Carlo simulation for the IMRT field with gantry angle 0° are shown in Fig. 7a and 7b as the thick solid lines. The measured dose distributions delivered by the leaf sequence files with and without correcting for the transmission and head scatter are shown in Fig.7a and 7b as the thin broken lines, respectively. The calculated and measured relative and absolute dose profiles along the leaf moving direction at the off-axis distance of 1.5cm (through the middle of the 22nd

leaf pairs) are shown in figure 8a and 8b. The measured dose distribution delivered by our corrected leaf sequences is in good agreement with that of Monte Carlo calculations. The differences between the isodose lines were within 2.5% or less than 2mm in the high dose gradient regions as shown in figure 7. Dose profiles shown in figure 8 also indicate that both the relative and absolute dose differences are within 2.0% of the maximum dose. As shown in Figure 8, when only transmission is corrected, the difference between the measured and calculated absolute doses is larger than that between the relative doses. For example, in the area B of Fig.8, the maximum absolute dose difference is as large as -6.0 % of the maximum dose, whereas the relative dose is lower than the calculated one by about 4.5%. In addition, it can be observed that the relative dose is higher than the calculated one by about 3.5% (in the area A shown in Fig.8) for the measured dose distributions using the uncorrected leaf sequences.

Figure 7 and 8 also show that the Monte Carlo-calculated doses in the low dose regions (less than 10%) are lower than the measured one about 3% of the maximum dose. This discrepancy is caused by the zero fluence beamlets in the desired fluence map, which was used in Monte Carlo calculation. These beamlets receive about 3% transmission radiation as shown in the table III.

Discussion

For step-and-shoot delivery, the effects of transmission and head scatter cannot be determined until a leaf sequence is generated. This entails an iterative approach to correct for the effects of transmission and head scatter. When head scatter is neglected, there are some special cases in which an analytical solution can be obtained from equation (5) by assuming $\partial F / \partial f_k = 0$ (k=1, ..., K). Simple examples of 1D IMRT fields consisted of 4 beamlets and 3 intensity levels are illustrated in figure 9. For case 1-3, analytical solutions can be obtained since the number of independent equations is less or equal to the number of correction factors (the number of variables, here is equal to 3). For case 4, there exists no analytical solution since the number of independent equations is larger than the number of correction factors. In general, an analytical solution does not exist

when head scatter is considered. Under such situations, the best we can do is to search for an optimum compromise using the algorithm proposed in this work. Our results indicate that the proposed method is robust and effective in minimizing the dosimetric influence of the transmission and head scatter in IMRT delivery.

For some disease sites, for instance, prostate and head & neck diseases, the desired intensity profiles produced by the optimization module tend to be highly complex. As a result, a large number of small segments, some are even formed by a single beamlet, are included in the leaf sequences. In these cases, head scatter might have significant influence on incident fluence due to the fast reduction of head scatter with the field size in the small field limit. The influence is even larger than that of transmission in some circumstances. To accurately determine head scatter distribution for each segment, we employed a three-source model.

It is interesting to point out that transmission and head scatter usually have opposite influence on the delivered doses. The head scatter correction tends to reduce the incident intensity values and requires the leaf sequence to be modified to increase beam-on-time. The transmission correction, on the contrary, tends to increase the incident intensity values and requires the leaf sequence to reduce beam-on-time. If only transmission is considered in the leaf sequence algorithm, the deviations from the desired intensity maps may become larger than if none of the two factors is corrected in the leaf sequence algorithm since the effects of transmission and head scatter may cancel each other partially. This is especially true when there are a large number of small segments in IMRT field. This has been observed in the measurements and calculations for a few clinical fields. Similar results are also reported recently by Azcona JD et al (11). In short, in order to obtain the dose distributions as close as that calculated by the inverse treatment planning system, both transmission and head scatter should be corrected accurately.

From Fig. 8a, we find that the relative dose at the areas of lower dose (area A in Fig. 8a) is higher than the calculated dose if head scatter and transmission are not corrected. This is because these areas are blocked by MLC much longer than other areas and receive the largest transmission contributions. However, there exist some areas (area B and C in Fig. 8a) where the relative doses are closer to the calculated ones if neither head scatter

nor transmission is corrected than if only transmission is corrected. In addition, as shown in fig.8, our measured and calculated results also indicate that the head scatter and transmission corrections have larger influences on the absolute dose (or intensity) distributions than on the relative dose (or intensity) distributions. As a consequence, if the details of head scatter and transmission relative distributions are ignored, the averaged effects for head scatter and transmission can be approximately corrected by an experimentally determined adjusting factor, which is similar to the fudge factor used by Azcona et al (11) and by the CORVUS inverse planning system. The deviations in absolute dose distributions can be reduced greatly by using a fudge factor if an accurate head scatter calculation model is not available or only transmission is taken into account.

When the number of intensity levels used to stratify the intensity profiles is increased, we observe that the deviations between the incident intensity map calculated by the corrected leaf sequences and the desired one decrease. This is because the number of segments usually increases with the number of intensity levels, providing more adjustable variables in the leaf sequence file.

Conclusions

Unlike conventional radiation treatment with static MLC fields, there are significant dosimetric issues that must be addressed when IMRT delivery is used. In this paper, an algorithm for correcting the effects of the transmission and head scatter in step-and-shoot leaf sequences is presented. The experimental data indicate that the deviations of the delivered fluence (dose) corrected using the algorithm from the desired ones are significantly decreased for both the relative and absolute distributions. While the proposed technique was applied to the Varian MLC, the methodology can be easily extended to deal with IMRT deliveries of other vendors.

Acknowledgements

We wish to thank Drs. M. Lee, M. Murphy, J. Kung, J.G. Li, T. Pawlicki, G. Luxton, and Arthur Boyer for useful discussions. This work was partly supported by a research grant

from the Department of Defense (BC996645) and a Research Scholar Award from the American Cancer Society (RSG-01-022-01-CCE).

Table I. The measured and calculated head scatter factors (*Sc*) for eight different beamlets in five randomly chosen segments of clinical prostate IM fields for Varian 2300C/D 15 MV photon beam. Diff= (Calculated S_c-measured S_c)/measured $S_c \times 100\%$.

Beamlet Num.	1	2	3	4	5	6	7	8
Calculated Sc	0.948	0.954	0.945	0.965	0.979	0.962	0.976	0.961
Measured Sc	0.942	0.959	0.939	0.972	0.975	0.954	0.969	0.955
Diff (%)	0.6%	-0.5%	0.6%	-0.7%	0.4%	0.8%	0.7%	0.4%

Table II. The intensity maps for a test field: (a) The calculated intensity map without corrections of head scatter and transmission; (b) The calculated intensity map only corrected for transmission; (c) The calculated intensity map corrected for both head scatter and transmission. The values in Table II are the absolute MU for each beamlet and the beamlets are indexed by their center positions (cm). The isocenter is at (0,0).

(a)	-4.5	-3.5	-2.5	-1.5	-0.5	0.5	1.5	2.5	4.5	4.5
4.5	30.9	30.9	31	31	31	31	31	31	30.9	30.9
3.5	30.9	30.9	31	31	31.1	31.1	31.1	31.1	31	31
2.5	31	31	31.1	31.1	31.1	31.1	31.1	31.1	31	31
1.5	31	31	31.1	31.1	31.1	31.1	31.1	31.1	31	31
0.5	31	31	31.1	31.1	31.2	31.2	31.1	31.1	31	31
-0.5	31	31	31.1	31.1	31.2	31.2	31.1	31.1	31	31
-1.5	31	31	31.1	31.1	31.2	31.2	31.1	31.1	31	31
-2.5	31	31	31.1	31.1	31.1	31.1	31.1	31.1	31	31
-3.5	30.9	30.9	31	31	31.1	31.1	31	31	31	31
-4.5	30.9	30.9	31	31	31	31	31	31	30.9	30.9

(b)	-4.5	-3.5	-2.5	-1.5	-0.5	0.5	1.5	2.5	4.5	4.5
4.5	28.8	28.8	28.9	28.9	28.9	28.9	28.9	28.9	28.8	28.8
3.5	28.9	28.9	29	29	29	29	29	29	28.9	28.9
2.5	28.9	28.9	29	29	29	29	29	29	28.9	28.9
1.5	29	29	29.1	29.1	29.1	29.1	29.1	29.1	29	29
0.5	29	29	29.1	29.1	29.1	29.1	29.1	29.1	29	29
-0.5	29	29	29.1	29.1	29.1	29.1	29.1	29.1	29	29
-1.5	29	29	29.1	29.1	29.1	29.1	29.1	29.1	29	29
-2.5	28.9	28.9	29	29	29	29	29	29	28.9	28.9
-3.5	28.9	28.9	29	29	29	29	29	29	28.9	28.9
-4.5	28.8	28.8	28.9	28.9	28.9	28.9	28.9	28.9	28.8	28.8

(c)	-4.5	-3.5	-2.5	-1.5	-0.5	0.5	1.5	2.5	4.5	4.5
4.5	29.9	29.9	29.9	29.9	29.9	29.9	29.9	29.9	29.9	29.9
3.5	30	30	30	30	30	30	30	30	30	30
2.5	30	30	30	30	30	30	30	30	30	30
1.5	30.1	30.1	30.1	30.1	30.1	30.1	30.1	30.1	30.1	30.1
0.5	30.1	30.1	30.1	30.1	30.1	30.1	30.1	30.1	30.1	30.1
-0.5	30.1	30.1	30.1	30.1	30.1	30.1	30.1	30.1	30.1	30.1
-1.5	30.1	30.1	30.1	30.1	30.1	30.1	30.1	30.1	30.1	30.1
-2.5	30	30	30	30	30	30	30	30	30	30
-3.5	30	30	30	30	30	30	30	30	30	30
-4.5	29.9	29.9	29.9	29.9	29.9	29.9	29.9	29.9	29.9	29.9

Table III. The intensity maps for the clinical IM field with gantry angle 0°: (a) The desired intensity map; (b) the calculated intensity map without corrections of head scatter and transmission; (c) The calculated intensity map only corrected for transmission; (d) The calculated intensity map corrected for both head scatter and transmission. The values in Table III are the absolute MU for each beamlet and the beamlets are indexed by their center positions (cm). The IMRT treatment isocenter is at (0,0).

(a)	-2.5	-1.5	-0.5	0.5	1.5	2.5	3.5
2.5	39.2	44.8	56	44.8	28	50.4	5.6
1.5	50.4	56	28	39.2	50.4	22.4	22.4
0.5	39.2	28	28	16.8	50.4	39.2	39.2
-0.5	56	56	50.4	56	50.4	22.4	0
-1.5	56	28	44.8	44.8	28	56	0
-2.5	16.8	5.6	16.8	44.8	56	39.2	0
-3.5	0	39.2	50.4	44.8	33.6	16.8	0
-4.5	0	44.8	56	16.8	22.4	0	0
-5.5	0	0	39.2	56	0	0	0

(b)	-2.5	-1.5	-0.5	0.5	1.5	2.5	3.5
2.5	38.9	44.3	55	44.5	28.5	49.6	7.1
1.5	49.8	55.2	28.7	39.3	49.9	23.1	23.1
0.5	39	28.5	28.8	18	50.1	39.2	39.2
-0.5	55.2	55.2	50.2	55.5	50	23.1	1.7
-1.5	55	28.8	45	45	28.8	54.9	1.7
-2.5	17.4	7.2	17.9	45.1	55.5	39.3	1.7
-3.5	1.7	38.6	49.4	44.9	34.1	17.9	1.7
-4.5	1.7	44.3	55	17.9	23.2	1.7	1.7
-5.5	1.7	1.7	38.4	54.4	1.7	1.7	1.7

(c)	-2.5	-1.5	-0.5	0.5	1.5	2.5	3.5
2.5	39.6	45.1	55.8	45.1	28.4	49.7	6.1
1.5	50.6	55.9	28.3	39.3	50	22.8	22.8
0.5	39.7	28	28.4	17.3	50.1	39.3	39.3
-0.5	55.9	55.9	50.2	56.1	50.1	22.7	1.8
-1.5	55.8	28.4	44.5	44.5	28.4	55.9	1.8
-2.5	16.8	5.6	17.3	44.5	55.9	39.7	1.8
-3.5	1.8	39.4	50.3	44.3	33.9	17.4	1.8
-4.5	1.8	45.1	55.8	17.5	22.4	1.8	1.8
-5.5	1.8	1.8	39.3	55.5	1.8	1.8	1.8

(d)	-2.5	-1.5	-0.5	0.5	1.5	2.5	3.5
2.5	37.8	43.3	54.2	43.5	27.2	48.7	5.5
1.5	48.9	54.4	27.4	38.2	49	21.9	21.8
0.5	37.9	27.2	27.5	16.6	49.2	38.1	38.1
-0.5	54.4	54.4	49.3	54.7	49.1	21.8	1.7
-1.5	54.2	27.5	44	44	27.5	54.1	1.7
-2.5	16	5.5	16.5	44	54.7	38.2	1.7
-3.5	1.7	37.5	48.5	43.9	32.9	16.5	1.7
-4.5	1.7	43.2	54.2	16.5	21.9	1.7	1.7
-5.5	1.7	1.7	37.4	53.6	1.7	1.7	1.7

Table IV. Correction factors of the fractional MUs for the IMRT field with gantry angle 0°. The number of intensity levels is set to 10. C_{tr}'s represent the correction factors only corrected for transmission and the C_{sctr}'s are the correction factors corrected for both head scatter and transmission. "+" implies that the fractional MU of this segment should be reduced by $\Delta f = C \times MU_{tot}$; "-" implies that the fractional MU of this segment should be increased by $\Delta f = C \times MU_{tot}$. MU_{tot} is the total irradiated MU for this IMRT field.

Segment Num.	1	2	3	4	5	6	7	8
C_{tr}	-0.0059	0.0201	-0.0109	-0.0025	0.0163	-0.0107	0.0007	0.0015
C_{sctr}	-0.0143	0.0208	-0.0130	-0.0063	0.0163	-0.0123	-0.0001	-0.0002

Segment Num.	9	10	11	12	13	14	15	16
C_{tr}	0.0016	0.0092	-0.0093	0.0042	-0.0035	-0.0014	0.0099	-0.0038
C_{sctr}	0.0011	0.0075	-0.0120	0.0059	-0.0056	-0.0047	0.0079	0.0111

Figure Captions

FIG.1. The procedure of correcting the effects of head scatter and transmission in step-and-shot leaf sequences.

FIG.2. The dose verification process for validating the algorithm.

FIG.3. The schematic diagram of the intuitive test field. The field includes five consecutive 2.0×10 cm^2 segments and attempts to produce a 10×10 cm^2 open beam.

FIG.4. The measured and calculated head scatter factors for square field size from 4 cm to 40 cm at isocenter for 15MV photon beam. All the data are normalized to the value of a 10×10 cm^2 field at SAD. The line and solid dots represent the calculated and measured data, respectively.

FIG.5. Two segments of clinical prostate IMRT fields. The four measured positions are labeled in the figure and the corresponding head scatter factors are listed data in Table I.

FIG.6. The measured relative (a) and absolute (b) dose profiles along the midline of the 21A-21B leaf pair in the isocenter plane at depth 5cm in solid water for the test field. The test field consists of five consecutive 2.0×10 cm^2 segments to produce a 10×10 cm^2 uniform fluence distribution of 30MU. The measured results of the single-segment 10×10 cm^2 open field with 30MU are shown as benchmark.

FIG.7. Comparison of the measured and Monte Carlo calculated isodose distributions in the isocenter plane at depth 3cm in solid water for an IMRT field. The measurements are performed using leaf sequences with (figure 7a) and without (figure 7b) correcting the transmission and header scatter effects. The thick solid lines indicate the calculated results and the thin broken lines are the measured results. The shown isodose lines are from 10% to 90% with 10% increment.

FIG.8. The calculated and measured relative (a) and absolute (b) dose profiles along the leaf moving direction at the off-axis distance of 1.5cm (through the middle of the 22nd leaf pairs) in the isocenter plane at depth 5cm in solid water for an IMRT field.

FIG.9. Simple 1D IMRT fields consisted of 4 beamlets and 3 intensity levels. For case 1-3, analytical solutions can be obtained if only transmission is taken into account since the number of independent equations is less or equal to the number of correction factors (the number of variables, here is equal to 3). For case 4, there exists no analytical solution since the number of independent equations is larger than the number of correction factors.

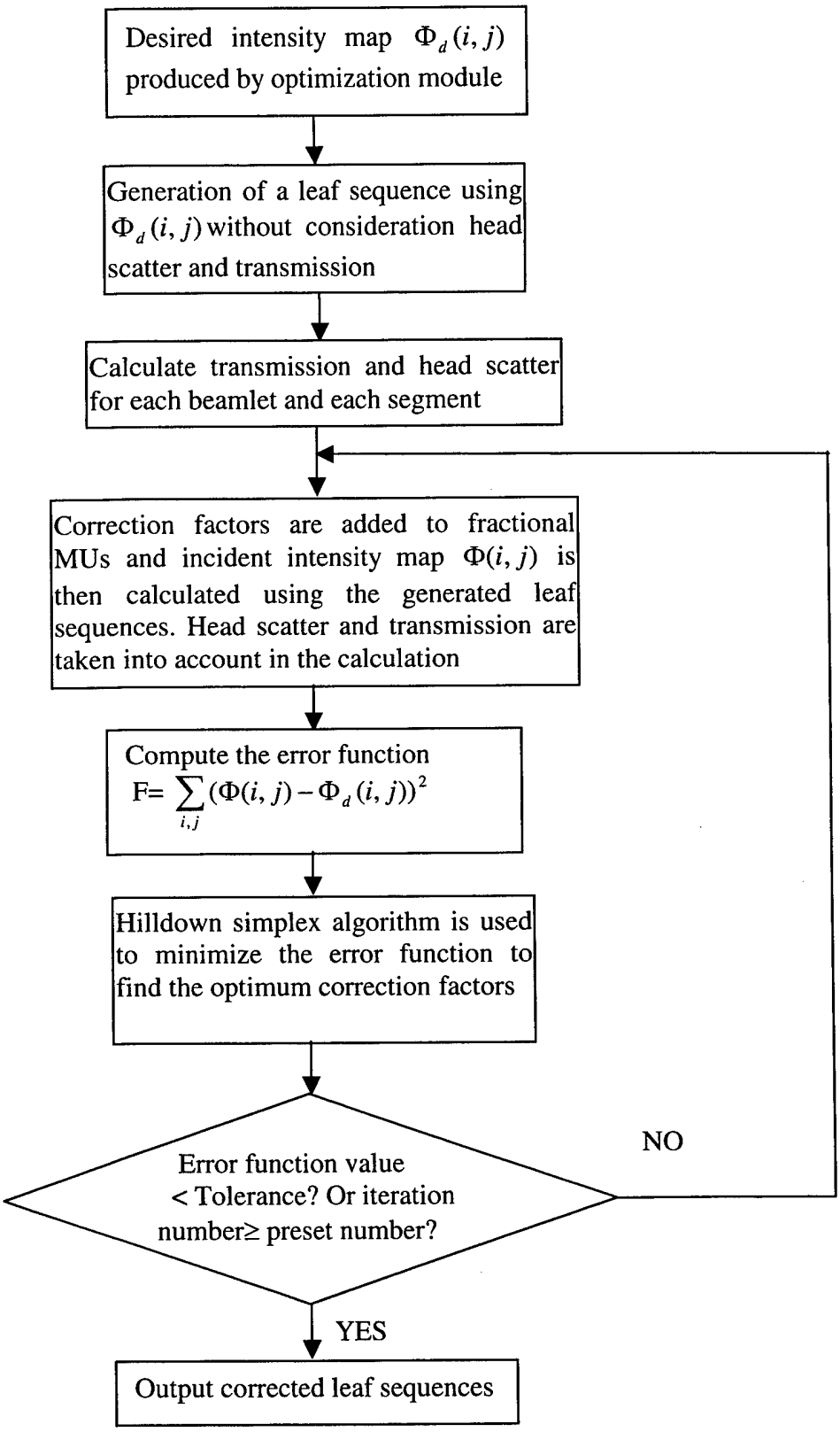
Desired intensity map $\Phi_d(i,j)$ produced by optimization module
Generation of a leaf sequence using $\Phi_d(i,j)$ without consideration head scatter and transmission
Calculate transmission and head scatter for each beamlet and each segment
Correction factors are added to fractional MUs and incident intensity map $\Phi(i,j)$ is then calculated using the generated leaf sequences. Head scatter and transmission are taken into account in the calculation
Compute the error function $F=\sum_{i,j}(\Phi(i,j)-\Phi_d(i,j))^2$
Hilldown simplex algorithm is used to minimize the error function to find the optimum correction factors
Error function value < Tolerance? Or iteration number≥ preset number?
NO
YES
Output corrected leaf sequences

FIG. 1

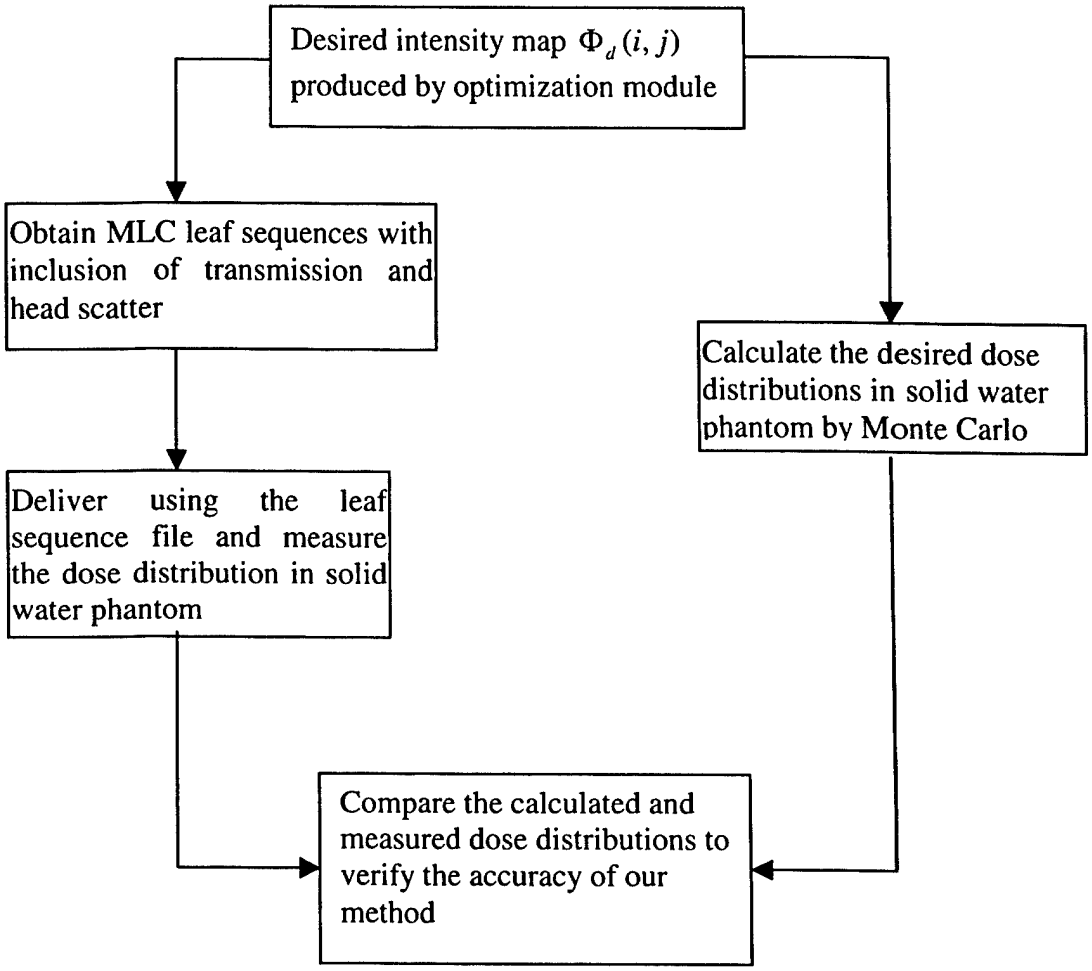
Desired intensity map $\Phi_d(i,j)$ produced by optimization module
Obtain MLC leaf sequences with inclusion of transmission and head scatter
Calculate the desired dose distributions in solid water phantom by Monte Carlo
Deliver using the leaf sequence file and measure the dose distribution in solid water phantom
Compare the calculated and measured dose distributions to verify the accuracy of our method

FIG. 2

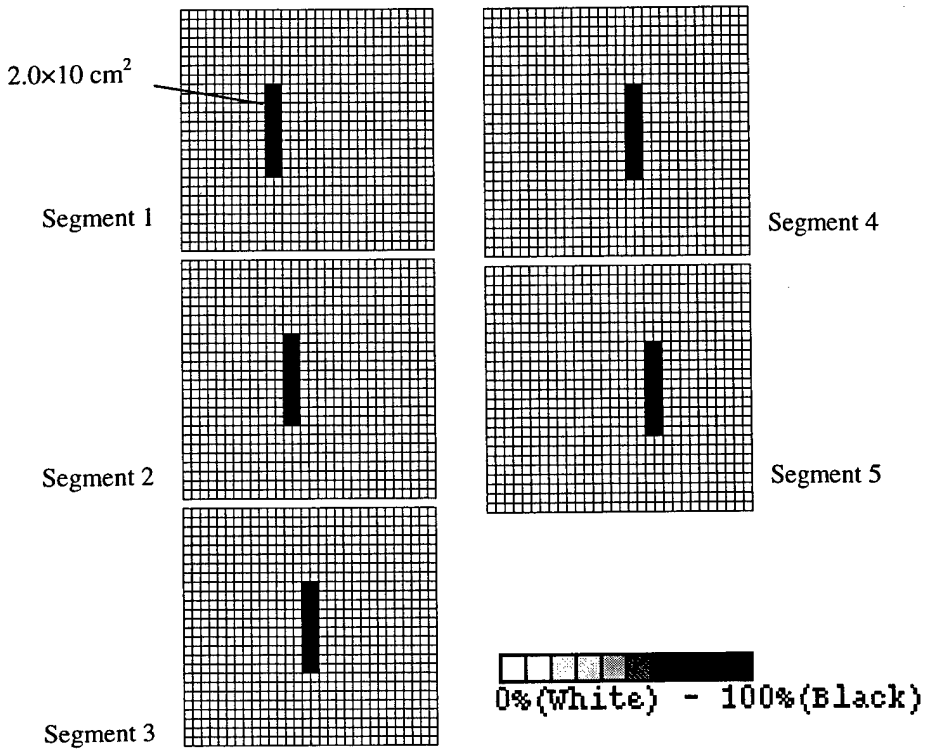
2.0×10 cm²
Segment 1
Segment 2
Segment 3
Segment 4
Segment 5
0%(White) - 100%(Black)

FIG.3

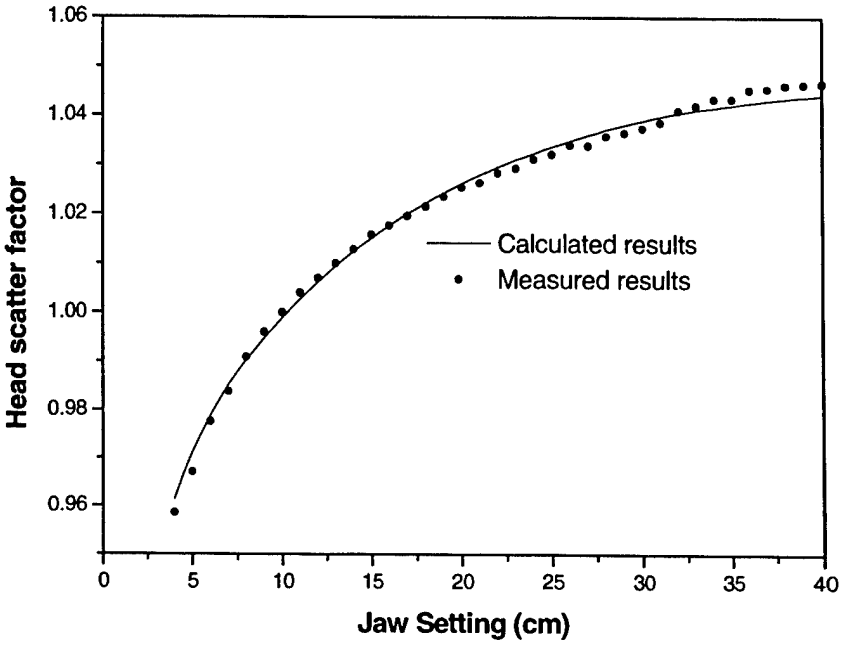
1.06
1.04
1.02
1.00
0.98
0.96
Head scatter factor
0
5
10
15
20
25
30
35
40
Jaw Setting (cm)
Calculated results
Measured results

Fig. 4

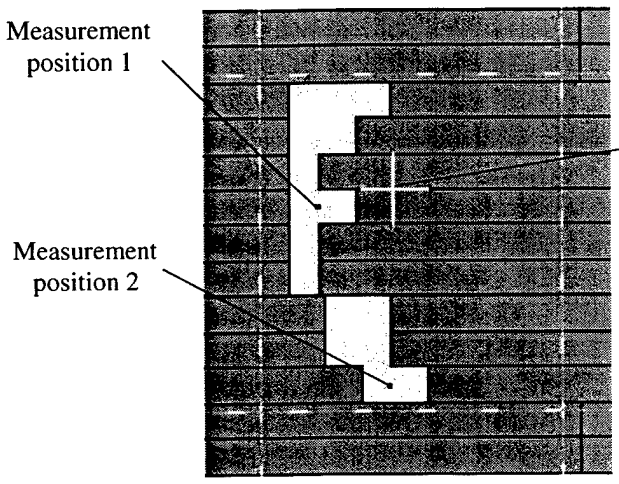
Measurement position 1
Measurement position 2

Fig. 5a

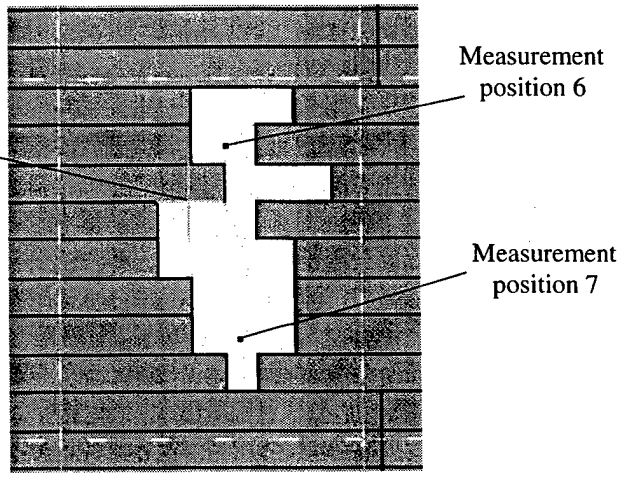
isosenter
Measurement position 6
Measurement position 7

Fig. 5b

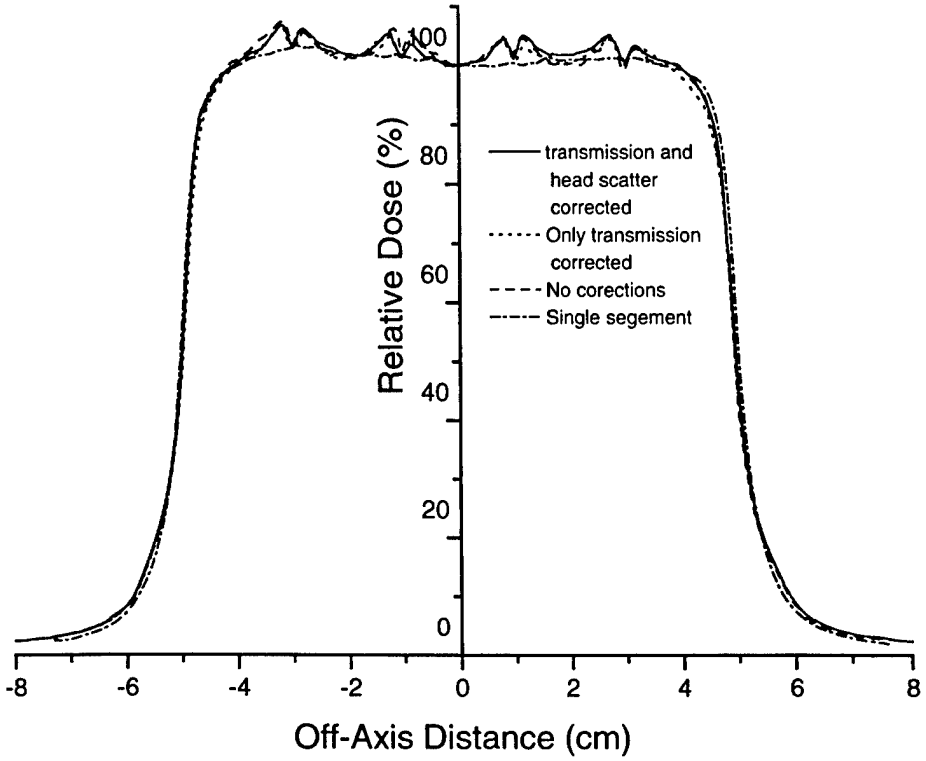
Relative Dose (%)
100
80
60
40
20
0
-8
-6
-4
-2
0
2
4
6
8
Off-Axis Distance (cm)
transmission and head scatter corrected
Only transmission corrected
No corections
Single segement

Fig. 6a

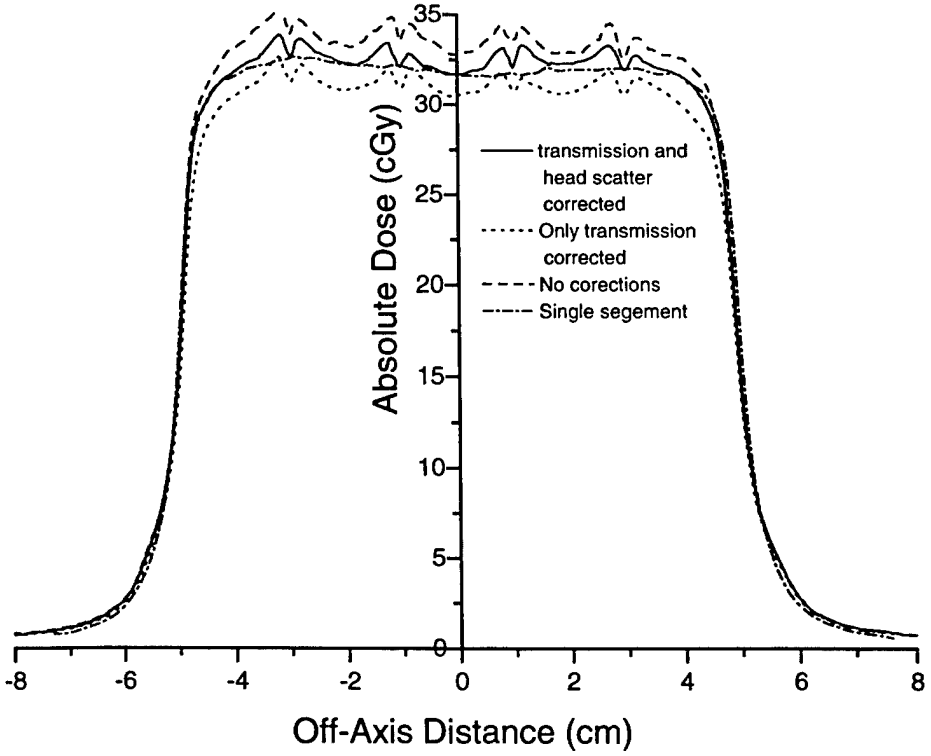
Absolute Dose (cGy)
35
30
25
20
15
10
5
0
-8
-6
-4
-2
0
2
4
6
8
Off-Axis Distance (cm)
transmission and head scatter corrected
Only transmission corrected
No corections
Single segement

Fig. 6b

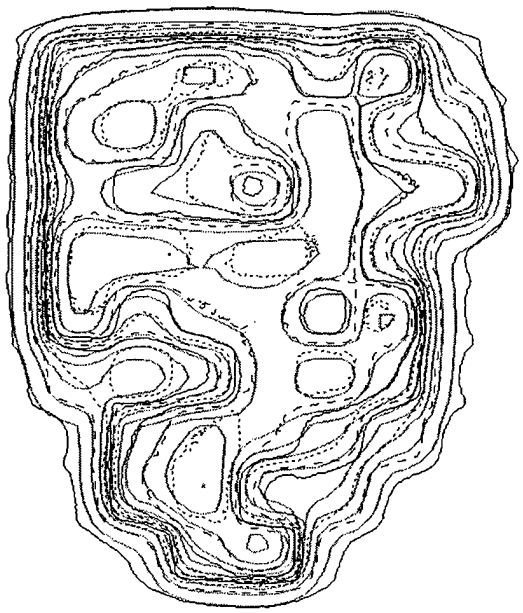

Fig. 7a

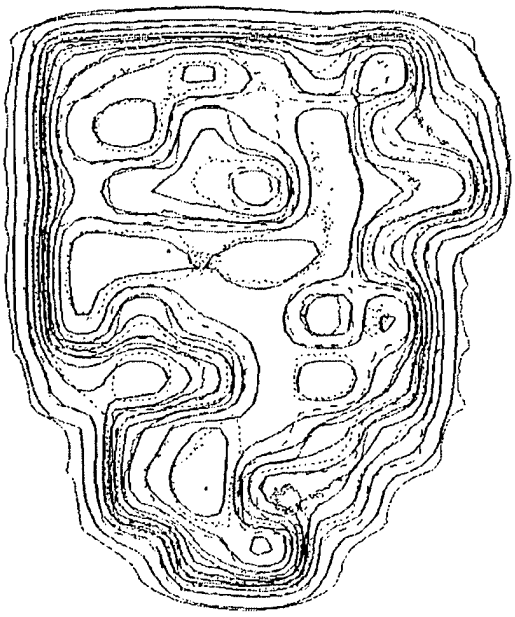

Fig. 7b

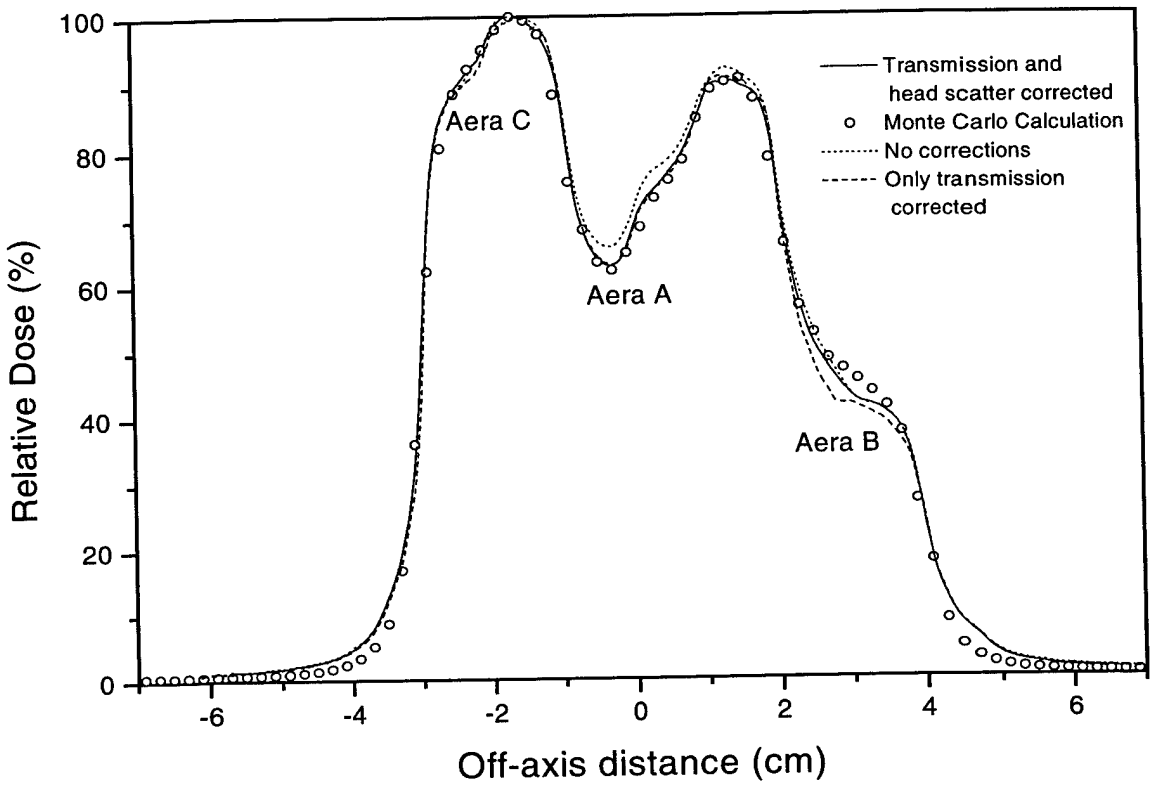
Relative Dose (%)
100
80
60
40
20
0
-6
-4
-2
0
2
4
6
Off-axis distance (cm)
Aera C
Aera A
Aera B
Transmission and head scatter corrected
Monte Carlo Calculation
No corrections
Only transmission corrected

Fig. 8a

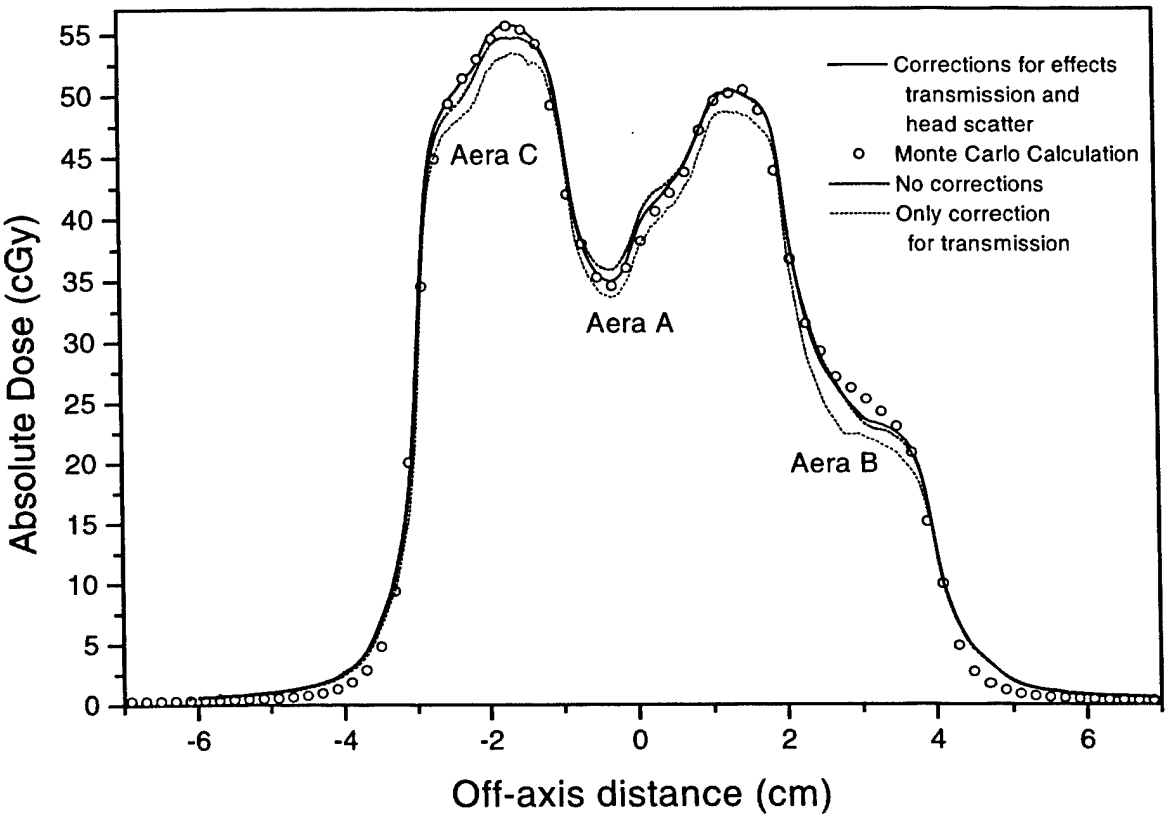
Absolute Dose (cGy)
Off-axis distance (cm)
Aera C
Aera A
Aera B
Corrections for effects transmission and head scatter
Monte Carlo Calculation
No corrections
Only correction for transmission

Fig. 8b

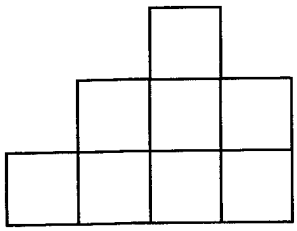

Case1

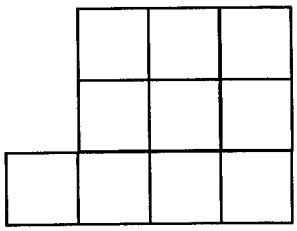

Case 2

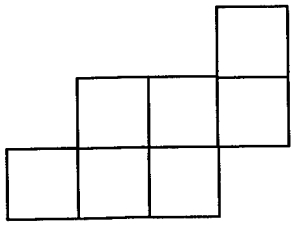

Case 3

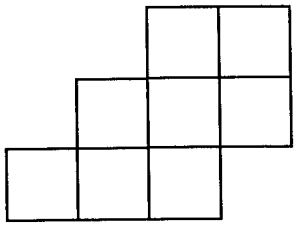

Case 4

Fig. 9

References

1. Bortfeld TR, Kahler DL, Waldron TJ, Boyer AL. X-ray field compensation with multileaf collimators. *International Journal of Radiation Oncology, Biology, Physics.* 1994;28:723-30.

2. Ma L, Boyer AL, Xing L, Ma CM. An optimized leaf-setting algorithm for beam intensity modulation using dynamic multileaf collimators. *Physics in Medicine & Biology.* 1998;43:1629-43.

3. Que W. Comparison of algorithms for multileaf collimator field segmentation. *Medical Physics.* 1999;26:2390-6.

4. Dai JR and Zhu Y P. Minimizing the number of segments in a delivery sequence for intensity-modulated radiation therapy with a multileaf collimator. *Medical Physics.* 2001; 28: 2113-2120.

5. Convey D J and Rosenbloom M E. The generation of intensity-modulated fields for conformal radiotherapy by dynamic collimation. *Physics in Medicine & Biology.* 1992; 37:1359-1374.

6. Spirou SV, Chui CS. Generation of arbitrary intensity profiles by dynamic jaws or multileaf collimators. *Medical Physics.* 1994;21:1031-41.

7. Svensson R, Kallman P, Brahme A. An analytical solution for the dynamic control of multileaf collimators. *Physics in Medicine & Biology.* 1994;39:37-61.

8. Stein J, Bortfeld T, Dorschel B, Schlegel W. Dynamic X-ray compensation for conformal radiotherapy by means of multi-leaf collimation. *Radiotherapy & Oncology.* 1994;32:163-73.

9. Xing L, Li JG. Computer verification of fluence maps in intensity modulated radiation therapy. *Medical Physics.* 2000;27:2084-92.

10. LoSasso T, Chui CS, Ling CC. Physical and dosimetric aspects of a multileaf collimation system used in the dynamic mode for implementing intensity modulated radiotherapy. *Medical Physics.* 1998;25:1919-27.

11. Azcona JD,. Siochi RAC and Azinovic I. Quality assurance in IMRT: Importance of the transmission through the jaws for an accurate calculation of doses calculation of absolute doses and relative distributions. *Medical Physics.* 2002; 29: 269-274.

12. Chui CS, Chan MF, Yorke E, Spirou S, and Ling CC. Delivery of intensity-modulated radiation therapy with a conventional multileaf collimator: Comparison of dynamic and segmental methods. *Medical Physics*. 2001; 28: 2441-2449.

13. LoSasso T, Chui CS, Ling CC. Comprehensive quality assurance for the delivery of intensity modulated radiotherapy with a multileaf collimator used in the dynamic mode. *Medical Physics*. 2001;28:2209-2219.

14. Dirkx ML, Heijmen BJ, van Santvoort JP. Leaf trajectory calculation for dynamic multileaf collimation to realize optimized fluence profiles. *Physics in Medicine & Biology*. 1998;43:1171-84.

15. Holmes T W. A method to incorporate leakage and head scatter corrections into tomotherapy inverse treatment planning algorithm. *Physics in Medicine & Biology*. 2000;45: 1211-1227.

16. Mohan R, Arnfield M, Tong S, Wu Q, and Siebers J. The impact of fluctuations in intensity patterns on the number of monitor units and the quality and accuracy of intensity modulated radiotherapy. *Medical Physics*. 2000; 27: 1226-1237.

17. Liu HH, Mackie TR, and McCullough EC. A dual source beam model used in convolution/superposition dose calculations for clinical megavoltage x-ray beams. *Medical Physics*. 1997;24: 1960-1974.

18. Kim S, Palta JR, Zhu TC, The equivalent square concept for the head scatter factor based on scatter from flattening filter. *Physics in Medicine & Biology*. 1998;43: 1593-1604.

19. Arnfield MR, Siebers, JV, Kim, JO; Wu, Q, Keall, PJ, Mohan R. A method for determining multileaf collimator transmission and scatter for dynamic intensity modulated radiotherapy *Medical Physics*. 2000; 27: 2231-2241.

20. Xing L, Curran B, Hill R, et al. Dosimetric verification of a commercial inverse treatment planning system. *Physics in Medicine & Biology*. 1999;44:463-78.

21. Siochi RA. Minimizing static intensity modulation delivery time using an intensity solid paradigm. *International Journal of Radiation Oncology, Biology, Physics*. 1999;43:671-80.

22. Xia P, Verhey LJ. Multileaf collimator leaf sequencing algorithm for intensity modulated beams with multiple static segments. *Medical Physics*. 1998;25:1424-34.

23. Ma CM, Pawlicki T, Jiang SB, Deng J, Li JS, Mok E, Kapur A, Xing L, Ma L, and Boyer AL. Monte Carlo verification of IMRT dose distributions from a commercial treatment planning optimization system. *Physics in Medicine & Biology*. 2000; 45: 2483-2495.

24. Keall PJ, Siebers JV, Arnfield MR, Kim JO, Mohan R. Monte Carlo dose calculations for dynamic IMRT treatments, *Physics in Medicine & Biology*. 2001;46:929-941.

25. Liu HH, Verhaegen F, Dong L. A method of simulating dynamic multileaf collimators using Monte Carlo techniques for intensity-modulated radiation therapy. *Physics in Medicine & Biology*. 2001;46: 2283-2298.